IRON-MAGNESIUM AMPHIBOLES: SYNTHESIS AND STABILITY WITH RESPECT TO TEMPERATURE, PRESSURE, OXYGEN FUGACITY, AND SULFUR FUGACITY

by

Robert K. Popp

Dissertation submitted to the Graduate Faculty of the
Virginia Polytechnic Institute and State University
in partial fulfillment of the requirements for the degree of
DOCTOR OF PHILOSOPHY
in
Geological Sciences

APPROVED:

M. C. Gilbert, Chairman

F. D. Bloss

J. C. Schug

G. V. Gibbs

D. A. Hewitt

August 1975

Blacksburg, Virginia

ACKNOWLEDGEMENTS

The writer wishes to express gratitude to his advisor, Dr. M. C. Gilbert, for his support and encouragement throughout the term of this study.

Drs. F. D. Bloss, G. V. Gibbs, J. R. Craig, and D. A. Hewitt offered invaluable advice concerning various portions of the research, and along with Dr. J. C. Schug, critically reviewed the manuscript.

Financial support was provided from National Science Foundation grants to M. C. Gilbert (GA 12479-A#1) and to J. R. Craig and M. C. Gilbert (GA 35674; DES 74-22684).

In addition, the aid of Drs. G. Nord, M. Ross, and E. Dwornik, U. S. Geological Survey, Reston, Virginia, Dr. L. Finger, Geophysical Laboratory, Washington, D. C., and F. Seifert, University of Bochum, Germany, is gratefully acknowledged.

TABLE OF CONTENTS

	Page
ACKNOWLEDGEMENTS	ii
LIST OF TABLES	v
LIST OF FIGURES	vi
Part I	1
Introduction	2
Experimental Procedures	5
Experimental Results	11
Relation Between Composition and X-ray Powder Pattern	27
Part II	35
Introduction	36
Experimental Methods	37
Phase Identification and Characterization	38
Phase Equilibria	40
Magnetite-Hematite Buffer	40
Nickel-Nickel Oxide Buffer	48
Fayalite-Magnetite Quartz Buffer	49
Geological Applications	56
Part III	63
Introduction	64
Calculated Sulfide-Silicate Equilibria	66
Experimental Procedures	71
Phase Identification and Characterization	73
Experimental Results	77
Preliminary Sulfurization Runs	77
Reversed Equilibrium Runs	80

TABLE OF CONTENTS (continued)

	Page
Determination of Oxygen Fugacity During Runs	89
Composition of the Vapor Phase	92
Log f_{O_2}-Log f_{S_2} Plot of Amphibole Stability	96
Amphibole Solution Models	100
Log K versus 1/T Plots; Enthalpy of Formation of Iron Amphibole	104
Geological Applications	110
REFERENCES	115
VITA	122

LIST OF TABLES

Table		Page
I-1	Unit cell parameters of amphiboles	14
I-2	Comparison of amphibole structure types.	20
I-3	Peak locations vs composition.	28
I-4	Predicted amphibole compositions	29
I-5	Synthesis run summaries.	30
I-6	Effect of oxygen fugacity on cell parameters	33
II-1	Runs at f_{O_2} defined by MH buffer	43
II-2	Runs at f_{O_2} defined by NNO buffer.	50
II-3	Runs at f_{O_2} defined by FMQ buffer.	54
III-1	Sources of error in calculated opx-po equilibrium. . . .	69
III-2	Results of runs using ruptured capsule method.	81
III-3	Results of double-charge capsule runs.	85
III-4	Revised FMQ-po equilibria.	93
III-5	Comparison of $K_{(21)}$ values	103
III-6A	Enthalpy of reaction values.	108
III-6B	Standard state enthalpies for selected silicates	108

LIST OF FIGURES

Figure		Page
I-1	Unit cell parameters of synthetic amphiboles	12
I-2	Unit cell volumes of amphiboles	13
I-3	Molar volumes of amphiboles	17
I-4	Electron diffraction pattern of synthetic amphibole	21
I-5	Electron diffraction pattern of natural anthophyllite	23
I-6	Relative X-ray structure factors of natural anthophyllite	25
II-1	Shift in amphibole compositions at f_{O_2} defined by MH buffer	41
II-2	Condensed T-X section at f_{O_2} defined by MH buffer	42
II-3	Isothermal sections at f_{O_2} defined by MH buffer	46
II-4	Shift in amphibole composition at f_{O_2} defined by NNO buffer	51
II-5	Extent of solid solution of silicates	52
II-6	Condensed T-X section at f_{O_2} defined by FMQ buffer	55
III-1	Calculated sulfide-orthopyroxene phase relations	67
III-2	Pertinent sulfurization curves	72
III-3	Results of initial sulfurization runs	79
III-4	Variation of amphibole and pyrrhotite composition with time	82
III-5a	Results of a well reversed experiment	84
III-5b	Starting configuration of reversal runs	84
III-6	Coexisting amphibole-pyrrhotite compositions	88
III-7	Calculated and experimental magnetite-pyrrhotite equilibrium	91
III-8	Contours of log f_{H_2O}	97

LIST OF FIGURES (continued)

Figure		Page
III-9	f_{O_2}-f_{S_2} stability of amphiboles.	99
III-10	Plot of a_{Fe}^{amph} vs X_{Fe}^{amph}	105
III-11	Log K vs 1/T plots for oxidation and sulfurization reactions	107

Part I: Synthesis and Unit Cell Parameters of Fe-Mg Amphiboles

Introduction

Amphiboles chemically approaching the join $Mg_7Si_8O_{22}(OH)_2$-$Fe_7Si_8O_{22}(OH)_2$ occur naturally as anthophyllite and as cummingtonite-grunerite. Although they are the least common of the major amphibole groups, natural specimens have been studied in considerable detail because they are important in understanding metamorphism of certain chemically restrictive (low Ca and Al) geological environments (e.g., Klein, 1966). Despite the considerable attention directed to natural specimens, iron-magnesium amphiboles are still poorly understood in terms of both phase equilibria and crystal chemistry. This is unfortunate since these are the chemically simplest amphiboles and should serve as end-member models for understanding the chemically more complex series.

Problems in the determination of phase relations on the join arise from the sluggishness of reactions as evinced by the difficulties in the synthesis of the Mg (anthophyllite) and Fe (grunerite) end-members (Greenwood, 1963; Forbes, 1971). Boyd (1955) reported synthesis of some intermediate compositions on the join at 1 kbar and temperatures in the range of 800°C, but he was unable to crystallize amphibole from its high temperature breakdown assemblage, hypersthene and quartz. Hinrichsen (1967) determined a T-X phase diagram for orthorhombic forms on the join at 2 kbar and temperatures in the range 500°-700°C. Both Hinrichsen and Boyd reported that the most iron-rich amphibole which could be synthesized contained approximately 60 mole % Fe end-member. Aside from these studies, detailed experimental investigations of intermediate members on the Mg-Fe join are lacking. Greenwood (1963) and Forbes

(1971) give detailed summaries of previous experimental studies relevant to the Mg and Fe end-member, respectively, and these will not be repeated here.

Amphiboles of the anthophyllite and cummingtonite-grunerite groups are known to crystallize in 3 of the 4 amphibole structure types so far identified: orthorhombic with space group *Pnma*, monoclinic *C*2/*m* and monoclinic $P2_1/m$. The protoamphibole structure type (Gibbs, 1961; space group *Pnmn*) has not been found in nature and accordingly is not represented. Papike *et al.*, (1969) have shown that the structure and stacking sequence of the double chains in the $P2_1/m$ structure most closely resemble that of the anthophyllite (*Pnma*) structure. Sueno *et al.* (1972) have demonstrated that $P2_1/m$ is the low temperature polymorph of the monoclinic *C*2/*m* type. The phase relationships between the anthophyllite and the cummingtonite (*C*2/*m*) structures are still unclear. Although some authors have evoked chemical explanations for the existence of these two structure types (e.g., Layton and Phillips, 1960), the two forms are known to coexist in nature with essentially the same chemical composition (Evans *et al.*, 1974). Routine optical and powder diffraction examination would probably not distinguish protoamphibole from anthophyllite.

This paper represents the first portion of a study intended to determine the stability of amphiboles on the join $Mg_7Si_8O_{22}(OH)_2$-$Fe_7Si_8O_{22}(OH)_2$ with respect to T, P, f_{O_2}, and f_{S_2}. The aim of this portion was to synthesize as large a range of compositions as possible, determine the structure type(s), and to quantify the relationship between unit cell parameters and composition. For use in further studies, a

simple but accurate method of relating amphibole composition to 2θ spacings on X-ray powder diffraction patterns was desired.

Experimental Procedures

Starting Materials

Starting materials for most of the amphibole syntheses were oxide mixes of the following: MgO (fired periclase) + Fe sponge + SiO_2 glass. However, a few experiments on the Fe end-member were made from an additional "oxygen balanced" oxide mix containing Fe_2O_3 in addition to the above materials. Reagents were dried and stored in a vacuum dessicator prior to weighing. Treatment of Fe sponge with hot H_2 gas resulted in a weight loss attributed to release of oxygen. Appropriate adjustments were made to produce stoichiometric starting materials.

After weighing, all mixes were ground under acetone in an automated agate mortar and pestle for one hour to achieve homogeneity. Portions of certain mixes were ground in the same apparatus up to an additional eight hours to determine the effect of smaller grain size on synthesis rates.

Mixes equivalent to whole-number Mg-Fe formula units across the join were made (i.e., $Mg_7Si_8O_{22}(OH)_2$, $Mg_6Fe_1Si_8O_{22}(OH)_2$, ..., $Mg_1Fe_6Si_8O_{22}(OH)_2$, $Fe_7Si_8O_{22}(OH)_2$). For the sake of simplicity, compositions will hereafter be referred to only by their Mg-Fe formula units (Mg_5Fe_2, etc.) or by mole % of the Fe end-member.

Apparatus, Buffering Techniques and Sample Containers

Most experiments were carried out in Tuttle-type pressure vessels essentially like that described by Ernst (1968, p. 34). Two systems, one with a 5 kbar pressure capacity and the other with a 7 kbar capacity were

used for various steps of the syntheses. Control of oxygen fugacity was normally accomplished with the solid-buffer technique of Eugster (Huebner, 1971), using sealed $Ag_{70}Pd_{30}$ inner capsules, and Au outer capsules. A number of runs, also in sealed $Ag_{70}Pd_{30}$, were carried out in a CH_4-C buffering system with a 1 kbar pressure capacity. This system is similar to the hydrothermal systems described above but utilizes methane as the pressure medium and graphite filler rods (Eugster and Skippen, 1967; Huebner, 1971).

Temperatures in all of the apparatus were measured by means of chromel-alumel thermocouples. Furnace-bomb assemblies were calibrated against 1 atm NaCl (800.5°C) and CsCl (646°C) melting points. Variations of 1°-3°C were typical for runs. Pressures were measured on Heise bourdon tube gauges, which were factory calibrated, and set to read 0.0 bars at one atm. Typical pressure variations during runs were $\pm$20 bars.

Phase Identification

Run products were routinely examined with the petrographic microscope and a Norelco X-ray powder diffractometer equipped with a graphite monochromator using Ni-filtered CuK_α radiation. Qualitative identification was made by scanning at 2°2θ/min between 8° and 70°2θ. Spacing data for the X-ray reflections were collected from four scans (two oscillations) run at 1/2° 2θ/min with synthetic $MgAl_2O_4$ spinel (a_o = 8.0831 Å) as an internal standard. Unit cell parameters were then obtained by a least-squares refinement using the computer program of Evans *et al.* (1963). All peaks were weighted equally. Grain size of the amphibole

averaged approximately 10-15μ × 1-2μ and thus precluded use of single crystal X-ray techniques.

Because of the small grain size, measurement of the principle indices of refraction could not be accomplished. However, an approximate refractive index of bulk amphibole was obtained (n = 1.620, Mg_6Fe_1; 1.632, Mg_5Fe_2; 1.644, Mg_4Fe_3; 1.660, Mg_3Fe_4; 1.674, Mg_2Fe_5; 1.690, Mg_1Fe_6). Estimation of the percentage amphibole in runs was based primarily on optical examination.

Optical and X-ray data are consistent with the presence of a single, homogeneous amphibole phase in all runs.

Synthesis Techniques

Because of possible partitioning of Fe and Mg between amphibole and other run products, unit cell parameters are reported only for runs which yielded greater than 95% amphibole. A number of different synthesis procedures were required to achieve these high yields.

Greenwood (1963) and Forbes (1971) have noted the difficulty of nucleation of the Mg and Fe end-members. However, this difficulty decreases for the intermediate compositions. The Mg_5Fe_2, Mg_4Fe_3, and Mg_3Fe_4 amphiboles were synthesized directly from oxide mixes plus excess H_2O to yields of greater than 95% at 2 kbar, f_{O_2} defined by the fayalite-magnetite-quartz (FMQ) buffer, and 750°, 700°, and 650°C, respectively. Compositions Mg_6Fe_1, Mg_2Fe_5, and Mg_1Fe_6 could not be directly synthesized. Nucleation of Mg_6Fe_1 was carried out by a method similar to that of Greenwood (1963). Initial crystallization of mix $+H_2O$ in silver capsules to talc + olivine at 650°C and 2 kbar was followed by reaction to talc +

olivine + cristobalite + orthopyroxene + amphibole at 820°C, 2 kbar, and a duration of one day. This assemblage + excess H_2O then produced yields of greater than 95% amphibole at 700°C, 2 kbar, and the FMQ buffer. The Mg_2Fe_5 and Mg_1Fe_6 amphiboles were synthesized by first crystallizing the mix $+H_2O$ at 700°C and 4-6 kbar for one week in silver capsules. This procedure yielded the assemblage: quartz + olivine + magnetite + amphibole $\pm$ pyroxene, which was then run with excess H_2O at 1 kbar and 600°C or 500°C, respectively, in the CH_4-C buffer system to complete the synthesis.

Run times necessary to produce yields of greater than 95% amphibole varied from 10 days in the case of Mg_5Fe_2 to 100 days for Mg_2Fe_5 and over 200 days for Mg_1Fe_6. Synthesis rates were increased by opening the capsules and redistributing the charge at intervals of 2-3 weeks.

Synthesis conditions are summarized in Table I-5.

Yields of about 50% amphibole have been achieved thus far for composition Mg_7 but the amphibole is not crystallized well enough to allow unit cell parameters to be determined. Although a number of different techniques have been used in attempting to synthesize the Fe end-member, yields of greater than 5% have not been realized. However, nucleation appears best for the well ground "reduced" mix at 4-6 kbar.

Amphiboles for which unit cell parameters are reported were synthesized at the FMQ buffer (except Mg_2Fe_5 and Mg_1Fe_6 as explained above). However, annealing at lower oxygen fugacities of the CH_4-C buffer (temperatures of synthesis, 1 kbar) produced no change in unit cell parameters (Table I-1). This is consistent with the results of Seifert and Virgo (1974) whose Mossbauer spectral studies detected no Fe^{3+} in a natural anthophyllite of approximate composition Mg_5Fe_2 annealed for

4 days at FMQ and 720°C. The effect of higher oxygen fugacity on unit cell parameters and on the stability of the amphiboles is discussed below and in Part II.

Determination of Crystal System

The amphiboles synthesized in this study cannot be characterized as monoclinic or orthorhombic on the basis of X-ray powder patterns alone. The method discussed by Cameron (1975) for distinguishing between cummingtonite and anthophyllite on the basis of the monoclinic 131 reflection at approximately 26°2θ CuK_{α} has not been found applicable. As discussed by Cameron, the monoclinic 131 peak may be overlapped by several minor anthophyllite peaks. A minor peak at 26°2θ is present in the synthetic amphibole patterns of this study but the distinction as to type of reflection cannot be made. All major peaks in the X-ray patterns can be indexed as either monoclinic or orthorhombic, and least-squares unit cell refinement gives equivalent standard errors.

Although grain size (10-15μ × 1-2μ average) is too small for single crystal X-ray studies, multi-crystal masses were mounted on a spindle stage and examined optically. Extinction angles for individual crystals within these larger masses could be determined. Parallel extinction resulted on all orientations observed, and on this basis, the amphiboles are assumed to be orthorhombic. Klein (1964) reported values of $Z \wedge c$ of 13°-20° for naturally occurring low-Ca cummingtonite-grunerites in the composition range 60-90 mole % Fe end-member. Rice *et al.* (1974) gave $Z \wedge c$ of 14°-15° for a natural magnesiocummingtonite of approximately 14

mole % Fe end-member. Amphiboles synthesized in this study have a composition range from 14-86 mole % Fe end-member.

Experimental Results

Unit cell parameters of the synthetic amphiboles are given in Table I-1, and are plotted against composition in Figures I-1 and I-2. The peaks listed in Table I-3 along with the 210 peak at approximately 10.7°2θ were used in the least squares refinement. The *c* dimension is based only on one reflection, 053, but a minor peak indexed as 202 at approximately 35°2θ was measurable in a number of the patterns; inclusion of this peak in the refinements did not significantly change the unit cell parameters. The data were refined assuming the anthophyllite space group *Pnma*. As a check for reproducibility, values were obtained from three independent synthesis runs for Mg_5Fe_2, and from two independent runs for the other compositions up to Mg_2Fe_5. In Figures I-1 and I-2 the error bars shown on the upper left represent typical one standard error values as given by the least squares refinement. Parameters for the Mg end-member are from Greenwood (1963) (Δ) and Cameron (1975) (●). Cameron re-indexed several of the high angle 2θ peaks reported by Greenwood and re-refined the data using Greenwood's 2θ values.

Curves relating individual unit cell parameters to composition were obtained by regression analysis using the Statistical Analysis System computer program designed by Barr and Goodnight (1972) which weights observations as 1/(standard error). Equations of first through fourth order were fit to the data assuming one, and then two, standard errors as given in Table I-1. The significance of the fits was determined by a t-test assuming $|t| = 2.0$ to be significant. Using one standard error weighting, fits of second or third order were obtained for all unit cell parameters.

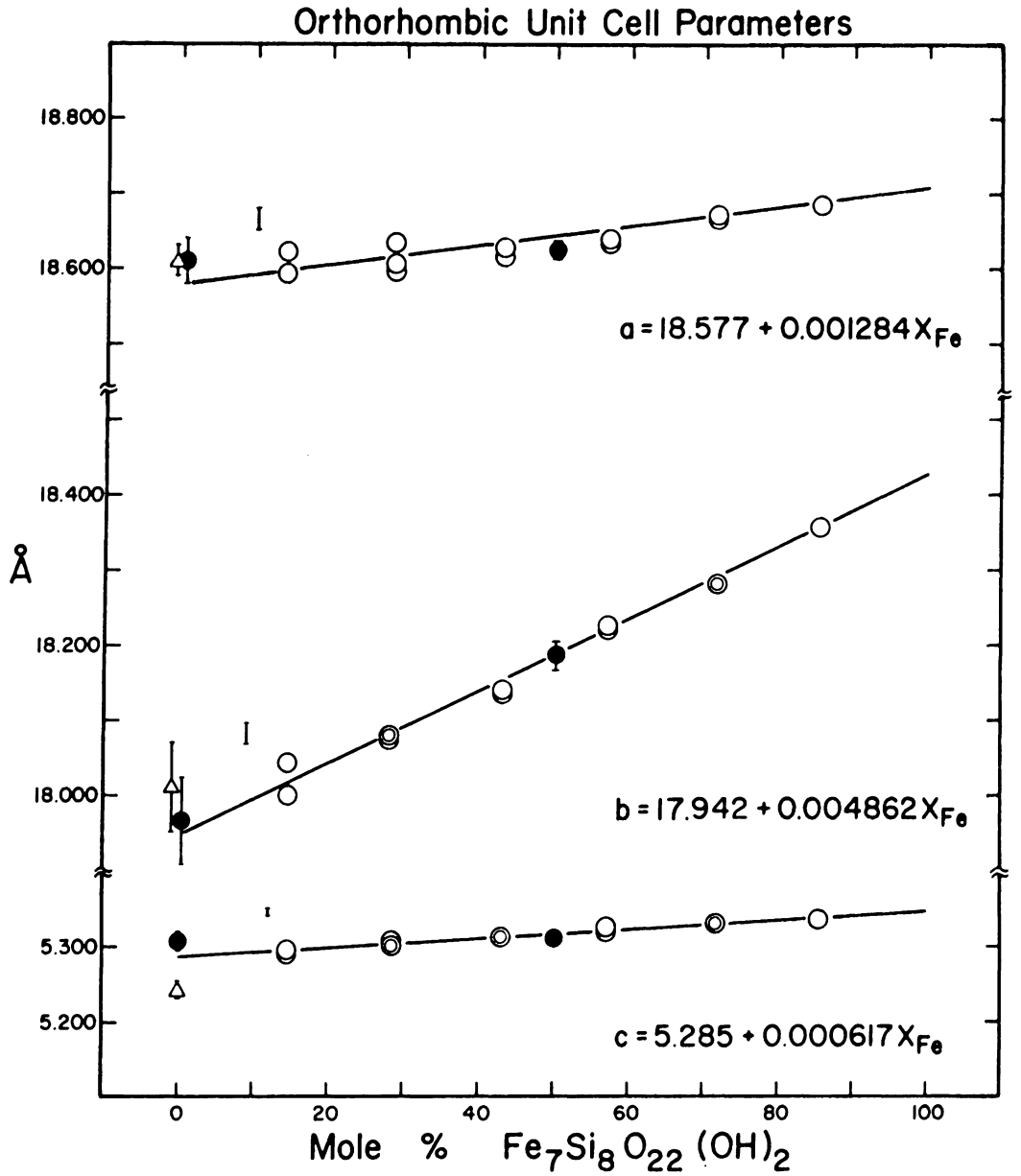

Figure I-1. Unit cell parameters of synthetic orthorhombic amphiboles. Open circles: This study. Double circles indicate identical values. Triangles: Greenwood (1963). Solid circles: Cameron (1975). Error bars at upper left indicate typical one standard error values. X_{Fe} = mole % Fe end-member.

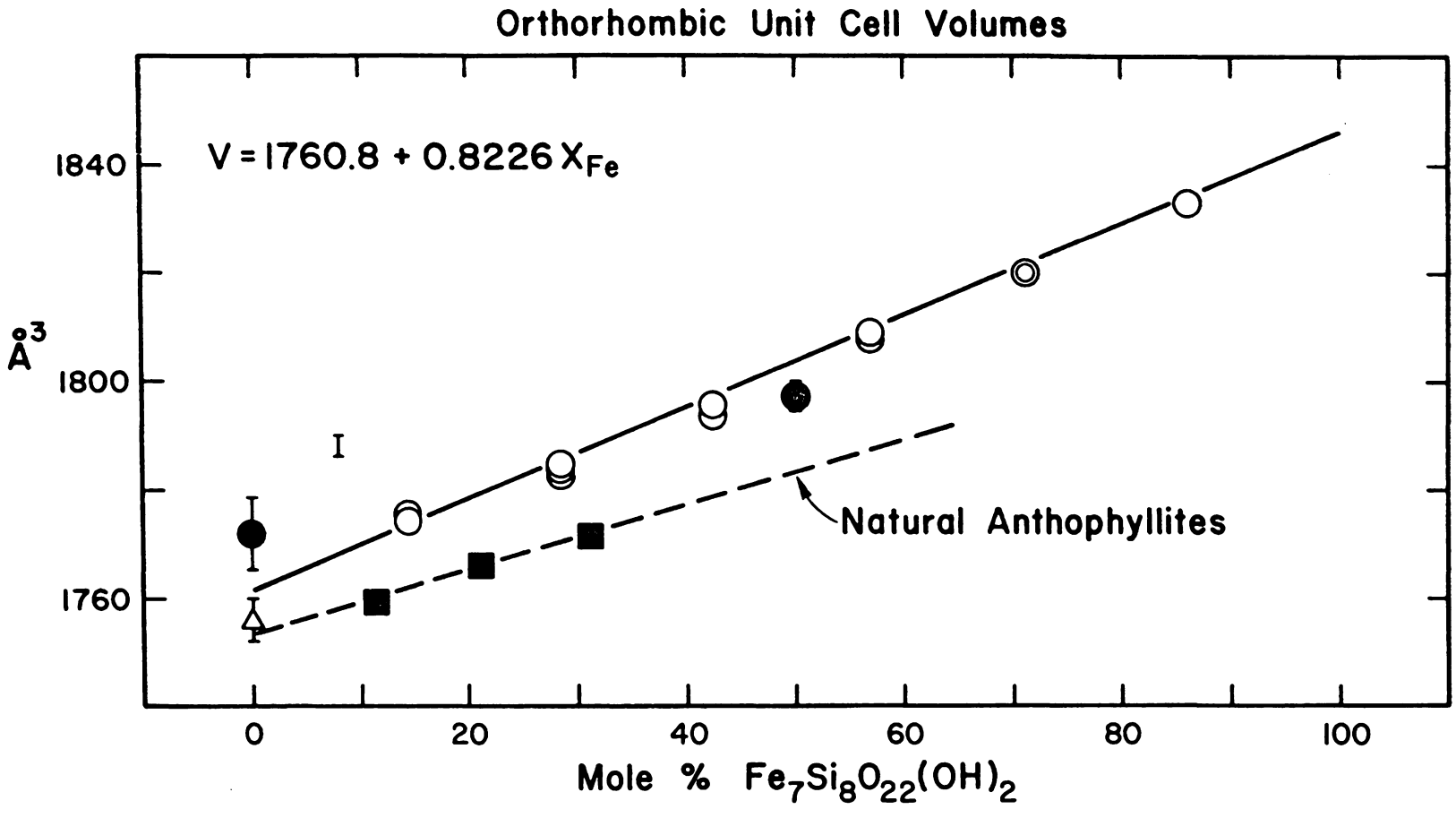

Figure I-2. Orthorhombic unit cell volumes of synthetic amphiboles. Symbols as in Fig. I-1. Solid squares: natural anthophyllites (Finger, 1970).

TABLE I-1. Orthorhombic Unit Cell Parameters
(Refined as Space Group *Pnma*)

Run #	Comp.	Mole % Fe_7	a(Å)	b	b(Å)	c(Å)	V(Å^3)
			Synthesized at FMQ				
145	Mg_6Fe_1	14.3	18.592(10)		18.045(10)	5.292(4)	1775.4(1.7)
290	Mg_6Fe_1	14.3	18.622(8)		17.999(14)	5.295(2)	1774.9(1.2)
26	Mg_5Fe_2	28.6	18.604(15)		18.088(10)	5.299(4)	1783.4(2.0)
68	Mg_5Fe_2	28.6	18.634(20)		18.077(11)	5.298(4)	1784.6(2.4)
125	Mg_5Fe_2	28.6	18.594(8)		18.078(5)	5.301(2)	1781.9(1.0)
82	Mg_4Fe_3	42.9	18.626(13)		18.139(9)	5.313(3)	1795.0(1.6)
149	Mg_4Fe_3	42.9	18.613(10)		18.136(7)	5.313(3)	1793.4(1.3)
80	Mg_3Fe_4	57.1	18.638(10)		18.227(7)	5.325(2)	1809.0(1.3)
150	Mg_3Fe_4	57.1	18.635(18)		18.223(12)	5.326(5)	1808.5(2.4)
			Synthesized at CH_4-C				
140	Mg_2Fe_5	71.4	18.669(11)		18.291(8)	5.329(3)	1819.8(1.5)
226	Mg_2Fe_5	71.4	18.672(3)		18.290(2)	5.329(1)	1819.8(0.4)
453	Mg_1Fe_6	85.7	18.686(7)		18.358(20)	5.336(2)	1830.3(1.3)
			Synthesized at FMQ and Annealed at CH_4-C				
178	Mg_4Fe_3	42.9	18.612(11)		18.141(8)	5.311(3)	1793.2(1.4)
177	Mg_3Fe_4	57.1	18.643(9)		18.222(6)	5.325(2)	1808.9(1.2)

Numbers in parentheses represent 1 standard error as given by the least squares refinement.

However, only first order (straight line) equations were significant when weighting of two standard errors was employed. Gibbs and Louisnathan (1971) estimated that in order for the standard error reported in least squares refinement to be a good estimate of that of the true population, the number of observations (m) should be at least ten times as large as the degrees of freedom (n). In the case where $m < 10n$, they recommend doubling the least squares standard error before applying statistical tests. Since $n = 3$ for the orthorhombic system and only 8-10 observations were used in the refinements, the fits obtained using two standard errors are preferred. Equations relating unit cell parameters to mole % of the Fe end-member (X_{Fe}) with the intercept and slope errors indicated in parentheses are:

$$a(\text{Å}) = 18.577(12) + 0.001284(190)\ X_{Fe}$$
$$b(\text{Å}) = 17.942(11) + 0.004862(170)\ X_{Fe}$$
$$c(\text{Å}) = 5.285(3) + 0.000617(50)\ X_{Fe}$$
$$V(\text{Å}) = 1760.8(1.7) + 0.8226(280)\ X_{Fe}$$

The straight line plot of unit cell volume vs. composition indicates the absence of a volume of mixing term as far as can be determined by X-ray powder diffraction.

Figure I-2 shows unit cell volumes refined on the anthophyllite space group (solid line), along with the values of Greenwood (Δ) (1963) and Cameron (●) (1975). The squares (■) are unit cell volumes of natural Al^{3+}-poor anthophyllites from Johansson (1930), Lindemann (1964), and Finger (1970). The dashed curve is a straight line fit to the three natural amphiboles. Finger (1970) noted the difference in molar volumes between these natural

anthophyllites and the cummingtonite-grunerite series of Klein and Waldbaum (1967). However, the synthetic, optically orthorhombic forms have molar volumes (Fig. I-3) that agree with those of the natural monoclinic rather than orthorhombic forms. Seifert (pers. comm., 1974) reports that the molar volume of a Mg_5Fe_2 form which he synthesized is consistent with the curve of Klein and Waldbaum (1967). In addition, the unit cell volume of $Mg_{3.5}Fe_{3.5}$ (Cameron, 1975), refined as *Pnma*, lies on the curve reported here within two standard errors reported by Cameron (see Figs. I-1 and I-2 of this study). Both of these amphiboles were also synthesized at the FMQ buffer.

Three possibilities can be evoked to explain the molar volume discrepancies: (1) order-disorder of Mg and Fe within the cation sites; (2) small amounts of Al^{3+} in the natural anthophyllites; (3) the synthetic amphiboles are orthorhombic but have not crystallized in the anthophyllite structure type.

Order-disorder apparently cannot account for the volume discrepancy. Seifert and Virgo (1974) have determined by Mossbauer spectra that equilibrium Fe-Mg distributions in the natural anthophyllite specimen of Finger (1970) are achieved in several days at 600°C and above, the temperature range utilized here. Seifert (pers. comm., 1974) also reports that the increase in unit cell volume accompanying disordering is too small to account for the observed difference. In support of this conclusion, an amphibole of composition Mg_5Fe_2 synthesized at 750°C, 2 kbar, and the FMQ buffer was annealed at 500°C, 2 kbar, and the FMQ buffer for two weeks. Unit cell parameters of the 500° sample (a = 18.594(5),

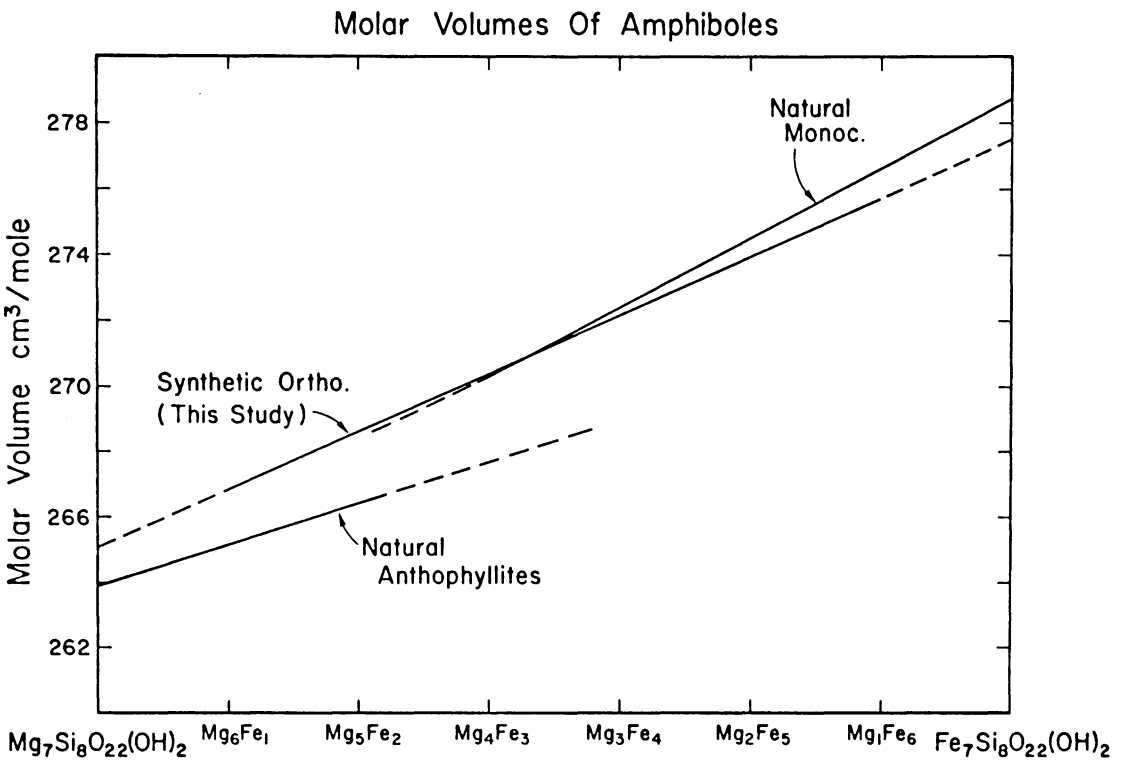

Figure I-3. Molar volumes of amphiboles. Curves represent synthetic orthorhombic forms (this study), natural monoclinic cummingtonites-grunerites (Klein and Waldbaum, 1967), and natural anthophyllites (Finger, 1970). Range of composition is shown by solid lines.

b = 18.078(4), c = 5.299(2), V = 1781.1(.7)) are not statistically different from the 750°C data (Table I-1).

Seifert (pers. comm., 1974) also reports that on the basis of his present studies on the join between Mg_5Fe_2 and Na-gedrite of composition, $Na_{0.5}Fe_2^{2+}Mg_{3.5}Al_{1.5}[Si_6Al_2...]$, the small amount of Al^{3+} in the natural anthophyllites plotted in Figures I-2 and I-3 cannot have a large enough effect to account for the observed volume difference.

In consideration of the third possibility, a brief discussion of the basic amphibole structure is helpful. Only those details relevant to the determination of the structure type are discussed. For background, the reader is referred to references cited in the Introduction and to diagrams such as that of Ernst (1968, Fig. 1, p. 5).

The amphibole structure consists of double chains of tetrahedra extending parallel to the c axis and interlocking to form sheets parallel to (100). These sheets are bound together by cations coordinated by apical oxygen and hydroxyl anions of adjacent sheets in a manner which requires a stagger of $\sim \pm c/3$ between adjacent tetrahedral chains. Two different types of tetrahedral chains have been identified in the amphibole structures solved to date. The tetrahedra in the A-chain form hexagonal rings, while those of the more distorted B-chain form ditrigonal rings. The B chain can be roughly approximated by a close-packing of oxygens and thus would theoretically be expected to occupy a smaller volume than the A chains.

The known amphibole structure types can be distinguished by the sequence of stacking vectors ($\pm c/3$) in the a^* direction and chain type.

Table I-2 summarizes the known structure types and gives the approximate a unit cell dimension.

In an attempt to determine the likelihood of hypothesis (3), electron diffraction patterns of a synthetic amphibole (Mg_5Fe_2) and a natural anthophyllite were obtained by G. L. Nord using the transmission electron microscope facilities at the U. S. Geological Survey, Reston, Virginia. Nord, M. Ross, also of the USGS, and G. V. Gibbs of VPI & SU aided in the interpretation of the diffraction patterns. L. Finger of the Geophysical Laboratory, Washington, D. C. provided a natural anthophyllite from the Minnesota River Valley (M14104) as well as a listing of observed X-ray structure factors from his (1970) refinement of the anthophyllite structure.

Figures I-4 and I-5 are $h0\ell$ electron diffraction patterns of synthetic amphibole Mg_5Fe_2 and natural anthophyllite, respectively, with the a^* and c^* directions and reciprocal unit repeat distances indicated. Figure I-6 is a graphic $h0\ell$ plot of the observed X-ray structure factors of natural anthophyllite.

A repeat of approximately 18.6 Å in the a^* direction, as well as an alternating ℓ-even = strong, ℓ-odd = weak distribution of intensities is observed in all three patterns. Fair agreement of the more detailed features exists between the electron and X-ray patterns of the anthophyllites. However, both are unlike the synthetic amphibole. The strong enhancement of every fourth intensity in the a^* direction suggests the presence of a $\sim$4.7 Å subcell within the synthetic structure which is not present in anthophyllite. Streaking in the a^* direction similar to that in Figure I-4 was observed in X-ray precession photographs of proto-

TABLE I-2. Comparison of Known Amphibole Structure Types

	Monoclinic $C2/m$	Monoclinic $P2_1/m$	Protoamphibole *Pnmn*	Anthophyllite *Pnma*
Stacking sequence in a^* direction	(+c/3) (+c/3)	(+c/3) (+c/3)	(+c/3) (-c/3)	(+c/3) (+c/3) (-c/3) (-c/3)
Chain types	A A	A B	A A	A B A B
a(Å)	∿9.5	∿9.5	∿9.5	∿18.6

Figure I-4. $h0\ell$ electron diffraction photograph of synthetic amphibole $Mg_5Fe_2Si_8O_{22}(OH)_2$. a^* and c^* directions and reciprocal distances representing 18.6 Å and 5.3 Å unit repeats are indicated.

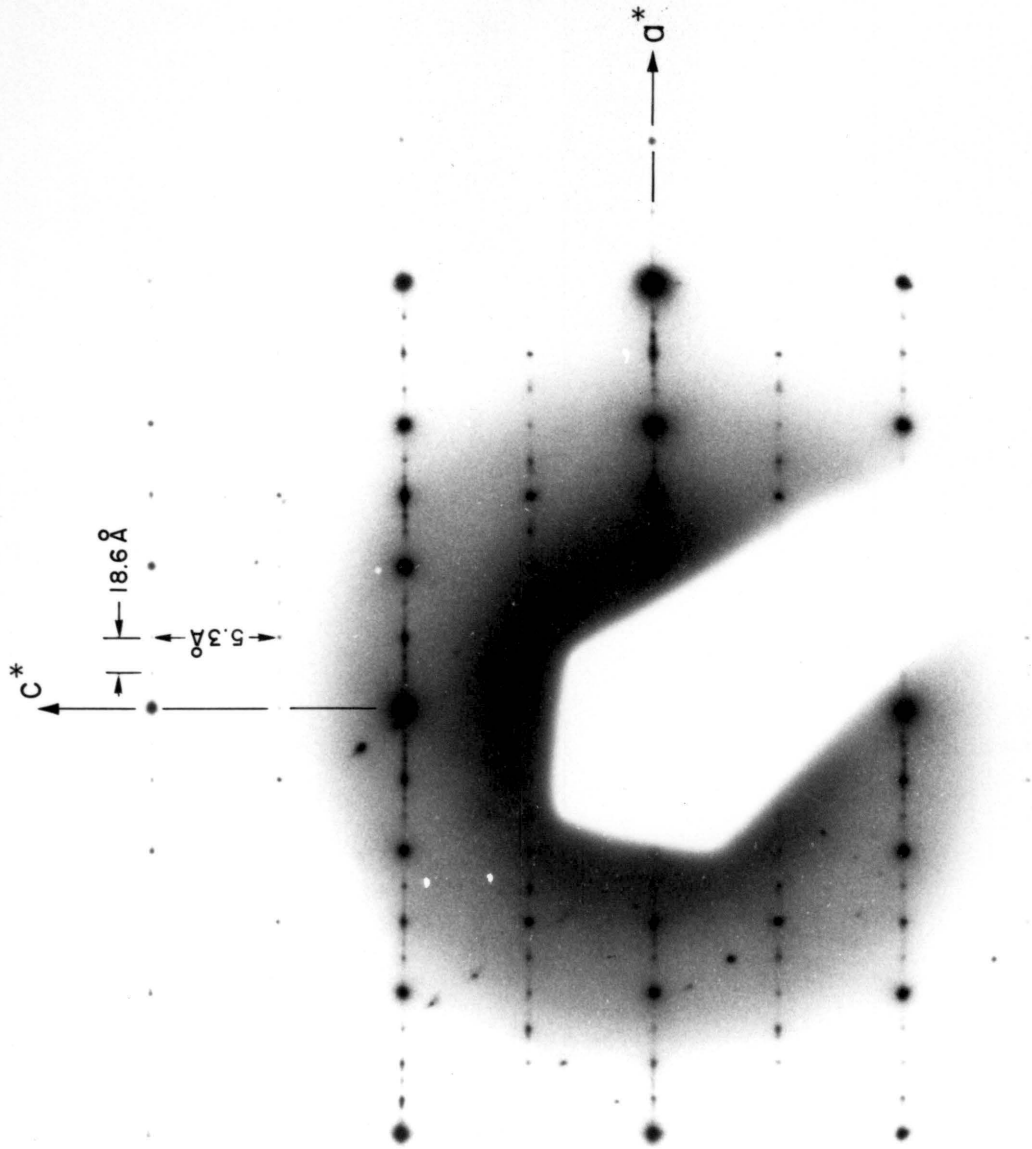
a*
18.6 Å
5.3Å
c*

Figure I-5. $h0\ell$ electron diffraction photograph of natural anthophyllite (Finger sample M14104). Symbols as in Figure I-4.

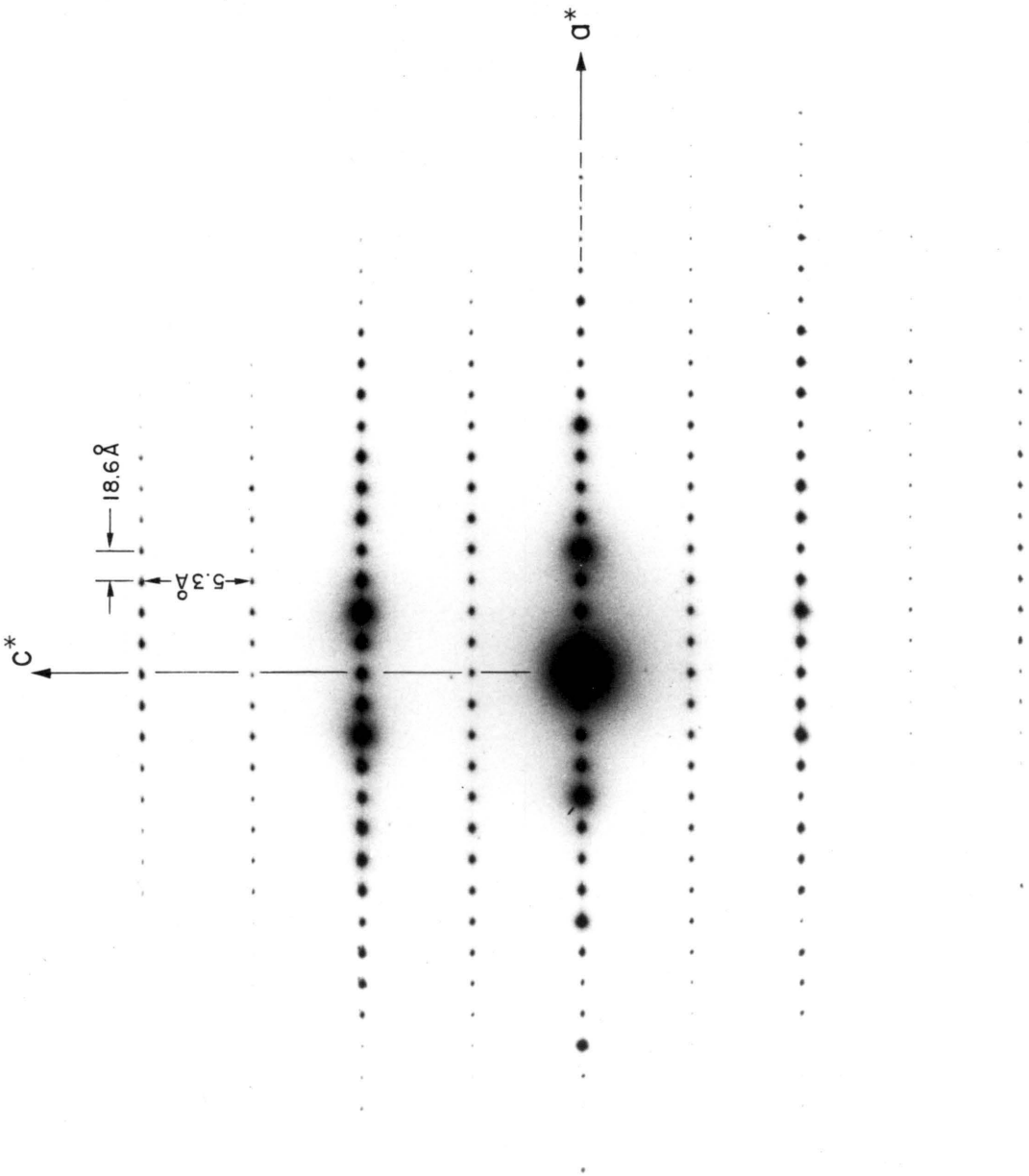
a*
18.6 Å
5.3 Å°
c*

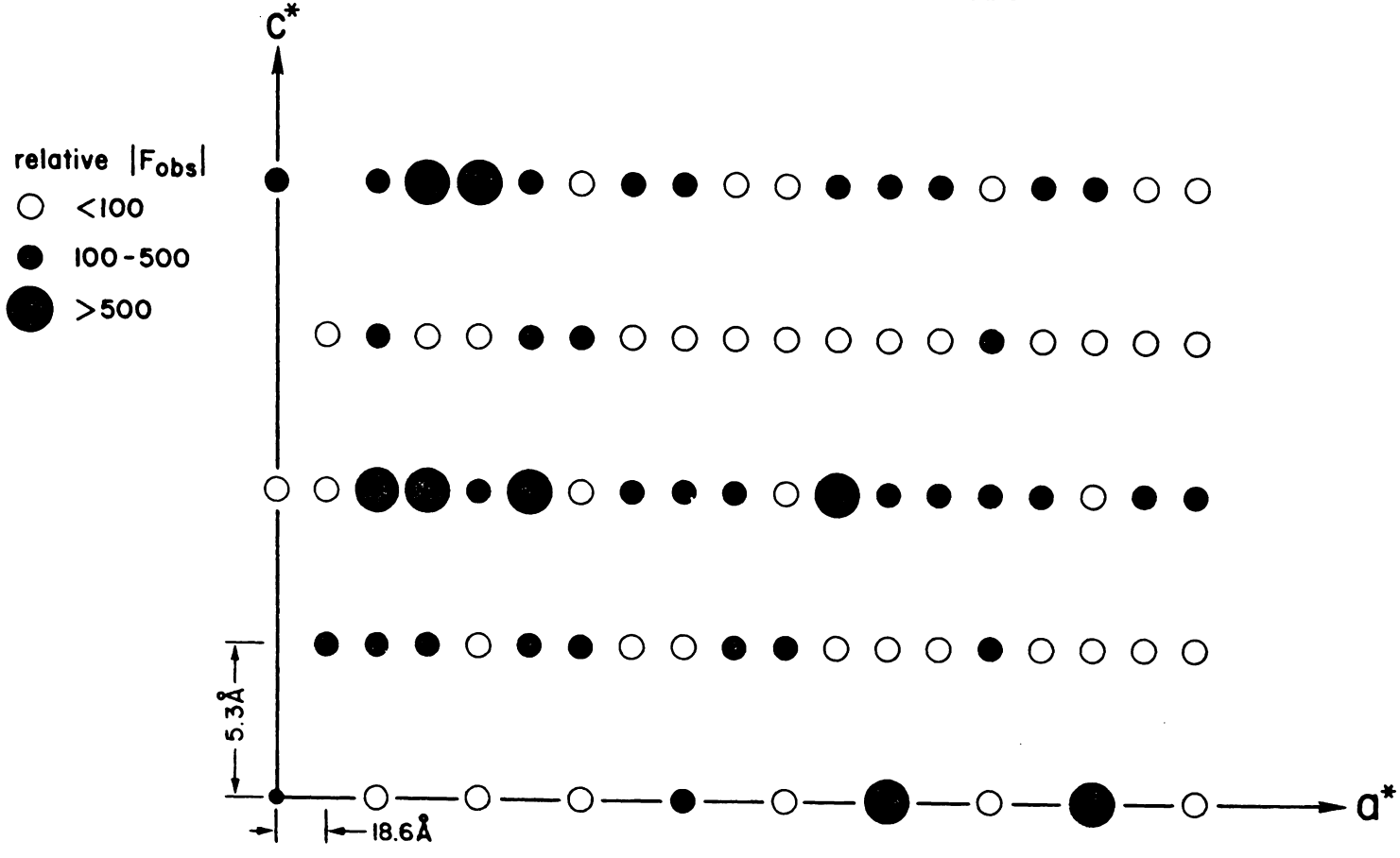

Figure I-6. Relative observed $h0\ell$ X-ray structure factors of the natural anthophyllite of Finger (1970).

amphibole by Gibbs (1969) and interpreted as indicating large numbers of stacking faults in the a^* direction.

From Figures I-4, I-5, I-6 and Table I-2, certain structure types can be rejected as inapplicable to these synthetic amphiboles. The electron diffraction patterns indicate that the synthetic amphiboles have not crystallized with the anthophyllite structure. Protoamphibole, which was originally considered a likely candidate because it has orthorhombic symmetry but contains only the larger A-type chains, is rejected because of its ∿9.5 Å a repeat. The $C2/m$ and $P2_1m$ structures are rejected because of both their ∿9.5 a unit cell repeat and monoclinic symmetry. Comparison with the appropriate X-ray precession photographs indicates that while twinned monoclinic amphiboles could produce additional reflections along a^*, they would not be likely to produce a regular 18.6 Å repeat such as that observed. M. Ross (pers. comm., 1975) has observed that epitaxial growth of talc (a = 5.3 Å, b = 9.2 Å, c = 18.9 Å) on natural anthophyllite can produce subcell reflections in X-ray precession photographs. Although talc and the subcell reflections in Figure I-4 show metric similarities, distribution of the intensities is unlike that of talc. In addition, the synthetic amphibole of Figure I-4 was obtained from a run that yielded essentially all (99+%) amphibole.

Thus it is concluded that the amphibole synthesized in this study has a structure type unlike any known amphibole. The structure has orthorhombic symmetry and approximate unit cell parameters a = ∿18.6 Å, b = ∿18.0 Å, c = ∿5.3 Å (composition Mg_5Fe_2). Its larger molar volume as compared to anthophyllite may indicate that it consists of only the larger A-type chains.

Relationship Between Composition and X-ray Powder Pattern

One of the goals of this study was to obtain a method of estimating accurate amphibole compositions from as few X-ray measurements as possible. Linear regression analysis of peak locations ($2\theta CuK_{\alpha}$) vs. composition was carried out for each reflection used in the least squares refinement of cell parameters. The 210 peak at approximately 10.7°2θ was not used because of the small shift in 2θ with interplanar spacing at low angles. From the equations in Table I-3 various individual peaks and combinations of peaks were tested for their accuracy in predicting compositions of the synthetic amphiboles of known composition. The results are shown in Table I-4. In the case where a combination of peaks was used the compositions given by the individual peaks were averaged to give the estimate of composition (e.g., in Table I-4, column 5, the composition given by the 040 peak, the 420 peak, and the 440 peak were averaged to give a final composition). The selection of combinations of peaks was based on their proximity on the X-ray powder pattern so as to provide the smallest 2θ range to be scanned.

In general, composition can be determined to within approximately 3-4 mole % Fe end-member. However, the maximum error encountered using the 440, 610 combination (9.4 mole % Fe end-member) is too large to be of practical use in estimating compositions. The other methods have maximum errors ranging from 3.2-5.6 mole %, representing the maximum error expected in estimating composition of any single unknown. It should be noted that there is a considerable range in the relative intensities of the peaks listed in Table I-3. The 610 and 440 peaks have by far the

TABLE I-3. Equations Relating Location of Major Peaks (2θ CuKα) to Amphibole Composition*

040:	$2\theta = 19.784 - 0.0052\ X_{Fe}$	$r = 0.9935$
420:	$2\theta = 21.559 - 0.0028\ X_{Fe}$	$r = 0.9815$
440:	$2\theta = 27.648 - 0.0047\ X_{Fe}$	$r = 0.9891$
610:	$2\theta = 29.261 - 0.0022\ X_{Fe}$	$r = 0.9338$
630:	$2\theta = 32.628 - 0.0040\ X_{Fe}$	$r = 0.9611$
2110:	$2\theta = 57.300 - 0.0154\ X_{Fe}$	$r = 0.9909$
053:	$2\theta = 58.379 - 0.0100\ X_{Fe}$	$r = 0.9899$

*X_{Fe} = mole % Fe end-member, r = correlation coefficient

TABLE I-4. Compositions Predicted from Various Combinations of Peaks

Run #	Composition of Mix (Mole % Fe_7)	040 440	420 440	040 420 440	440	440 610	2110 053
	X_{real}			$X_{observed}$			
145	14.3	17.5	17.8	17.4	18.5	19.0	18.0
290	14.3	13.9	19.1	18.8	18.1	22.7	-*
26	28.6	29.8	29.0	29.3	29.8	28.8	27.9
125	28.6	24.6	23.8	24.6	23.0	19.2	27.2
68	28.6	29.1	29.9	29.8	28.3	32.8	25.5
82	42.9	42.2	43.4	43.0	42.1	41.7	41.5
149	42.9	40.5	40.5	40.0	39.4	36.1	41.1
150	57.1	56.4	59.5	58.2	57.2	58.8	59.8
80	57.1	56.7	55.6	55.5	58.0	57.0	60.0
140	71.4	71.8	73.4	73.8	68.9	68.8	70.8
226	71.4	72.7	71.2	71.3	73.8	74.4	73.6
453	8.57	-	84.9	-	87.7	85.7	-
$\frac{\Sigma\lvert X_{real}-X_{obs}\rvert}{N}$		1.6	2.2	2.0	2.5	3.5	2.0
$\lvert X_{real}-X_{obs}\rvert_{max}$		3.2	4.8	4.5	5.6	9.4	3.7

**Entry left blank indicates peak not measurable in powder pattern.*

TABLE I-5. Run Summaries

Run #	Comp.	T(°C)	P(kbar)	Buffer	Dur(days)*	Run Products**
145	Mg_6Fe_1	650	2	none	2	T+Ol
		815	2	none	1	A(20)+T+Ol+C+Q+P
		700	2	FMQ	61(1)	A(99)+P+Q
290	Mg_6Fe_1	650	2	none	1	T+Ol
		820	2	none	1	A(20)+Px+Q+Ol
		700	2	FMQ	44(2)	A(99)+Px+Q
68	Mg_5Fe_2	750	2	FMQ	23	A(100)
26	Mg_5Fe_2	700	2	FMQ	7	A(50)+T+Ol
		750	2	FMQ	10	A(100)
125	Mg_5Fe_2	750	2	FMQ	30	A(100)
82	Mg_4Fe_3	700	2	FMQ	35(1)	A(98)+Q+Ol
149	Mg_4Fe_3	700	2	FMQ	45(1)	A(98)+Q+Ol
80	Mg_3Fe_4	700	2	FMQ	19	A(50)+Q+Ol
		650	2	FMQ	17	A(99)+Q+Ol
150	Mg_3Fe_4	650	2	FMQ	51(1)	A(99)+Q+Ol
140	Mg_2Fe_5	700	4	none	26	A(40)+Q+Ol
		600	1	CH_4-C	102(3)	A(95)+Q+Ol
226	Mg_2Fe_5	700	4	none	6	A(5)+Q+Ol+K
		600	1	CH_4-C	101(5)	A(99)+Q+Ol
486	Mg_1Fe_6	700	6	none	12	A(5)+Q+Ol+P
		600	1	CH_4-C	63(2)	A(30)+Q+Ol+P+M
		550	1	CH_4-C	105(3)	A(60)+Q+Ol+M
		500	1	CH_4-C	35	A(98)+Q+Ol
178	Mg_4Fe_3	700	2	FMQ	35(1)	A(98)+Q+Ol
		700	1	CH_4-C	14	A(98+Q+Ol
177	Mg_3Fe_4	700	2	FMQ	19	A(50)+Q+Ol
		650	2	FMQ	17	A(99)+Q+Ol
		650	1	CH_4-C	14	A(99)+Q+Ol

Number in parentheses indicates number of times capsule was opened and charge examined optically and with X-ray methods.

**Starting material for first run of each series was oxide mix + H_2O. Numbers in parentheses indicate % amphibole in charge. Abbreviations: A - amphibole, K - keatite, M - magnetite, Ol - olivine, P - orthopyroxene, T - talc, C - cristobalite.*

largest relative intensities in the X-ray pattern. The 440 peak is distinguishable in X-ray patterns containing as little as 10-20% amphibole. Thus compositions on the join should be determinable to at worst 5-6 mole %, even in samples containing small percentages of amphibole.

Effect of Oxygen Fugacity on X-ray Determinative Curves

It was important to determine the effect, if any, of f_{O_2} on the X-ray determinative curves for amphibole composition. Accordingly, amphiboles synthesized at one buffer (generally FMQ) were annealed at oxygen fugacities defined by different buffers for periods of at least two weeks. Cell parameters of the annealed amphiboles were then determined in the same manner as described above.

Some difficulties were encountered using the NNO solid buffer. Runs of amphibole + H_2O were carried out at 2 kbar and temperatures in the range of 600°-750°C in platinum capsules. After runs, the charges consisted of Mg-enriched amphibole and up to 20% quartz but no additional Fe-containing phases. Following removal of the charge, the capsules were observed to be magnetic and thus it was apparent that loss of iron from charge to capsule had occurred. In support of this conclusion, it was noted that the amount of quartz (i.e., amount of iron lost to the capsule) increased with run temperature. Therefore, an attempt to determine the effect of f_{O_2} at NNO buffer on unit cell parameters was carried out in Shaw apparatus (Shaw, 1967) at 1 kbar total pressure. At the low f_{H_2} equivalent to the NNO buffer, accurate control of P_{H_2} and diffusion rates across the Pt membrane posed some problems resulting in an f_{H_2} of 7 ± 2 kbar. For comparison, Eugster and Skippen (1967) gave a value of f_{H_2} =

4.5 bar at 700°, 1 kbar for the assemblage Ni-NiO-H_2O and a value of f_{H_2} = 12.8 bar at 700°C, 1 kbar was calculated for the assemblage FMQ-H_2O from the data of Wones and Gilbert (1969), Burnham *et al.* (1969), and the JANAF Tables (1971). Thus even if f_{O_2} was at values lower than that of the NNO buffer, it still was considerably higher than that of the FMQ buffer.

Table I-6 summarizes unit cell parameters of runs made at various oxygen fugacities. Statistically no differences in unit cell parameters of the amphiboles as a function of f_{O_2} exist. This result is somewhat surprising since variation of unit cell parameters with f_{O_2} and temperature has been reported for a number of hydroxy-silicates (e.g., biotite: Eugster and Wones, 1962; ferrotremolite: Ernst, 1966). This variation is generally attributed to the solution of oxy-silicates (e.g., oxy-amphibole) by the reaction $Fe^{2+} + OH^- \rightarrow Fe^{3+} + O^{2-} + H$. Substitution of the smaller Fe^{3+} ions has the effect of decreasing unit cell parameters. In Mossbauer spectral studies, Seifert and Virgo (1974) were unable to detect Fe^{3+} in the structure of an amphibole of approximate composition Mg_5Fe_2 annealed at 720°C and the FMQ buffer for four days. In light of this result, annealing at f_{O_2} lower than the FMQ buffer would not be expected to produce any changes in unit cell parameters attributed to variation of Fe^{3+}/Fe^{2+} ratio. The amount of solid solution of oxy-amphibole should be greater at f_{O_2} defined by MH buffer. However, only very Mg-rich amphiboles are stable at these higher oxygen fugacities and the total iron content may not be large enough for the unit cell parameters to reflect any change. It is thus concluded that oxy-amphibole, if present, cannot be detected by changes in unit cell parameters as measured in this study.

TABLE I-6. Unit Cell Parameters for Amphiboles Annealed at Various f_{O_2} (All Runs had a Duration of at Least Two Weeks)

T(°C)	P(kbar)	Buffer	a(Å)	b(Å)	c(Å)	V(Å^3)
			Mg_6Fe_1			
700	2.0	H-M	18.610(12)	18.007(12)	5.291(2)	1773.3(1.3)
650	2.0	H-M	18.584(17)	18.017(5)	5.291(2)	1771.8(1.0)
700	2.0	FMQ*	18.607(9)	18.022(12)	5.293(2)	1775.0(1.7)
			Mg_4Fe_3			
700	1.0	CH_4-C	18.612(11)	18.141(8)	5.311(3)	1793.2(1.4)
700	1.0	Shaw**	18.624(12)	18.136(8)	5.311(3)	1794.0(1.5)
700	2.0	FMQ*	18.620(11)	18.138(8)	5.313(3)	1794.2(1.5)
			Mg_3Fe_4			
650	1.0	CH_4-C	18.643(9)	18.222(6)	5.325(2)	1808.9(1.2)
650	2.0	FMQ*	18.637(12)	18.225(10)	5.326(3)	1808.8(1.9)

**FMQ value denotes average of determinations on two separate runs.*

***f_{H_2} = 7 ± 2 bars; f_{H_2} of FMQ = 12.8 bars; f_{H_2} of N-NO = 4.5 bars.*

Based on the above discussion, the X-ray determinative curves are assumed to be applicable, without correction, over the range of temperature and f_{O_2} of this study.

Part II: Stability of Fe-Mg Amphiboles with Respect to Oxygen Fugacity

Introduction

Part II concerns the stability of amphiboles on the join $Mg_7Si_8O_{22}(OH)_2$-$Fe_7Si_8O_{22}(OH)_2$. Previous experimental work on this join is limited. Studies of the Mg and Fe end-members (Greenwood, 1963; Forbes, 1971) and the early reconnaissance study of Boyd (1955) were discussed in Part I. Hinrichsen (1967) synthesized orthorhombic amphiboles on the join at P_{H_2O} = 1 kbar, 500° - 700°C and at f_{O_2} purportedly defined by the iron-wustite (IW) and iron-magnetite (IM) buffers. His T-X phase diagram, although stated to be based upon reversed experiments, cannot be directly evaluated and appears to be based on synthesis experiments. Recently, Cameron (1975) determined the upper thermal stability of an intermediate orthorhombic amphibole of 50 mole % Fe end-member.

Several studies, while not restricted chemically to only the Fe-Mg amphiboles, presented results relevant to amphiboles on the join. Cameron (1975) investigated the join $Mg_{3.5}Fe_{3.5}Si_8O_{22}(OH)_2$-$Ca_2Mg_{2.5}Fe_{2.5}Si_8O_{22}(OH)_2$ at P_{H_2O} = 2 kbar, f_{O_2} defined by the FMQ buffer, and 500°-800°C. Schurmann (1974) has investigated the joins: ferrotremolite-grunerite; and $ferrotremolite_{50}$ $grunerite_{50}$-$tremolite_{50}$ $anthophyllite_{50}$ in the range P_{H_2O} = 1-6 kbar, 450°-700°C, and f_{O_2} defined by the IW and IM buffers.

Despite the results of the above mentioned studies, phase relations of the Fe-Mg amphiboles are still poorly understood. This section describes the results of a hydrothermal investigation of the phase relations of amphiboles on the join at P_{H_2O} = 2 kbar, in the temperature range 600°-700°C, and a range of oxygen fugacities defined by the MH, NNO, and FMQ buffers.

Experimental Methods

Starting materials for runs consisted of: (a) Amphiboles: synthesized to yields of >95% as described in Part I. (b) Magnetite + SiO_2 glass: mixed together in appropriate amounts to yield the pure iron end-member amphibole. Magnetite was synthesized from reagent grade amorphous Fe_3O_4 at 700°C, 2 kbar in Au capsules. (c) Products of previous runs.

Solid starting materials plus a measured amount of distilled H_2O were sealed into $Ag_{70}Pd_{30}$ capsules, or into Pt capsules when the Ni-NiO buffer was employed. These capsules were then sealed into large Au capsules along with the appropriate solid buffer assemblage plus H_2O, or were loaded directly into bombs when the CH_4-C buffering apparatus was used.

Runs were carried out in hydrothermal and CH_4-C buffering vessels described in Part I. Temperature fluctuations of $\pm 3°$ and pressure variations of ± 20 bar were typical.

The solid buffer technique of Eugster (Huebner, 1971) was used to define f_{O_2} at the magnetite-hematite (MH), nickel-nickel oxide (NNO) and fayalite-magnetite-quartz (FMQ) buffers. Buffering at methane-graphite (CH_4-C) was accomplished in the system described above and in Part I. All runs were checked for the presence of H_2O in the inner and outer capsules (where used) upon opening. All buffers were checked by either optical or X-ray methods.

Phase Identification and Characterization

Run products were examined with the petrographic microscope and by X-ray powder diffraction using a Norelco (Ni-filtered CuK_α radiation) diffractometer equipped with a graphite monochromator.

Amphiboles occurred as needle-like grains averaging 1-2μ by 10-15μ often intergrown as fibrous masses. Compositions were determined by the X-ray method described in Part I. X-ray scans for compositional determination were run at 1/2°2θ/min using synthetic $MgAl_2O_4$ spinel (a_o = 8.0831) as an internal standard. Centers of peaks were located at 2/3 peak height. In most runs, sufficient amphibole was present to allow for the 040, 420, and 440 peaks to be used in the determination and therefore compositions are assumed accurate to between 2 and 4 mole % Fe end-member (see Table I-4).

In a small number of the runs at the MH buffer, especially those in which there was considerable reaction of amphibole, inclined extinction of 0°-10° was observed on a small proportion of the grains (1-5% of total amphibole). Thus clinoamphibole must be nucleating from the decomposition of orthoamphibole. Since the total percentage of monoclinic amphibole was small and the molar volumes (i.e., unit cell parameters) of the synthetic orthoamphiboles are roughly equivalent to the natural *C2/m* monoclinic amphiboles, the determinative curves should still reflect the appropriate chemical composition, provided there is no preferential segregation of Fe and Mg between the two structure types.

Magnetite or hematite, depending upon f_{O_2}, occurred in run products as equant grains ranging in size from 30μ down to <1μ. Very small grains

often coated, and in some cases appeared to be included within, amphibole. Magnetite was always anhedral to subhedral whereas the larger hematite grains commonly occurred as hexagonal plates.

Quartz, where formed as a product of amphibole decomposition, ranged from very small (<1μ) anhedral grains to doubly terminated prisms up to 30μ in length. The assemblage SiO_2 glass + magnetite was added to a number of runs, and quartz which crystallized from silica glass occurred as equant, anhedral grains up to 40μ. This quartz generally could be distinguished from quartz formed by amphibole decomposition.

Talc occurred only in the lower temperature runs. Optically it appeared as small shred-like grains often intergrown into larger clumps. When finely dispersed, it was almost impossible to distinguish from fine grained quartz, and thus X-ray methods were primarily used for its identification. When sufficient amounts were present, iron content was estimated using the location of the 003 peak (Forbes, 1969).

Olivine occurred as a high temperature decomposition phase of the most Fe-rich amphiboles. It occurred as equant grains generally 1-10μ, but up to 50μ in certain runs. The amount of olivine in any run was not sufficient to allow estimation of composition by X-ray methods.

Pyroxene is a high temperature decomposition product of amphiboles across most of the join. It always was much coarser grained than amphibole, often occurring as 300μ × 30μ laths and rarely up to 1 mm in length. All pyroxene observed had parallel extinction and was assumed orthorhombic.

Phase Equilibria

Magnetite-Hematite Buffer

The phase relations on the join $Mg_7...Fe_7Si_8O_{22}(OH)_2$ have been investigated at oxygen fugacities defined by the MH buffer at 2 kbar in the range 600°-725°C. Reaction rates at lower temperatures are too slow for experiments to be practical. At temperatures higher than 725° diffusion of H_2 through the large outer Au capsules is so rapid that the buffer can not be maintained longer than three to four days.

Critical run data is summarized in Table II-1 and phase relations are shown in Figures II-1 and II-2.

Steepness of the curve separating the fields Amphibole from Amph + Qtz + Hm + Mt (Fig. II-1), necessitated determination by monitoring changes in amphibole composition. Runs starting with essentially all amphibole (>95%) in the Amph + Qtz + Hm + Mt field reacted to yield Mg-enriched amphibole, quartz, hematite, and magnetite while those in the Amphibole field showed no significant shift in composition. Even though small amounts of quartz, hematite, and magnetite were observed optically, runs #436 and #460 (Table II-1) are interpreted as lying in the amphibole field because the amphiboles show no shift in composition. The starting materials for these two runs contained ∿2% quartz + pyroxene + olivine in addition to amphibole. Neither pyroxene nor olivine was observed in the run products and the presence of iron oxides is attributed to oxidation of these phases.

Runs starting with the assemblage amphibole + magnetite and SiO_2 glass in amounts chemically equivalent to amphibole of composition Fe_7Si_8

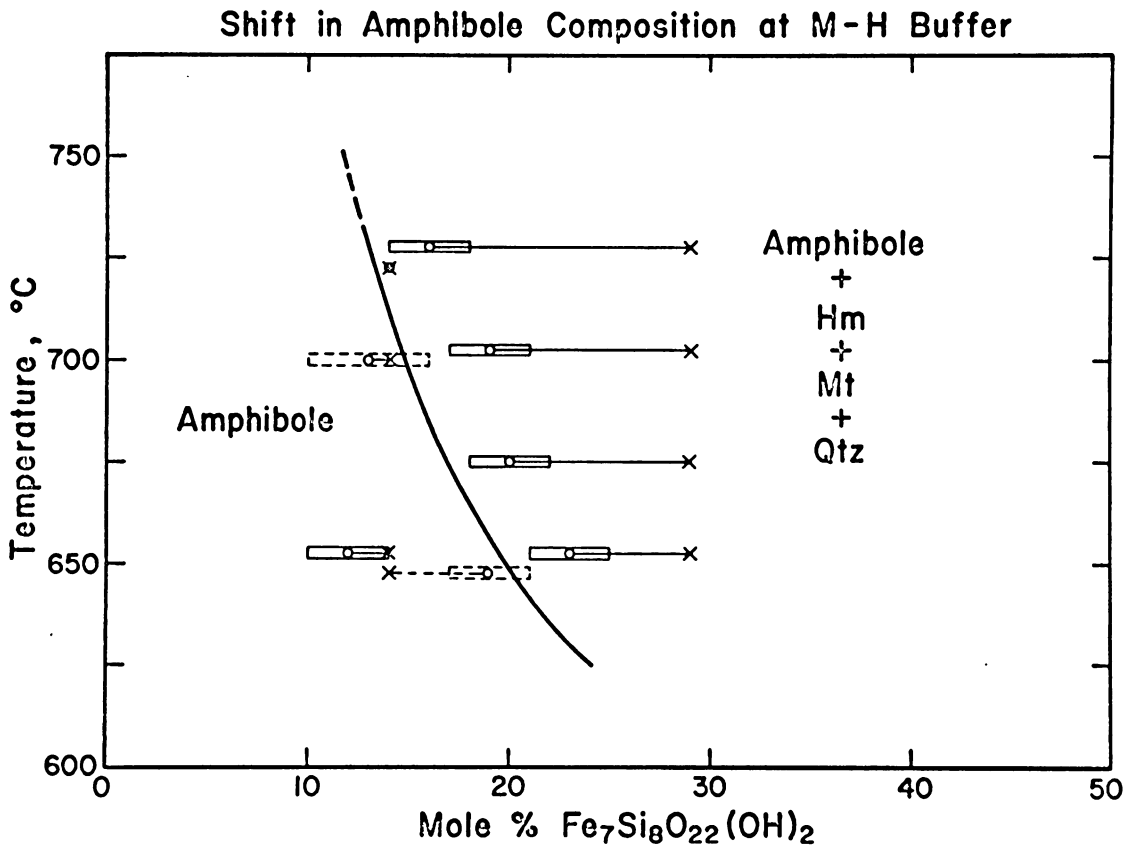

Figure II-1. Shift in amphibole composition at f_{O_2} defined by magnetite-hematite (MH) buffer. Error bars represent uncertainty in amphibole composition. Starting materials denoted by X: solid lines = amphibole + H_2O; dashed lines = amphibole + magnetite + silica glass + H_2O.

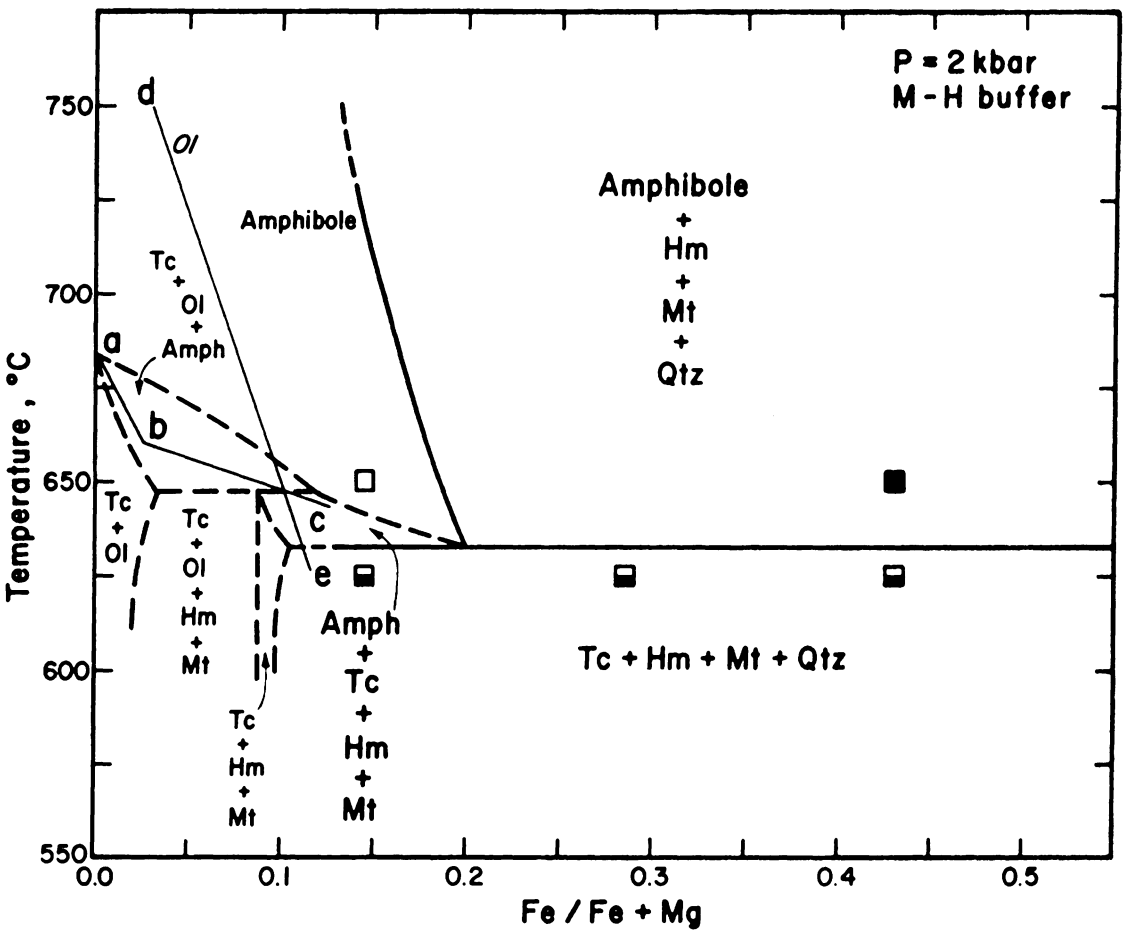

Figure II-2. Condensed T-X section of phase relations on the Mg_7-$Fe_7Si_8O_{22}(OH)_2$ join at 2 kbar and f_{O_2} defined by magnetite-hematite (MH) buffer. Symbols: solid and open, growth of high temperature assemblages at the expense of talc; half shaded, growth of talc. See text for discussion.

TABLE II-1. Runs at f_{O_2} Defined by MH Buffer, 2 kbar

Run #	T(°C)	Duration (days)	Reactants[b]	Products[a]
303	725	15	A(28.6)	A(16,2)[c]+Q+H+M
315	702	15	A(28.6)	A(19,2)+Q+H+M
397	676	21	A(28.6)	A(20,2)+Q+H+M
409	651	20	A(28.6)	A(23,2)+Q+H+M
436	724	14	A(14.3)	A(14,3)+[q+h+m][d]
460	651	16	A(14.3)	A(12,2)+[q+h+m][d]
521	698	20	A(14.3)+M+Q	A(13,3)+Q+H+M
545	649	23	A(14.3)+M+Q	A(19,2)+Q+H+M
424	625	21	A(14.3)	A+Q+H+M+T
381	625	21	A(28.6)	A+Q+H+M+t?
371	623	23	A(42.9)	A+Q+H+M+T
461	650	16	A+Q+H+M+T-(14.3)[e]	A+[q+h+m]
546	650	23	A+Q+H+M+T-(42.9)[e]	A+Q+H+M+t?

a - *Abbreviations: A - amphibole, Q - quartz, H - hematite, M - magnetite, T - talc. Lower case symbols indicate phase present in minor amounts. [ ] indicate presumed metastability.*

b - *Starting amphibole composition indicated in mole % Fe end-member.*

c - *Numbers in parentheses indicate amphibole composition (mole % Fe) and uncertainty (follows comma)*

d - *Only very minor amounts of quartz, hematite, and magnetite. May represent breakdown of the non-amphibole phases in the starting material (see text).*

e - *Represents bulk composition of the run, rather than only the amphibole composition.*

permit the starting amphiboles to react to more Fe-rich compositions. A reversed phase boundary was determined at 650°C and was inferred at higher temperatures.

Figure II-2 is a condensed T-X section of the phase relations on the join at 2 kbar. Pertinent reversals are shown by the rectangular symbols, which represent the temperature uncertainty. Since the reaction talc + hematite + magnetite + quartz → amphibole + hematite + magnetite + quartz is isothermal (as it does not depend on composition), the high temperature side can be located by a decrease in the amount of talc present rather than by its complete disappearance (*cf.* runs #461, #546, Table II-1).

The phase relations shown in the Mg-rich portion of the join were constructed by combining the data of this study with previously published data to produce *one possible* set of internally consistent phase relations. Reaction of the Mg_7 amphibole was taken as the center of Greenwood's (1963) reversal bracket. The slope and shape of the Amph + Tc + Ol loop was estimated from the phase diagram of Hinrichsen (1967) Curve d-e represents the maximum Fe/(Mg + Fe) of olivine at 2 kbar and MH buffer as determined by Fisher (1967). Line a-b-c indicates the composition of olivine coexisting in equilibrium with amphibole and talc in the Amph + Tc + Ol field. For segment a-b, it is assumed that iron is preferentially segregated into olivine over talc. At point b olivine coexists with the most iron-rich talc stable at the temperature and oxygen fugacity (Forbes, 1969). At the temperature of intersection of curves b-c and d-e a tie line switch occurs (Fig. II-3c) and the set of phase assemblages shown by the dashed lines (Fig. II-2) results.

There are a number of obvious factors that could complicate or alter the phase relations shown in the Mg-rich end of the join. The stability of pyroxene has been neglected since no data on its stability at f_{O_2} defined by the MH buffer are available. Although pyroxene is to be expected as a high temperature breakdown phase of amphibole, it could possibly occur in the system at lower temperatures as a product of the oxidation of amphibole. The occurrence of minnesotaite, the iron analog of talc, would also alter the configuration of the system. However, lattice spacings of the 003 reflection indicate very low iron contents consistent with those of Forbes (1969). These complications would alter only the Mg-rich side of the join and have no effect on the data original to this study.

Figure II-3 shows schematic isothermal sections of the lower temperature phase relations inferred from Figure II-2 and high temperature phase relations inferred from Greenwood (1963), Cameron (1975), and results of this study. Phases are shown projected from an H_2O apex onto a ternary molar ratio Si-Mg-"Fe" plane. The range of olivine (ol), amphibole (a), and talc (tc) solid solutions (indicated by the heavy dark bars) have been expanded over those shown in Figure II-2. This was done only to facilitate viewing, and the geometric details are still correct. The range of pyroxene (px) solution is hypothetical but was estimated assuming Fe to be preferentially segregated into pyroxene over amphibole, and into olivine over pyroxene (Ramberg, 1952). Bulk compositions of runs lie on the amphibole join but coexist with a free vapor phase.

Reactions (1)-(7) account for the tie line shifts shown graphically in Figure II-3. For reactions (6) and (7) compositions of phases and

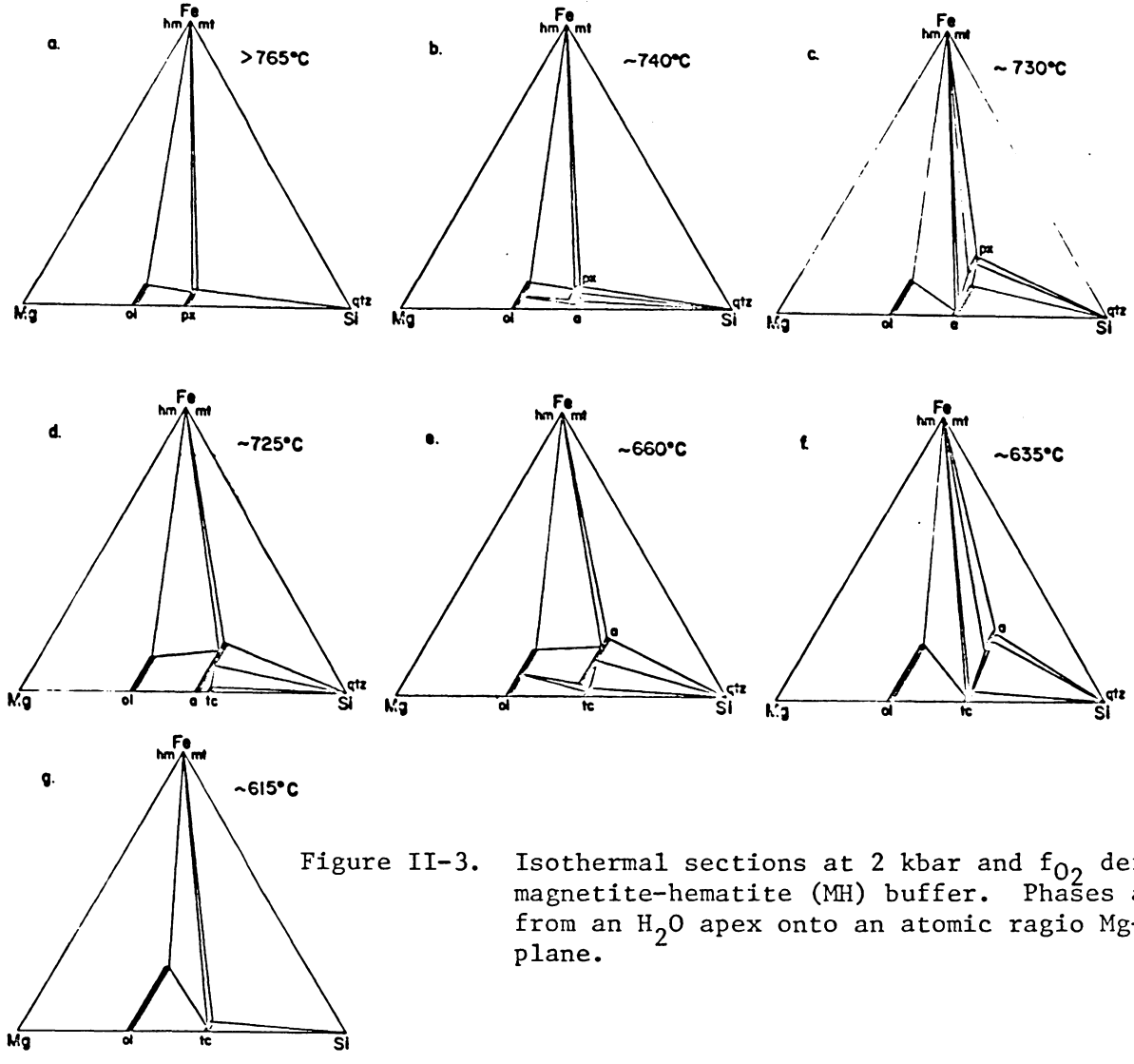

Figure II-3. Isothermal sections at 2 kbar and f_{O_2} defined by magnetite-hematite (MH) buffer. Phases are projected from an H_2O apex onto an atomic ragio Mg-"Fe"-Si plane.

temperatures were estimated from Figure II-2 and molecular coefficients are rounded off to the nearest 0.01. The remainder are written as reactions between solid solutions of unknown Fe:Mg ratios. Reactions (3) and (4) cannot be balanced without knowledge of the compositions of the silicate phases. It is important to note that temperature estimates for reactions (2)-(4) are hypothetical.

$\sim$765°C (1)

$$7(Mg,Fe)SiO_3 + SiO_2 + H_2O \rightarrow (Mg,Fe)_7Si_8O_{22}(OH)_2$$

pyroxene quartz vapor amphibole

$\sim$745°C (2)

$$9(Mg,Fe)SiO_3 + H_2O \rightarrow (Mg,Fe)_2SiO_4 + (Mg,Fe)_7Si_8O_{22}(OH)_2$$

pyroxene vapor olivine amphibole

$\sim$735°C (3)

$$(Mg,Fe)SiO_3 + (Mg,Fe)_2SiO_4 + H_2O + O_2 \rightarrow (Mg,Fe)_7Si_8O_{22}(OH)_2 + FeO_4$$

pyroxene olivine vapor amphibole magnetite

$\sim$730°C (4)

$$(Mg,Fe)SiO_3 + H_2O + O_2 \rightarrow (Mg,Fe)_7Si_8O_{22}(OH)_2 + FeO_4 + SiO_2$$

pyroxene vapor amphibole magnetite quartz

$\sim$680°C (5)

$$5(Mg,Fe)_7Si_8O_{22}(OH)_2 + 4\ H_2O \rightarrow 4(Mg,Fe)_2SiO_4 + 9(Mg,Fe)_3Si_4O_{10}(OH)_2$$

amphibole vapor olivine talc

$\sim$645°C (6)

$$5\ Mg_5Fe_2Si_8O_{22}(OH)_2 + 2.72\ Mg_{1.8}Fe_{0.2}SiO_4 + 5.68\ H_2O + 1.4\ O_2 \rightarrow$$

amphibole olivine vapor

$$10.68\ Mg_{2.8}Fe_{0.2}Si_4O_{10}(OH)_2 + 2.8\ Fe_3O_4$$

talc magnetite

$\sim$630°C (7)

$$2.8\ Mg_{5.5}Fe_{1.5}Si_8O_{22}(OH)_2 + 2.7\ H_2O + 0.59\ O_2 \rightarrow$$

amphibole vapor

$$5.5\ Mg_{2.8}Fe_{0.2}Si_4O_{10}(OH)_2 + 0.4\ SiO_2 + 1.07\ Fe_3O_4$$

talc quartz magnetite

Nickel-Nickel Oxide Buffer

As a result of the loss of iron from charges to platinum capsules at the NNO buffer discussed in Part I, runs could not effectively be maintained on the amphibole join at this buffer. However, the location of the curve representing oxidation of amphibole to magnetite, quartz, and vapor (i.e., location of the most Fe-rich amphibole which is stable) could be determined. Magnetite plus SiO_2 glass in the proportion equivalent to an amphibole of composition Fe_7Si_8 was sealed into Pt capsules with distilled H_2O plus synthetic amphibole. As discussed in relation to experiments at the MH buffer, this assemblage allows the amphibole to shift to either more Mg-rich or Fe-rich compositions as dictated by the equilibrium assemblage. Sufficient magnetite and SiO_2 was added to assure that the initial bulk composition lay well within the amphibole + magnetite + quartz field (e.g., Fig. II-3d). Even substantial loss of iron to

the capsule from such compositions will change neither the equilibrium assemblage nor the amphibole composition.

Results of runs at the NNO buffer at P_{total} = 2 kbar are summarized in Table II-2 and shifts in amphibole compositions are plotted versus temperature in Figure II-4. Comparison of the maximum extent of the amphibole solid solution with that of biotites (Wones and Eugster; 1965) and olivines (Fisher; 1967) at the MH and NNO buffers is shown in Figure II-5. Curves plotted separate the fields of stable solid solution from the fields in which amphibole, biotite, or olivine coexist with an iron oxide plus the appropriate breakdown assemblage. The compositional ranges of all three mineral groups at f_{O_2} defined by NNO are greatly expanded over those at MH.

The extent of olivine and amphibole solution at the NNO buffer are such that the most Fe-rich amphibole coexists with magnetite and quartz rather than olivine and quartz over the range of temperatures in Figure II-5. This is verified by the absence of olivine in run products. The absence of pyroxene in equilibrium with amphibole and quartz in run products indicates that the pyroxene solid solution cannot extend past approximately Fe/(Fe + Mg) = 0.65 at 700°C and 0.75 at 650°C for f_{O_2} defined by the NNO buffer.

Fayalite-Magnetite-Quartz Buffer

A preliminary series of runs to determine the upper thermal stability of amphiboles on the join was carried out at oxygen fugacity defined by the FMQ buffer. Starting materials for all runs were either amphibole + H_2O or amphibole + decomposition products + H_2O, but in the latter case

TABLE II-2. Shift in Amphibole Composition at Nickel-Nickel Oxide Buffer (2 kbar)

Run #	T(°C)	Duration (days)	Starting Amphibole[a]	Final Assemblage[b]
515	673	33	Mg_3Fe_4	A(56) + M + Q
516	600	33	Mg_3Fe_4	A(62) + M + Q
547	701	35	Mg_2Fe_5	A(59) + M + Q
548	603	35	Mg_2Fe_5	A(68) + M + Q
566	700	29	Mg_3Fe_4	A(57) + M + Q
573	650	28	Mg_2Fe_5	A(68) + M + Q
574	626	28	Mg_4Fe_3	A(50) + M + Q
575	725	28	Mg_4Fe_3	A(50) + M + Q

a - *All runs started with amphibole + H_2O + magnetite + silica glass.*

b - *Abbreviations: A - amphibole (numbers in parentheses represent composition expressed as mole % Fe end-member (± 3); M - magnetite; Q - quartz.*

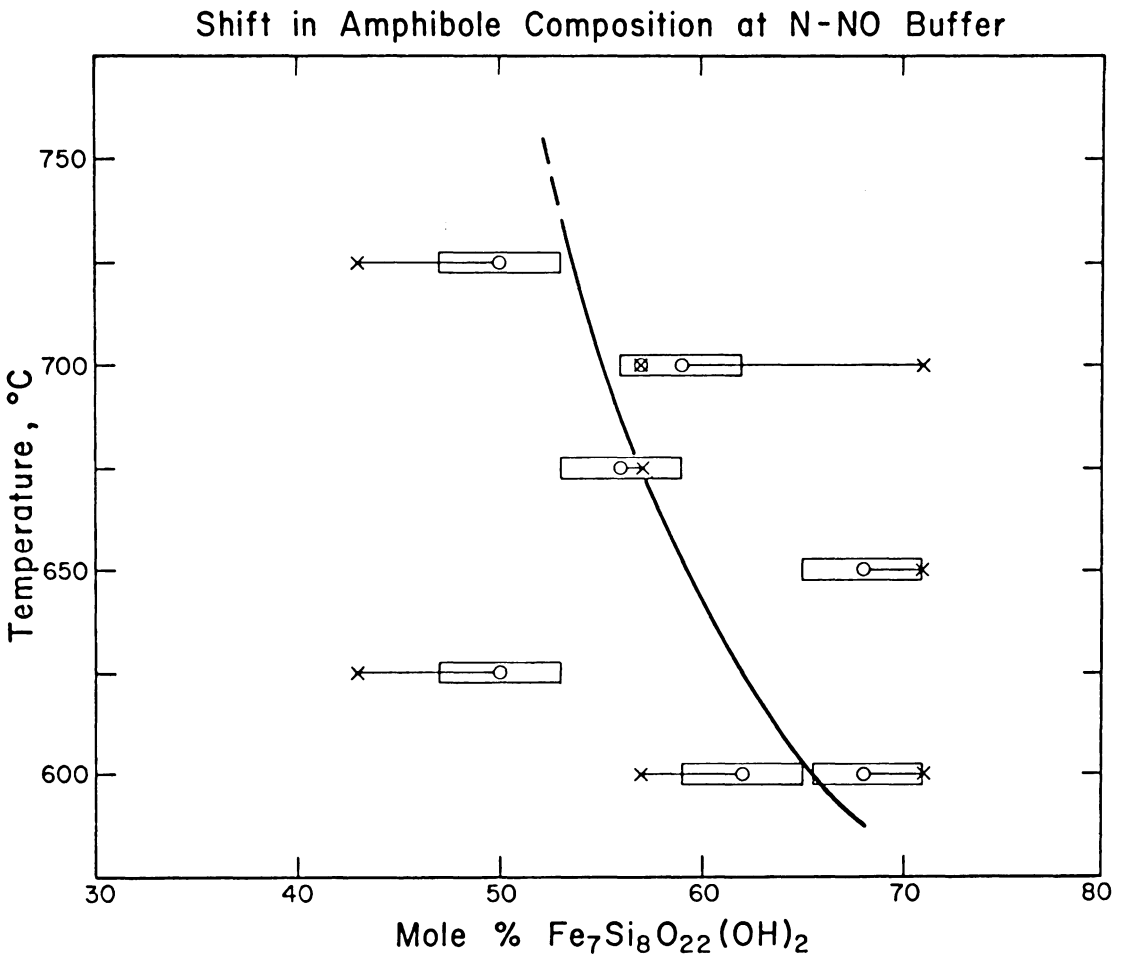

Figure II-4. Shift of amphibole composition at f_{O_2} defined by the nickel-nickel oxide (NNO) buffer. Starting materials for all runs were amphibole (composition denoted by X) + magnetite + silica glass + H_2O. Error bars indicate uncertainty in measurement of amphibole composition.

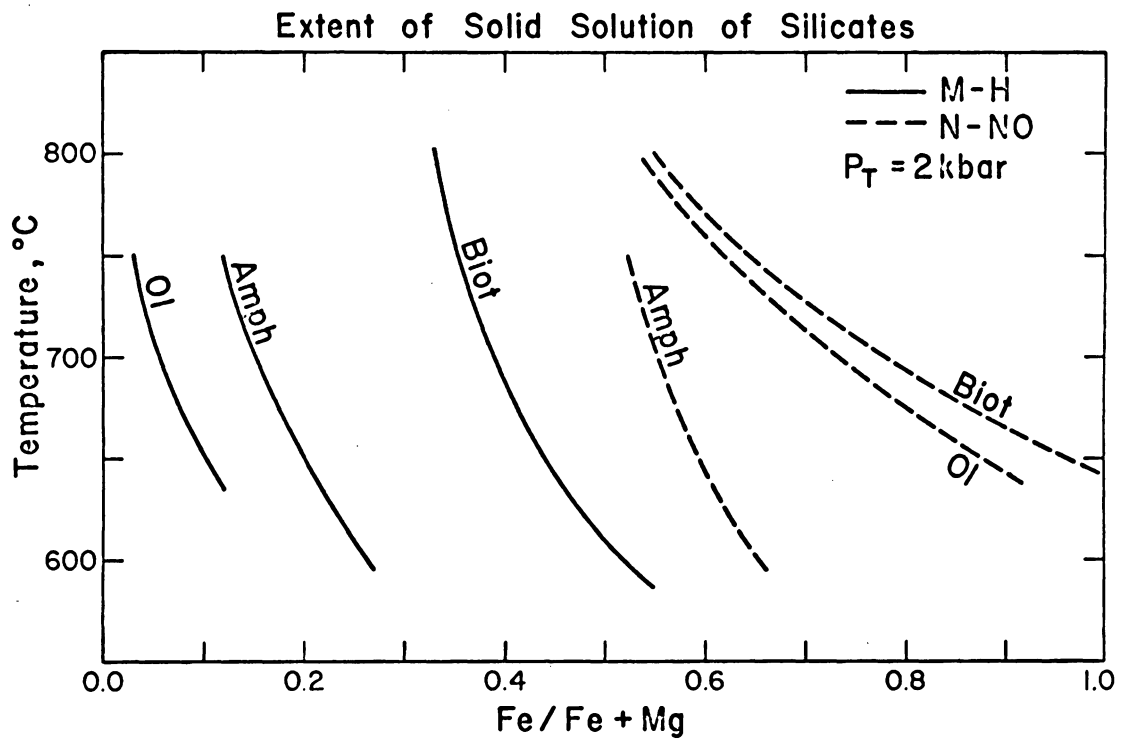

Figure II-5. Extent of solid solution of silicates. Amphibole, this study; biotite, Wones and Eugster, 1965; olivine, Fisher, 1967.

the bulk composition was amphibole + H_2O. Results are given in Table II-3 and plotted with previously published data in Figure II-6.

The boundary separating the Amph and Amph + Px + Qtz fields was drawn to satisfy the reversal bracket of Greenwood, the high temperature reversal at 14.3 mole % Fe end-member of this study, and the low temperature reversal of Cameron at 50%. The curve between the Amph + Px + Qtz and Px + Qtz fields satisfies Greenwood's bracket and the low temperature reversal of Cameron, and has been extrapolated to more Fe-rich compositions. The isotherm limiting the upper stability of the Amph + Ol + Qtz field was located at a temperature which is lower than the high temperature side of the reaction (square bracket, Fig. II-6), but which confines the field to the more Fe-rich side of the join. The lower thermal stability of the Amph + Ol + Qtz field was drawn to satisfy the reversal bracket of this study and was extrapolated to a hypothetical breakdown temperature of ∿625°C for the Fe end-member. Forbes (1971) synthesized Fe end-member grunerite at 610°C at the iron-magnetite buffer and at 555°C at the NNO buffer. The higher temperature phase relations in the most Fe-rich portion of Figure II-6 are hypothetical. The slopes of the curves limiting the Ol + Px + Qtz field assume olivine to be the high temperature phase rather than pyroxene.

TABLE II-3. Results of Runs at f_{O_2} Defined by the Fayalite-Magnetite-Quartz Buffer at P_{total} = 2 kbar

Run #	T(°C)	Duration (days)	Composition (Mole % Fe_7)	Starting Material	Products
290	700	44	Mg_6Fe_1(14.3)	A + P + Q	A
128	750	48	Mg_6Fe_1(14.3)	A + P + Q	A + P + Q
577	752	22	Mg_6Fe_1(14.3)	A	A + P + Q
455	714	15	Mg_5Fe_2(28.6)	A	A
431	748	8	Mg_5Fe_2(28.6)	A	A + Px + Q
368	750	5	Mg_4Fe_3(42.9)	A	A
399	761	10	Mg_4Fe_3(42.9)	A	A + Px + Q
459	724	8	Mg_3Fe_4(57.1)	A	A
550	740	27	Mg_3Fe_4(57.1)	A	A + Px + Q
457	751	16	Mg_2Fe_5(71.4)	A	A + P + Q
402	720	8	Mg_2Fe_5(71.4)	A	A + Ol +Q
576	648	26	Mg_2Fe_5(71.4)	A + Ol + Q	A

Abbreviations: A - amphibole; P - orthopyroxene; Q - quartz, Ol - olivine.

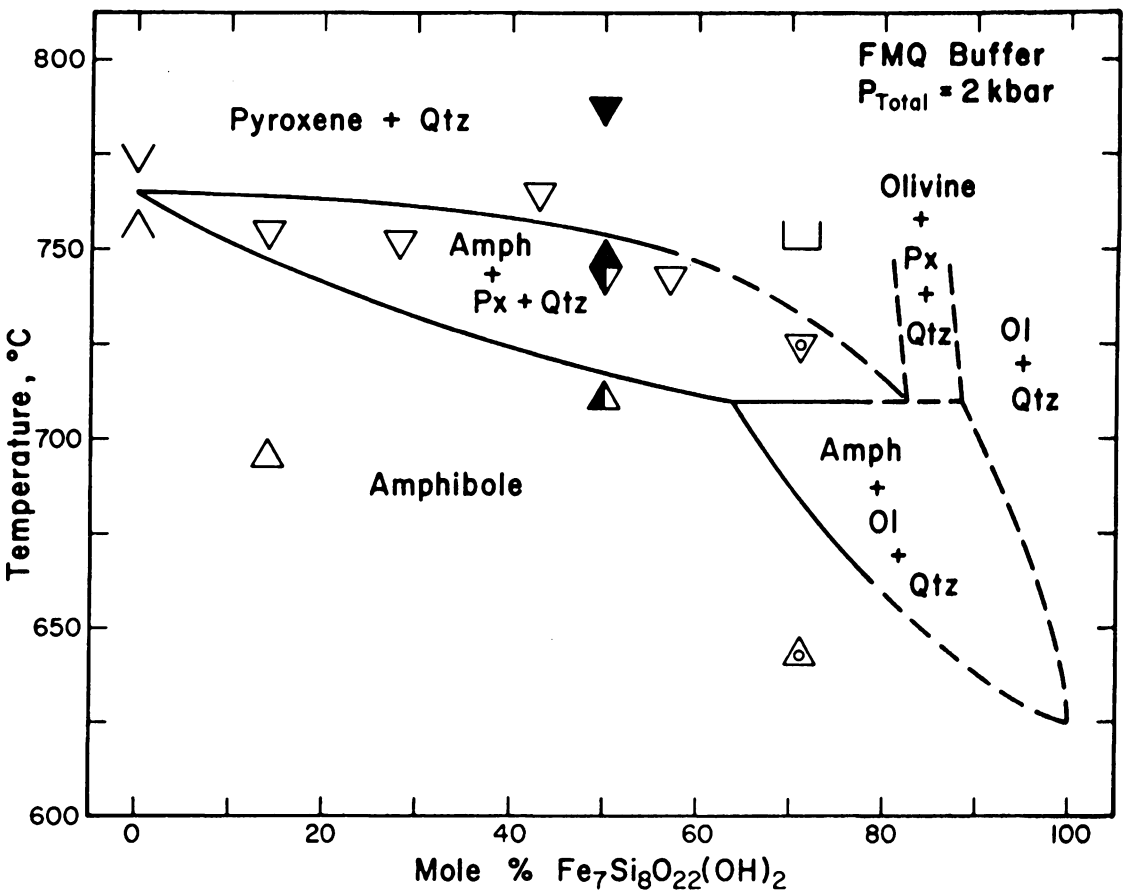

Figure II-6. Condensed T-X section of phase relations on the Mg_7-Fe_7 join at f_{O_2} defined by the fayalite-magnetite-quartz (FMQ) buffer. Symbols: arrows, Greenwood (1963); solid and half-shaded triangles, Cameron (1975). This study: open triangles, Amph → Amph + Px + Qtz; triangles with circles, Amph → Amph + Ol + Qtz; square bracket, Amph + Ol + Qtz → Amph + Px + Qtz.

Geological Applications

The results of this study can be applied to some natural amphibole-bearing assemblages if certain assumptions are made and a number of cautions noted. The amphiboles investigated here have orthorhombic symmetry but space group symmetry apparently different from any known amphibole. However, assuming the energy differences among the structure types of the synthetic amphibole, anthophyllite, and cummingtonite-grunerite to be small, the experimental results may be expected to give a close approach to the stabilities of chemically equivalent members of both natural groups. Rare nucleation of small amounts of monoclinic amphibole during breakdown of the synthetic material during runs may support this assumption.

Experiments were all carried out under conditions of P_{H_2O} essentially equal to P_{total}, whereas natural amphibole assemblages have generally equilibrated with a vapor phase of unknown composition, commonly containing at least H_2O, CO_2, CH_4, CO, and S_2. Under conditions of $P_{H_2O} = P_{total}$, experimental results such as depicted in Figure II-6 indicate maximum temperatures for amphibole stability; under conditions of $P_{H_2O} < P_{total}$, temperatures of thermal decomposition decrease.

The chemical complexity of most natural assemblages generally prohibits direct application of the experimental results. However, if possible effects of other components on phase relations can be ascertained, then the experimental data can be applied to amphiboles that approach the pure Mg-Fe join.

Metamorphosed Iron Formations

Iron-magnesium amphiboles are important constituents of regionally metamorphosed iron formations in the Labrador Trough (Mueller, 1960; Kranck, 1961; Klein, 1966; Butler, 1969). From the results of this study, estimates of temperatures of formation can be made for certain assemblages.

Mueller (1960) reported cummingtonite (Fe/(Fe + Mg) = 0.23, Mn/(Fe + Mg + Mn) = 0.02) coexisting with hematite (hm) + magnetite (mt) + quartz (qtz) + talc (tc) + actinolite from the Bloom Lake area, Labrador. Cameron (1975) has estimated temperatures of metamorphism in the range 550°-600°C based on coexisting cummingtonite-actinolite compositions. At $P_{H_2O} = P_{total}$ and f_{O_2} defined by the MH buffer, amphibole reacts to form talc below ∿630°C (Fig. II-2). The maximum extent of solid solution at this temperature (Fe/(Fe + Mg) = 0.22) agrees well with the observed natural composition. The presence of talc may indicate either amphibole breakdown or a bulk composition which lies off of the join investigated.

Klein (1966) reported both anthophyllite and cummingtonite from the Wabush Lake area, approximately 20 miles northeast of Bloom Lake. Klein's T-P estimate for metamorphism of < ∿600°C and 6-10 kbar has been revised by Cameron (1975) to 550°-600°C and <5 kbar based on coexisting cummingtonite-actinolite and the aluminum silicate phase diagram of Richardson *et al.* (1969). Anthophyllite (Fe/(Fe + Mg) = 0.19, Fe/(Fe + Mg + Ca + Mn) = 0.18) rimmed by talc coexists with hm + qtz at the Smallwood mine. If the talc rims are taken to represent amphibole breakdown, a temperature of < ∿630°C is implied from Figure II-2. Depletion of iron below the

0.22 atomic ratio value in this amphibole may be the result of a higher f_{O_2} as indicated by the absence of magnetite. Klein also reported mangano-cummingtonite (Fe/(Fe + Mg + Mn) = 0.20, Mn/(Fe + Mg + Mn) = 0.25) coexisting with hm + mt + qtz from the Wabush #4 deposit. This composition indicates that the extent of solid solution of Fe-end member at the HM buffer is apparently little affected by the addition of Mn to the amphibole. Only one assemblage reported by Klein (1966) contains Ca-free orthopyroxene: 25% cummingtonite, Fe/(Fe + Mg) = 0.78; 25% orthopyroxene, Fe/(Fe + Mg) = 0.80; 25% siderite; 25% quartz. The presence of the carbonate indicates $P_{H_2O} < P_{total}$, a conclusion also necessitated by the assemblage amph + opx + qtz at temperatures in the range of 600°C.

The amphibole composition from an additional assemblage at the Wabush #6 deposit consisting of anthophyllite (Fe/(Fe + Mg) = 0.24, Fe/(Fe + Mg + Ca + Mn) = 0.17) + hm + mt + qtz (Chakraborty, 1963) is also in good agreement with experimentally determined compositions at f_{O_2} defined by the MH buffer.

Somewhat more intense conditions of metamorphism have been estimated in the area of Mt. Reed and Gagnon, Quebec areas approximately 70 miles southwest of Bloom Lake. Based on the occurrence of granitic migmatites and on the assemblage muscovite + quartz, Butler (1969) estimated temperatures of 600°-700°C in the Gagnon area. The occurrence of kyanite implies pressures of ∿5.5 kbar at 600°C and ∿7.5 kbar at 700°C (Richardson *et al.*, 1969). Kranck (1961) and Butler (1969) report common assemblages of grunerite (Fe/(Fe + Mg) = 0.45 to 0.70), orthopyroxene, clinopyroxene, quartz, and calcite. Under conditions of $P_{H_2O} = P_{total}$ the somewhat higher pressures in the Gagnon region as compared to those of

the experimental conditions would increase the upper thermal stability of amphibole; however, the presence of calcite again implies $P_{H_2O} < P_{total}$. Applying the phase relations of Figure II-6, minimum temperatures in the range 715°-725°C are obtained for the assemblage amphibole + pyroxene for $P_{H_2O} = P_{total}$. However, under conditions of $P_{H_2O} < P_{total}$ this temperature can be considerably lower. Although such estimates may not be quantitatively exact, the common occurrence of cummingtonite + orthopyroxene + quartz generally indicates higher temperatures of metamorphism as compared to the Wabush Lake area, a conclusion also reached by Butler (1969) and Cameron (1975). A carbonate-free assemblage of cummingtonite (Fe/(Fe + Mg + Ca + Mn) = 0.50), magnetite, and quartz, also reported by Butler can be used to estimate f_{O_2}. In the range 600°-700°C such amphibole compositions are appropriate to the oxygen fugacity range of the NNO buffer (Fig. II-4). It is important to note, however, that gradients in f_{O_2} may exist over distances on the order of centimeters in metamorphic terranes and thus such estimates of f_{O_2} apply only to the specific assemblage. The absence of orthopyroxene from the cummingtonite + magnetite + quartz assemblage may also indicate a higher P_{H_2O} as compared to the orthopyroxene-bearing assemblages.

Considerable attention has been directed to mineral assemblages produced in iron formations by contact metamorphism associated with emplacement of the Duluth Gabbro in northern Minnesota (e.g., Gunderson and Schwartz, 1962; French, 1968; Bonnichsen, 1969; Simmons *et al.*, 1974). Retrograde assemblages of cummingtonite replacing orthopyroxene and olivine have been reported adjacent to the contact with the gabbro in the Biwabik and Gunflint iron formations. Textural relations are normally

quite complex and commonly complicated by exsolution features in pyroxenes and amphiboles. In addition, presence of significant Ca in certain phases complicates interpretation. However, Figure II-6 can be applied to these assemblages in a general way. Retrograde cummingtonite in the compositional range Fe/(Fe + Mg + Ca) = 0.6-0.8, orthopyroxene in the range Fe/(Fe + Mg + Ca) = 0.6-0.8, and olivines in the range Fe/(Fe + Mg) = 0.75-0.95 are reported by Bonnichsen (1969) and Simmons *et al.* (1974). From Figure II-6, at $P_{H_2O} = P_{total}$ and f_{O_2} defined by the FMQ buffer, the coexistence of amphibole, orthopyroxene, and olivine of such compositions indicates a temperature of ∿715°C. Estimates of P_{total} somewhat greater than 2 kbar, $P_{H_2O} < P_{total}$, f_{O_2} close to the FMQ buffer, and T > 800°C have been placed on the conditions of metamorphism at the gabbro contact by Simmons *et al.* (1974). Oxygen isotope ratios of quartz-magnetite pairs (Perry and Bonnichsen, 1966) indicate temperatures of 700°-750°C for the contact with the Biwabik formation. However, the isotope temperatures represent the minimum temperature of equilibration. Since cummingtonite-orthopyroxene-olivine represents a retrograde assemblage, the estimate of ∿715°C for this assemblage is consistent with the higher temperature estimates for the peak of metamorphism.

Regional Metamorphism

Rocks of the granulite facies are commonly marked by the appearance of orthopyroxene in place of Ca-free amphiboles such as gedrite, cummingtonite, or anthophyllite (e.g., Winkler, 1967, Ch. 11). Thus the breakdown of amphibole to pyroxene + quartz + H_2O shown in Figure II-6 could be taken to represent the transition from the amphibolite to the granulite

facies for $P_{H_2O} = P_{total}$. However, Winkler (1967) suggests that $P_{H_2O} < P_{total}$ generally prevails for the formation of granulite rocks and thus only maximum possible temperatures of formation can be determined. Because the actual value of P_{H_2O} is generally unknown for granulite facies rocks, only a single example is discussed below.

Retrograde reaction of orthopyroxene to cummingtonite in basic rocks of the granulite facies in the Granite Falls-Montevideo area, Minnesota was reported by Himmelberg and Phinney (1967). Chemical analyses of two coexisting pairs are reported: cummingtonite (Fe/(Fe + Mg) = 0.43)-orthopyroxene (Fe/(Fe + Mg) = 0.61); cummingtonite (Fe/(Fe + Mg) = 0.43)-orthopyroxene (Fe/(Fe + Mg) = 0.50). Maximum temperature estimates for these assemblages of ∿725°C at P_{H_2O} = 2 kbar result from Figure II-6. However, in the absence of knowledge of P_{total} and especially P_{H_2O} such estimates may be of limited value.

In summary, the results of this study can be used to estimate temperatures of formation of natural metamorphic assemblages provided assumptions concerning P_{H_2O} can be made. At oxygen fugacities defined by the FMQ buffer the assemblage amphibole + orthopyroxene + olivine + quartz is stable only at a single temperature for constant P_{H_2O} (Fig. II-6) and thus should be useful in limiting temperature of metamorphism. Figure II-6 should also be useful in placing approximate temperatures on progressive metamorphism based on general diagrams such as that of French (1968, Fig. 23) depicting the appearance of orthopyroxene and fayalite in cummingtonite-grunerite assemblages with increasing grade of metamorphism.

Extrusive Igneous Rocks

Ewart *et al.* (1971) have reported phenocrysts of cummingtonite, hypersthene, quartz, and plagioclase in rhyolitic volcanic rocks of the Taupo region of New Zealand. Chemical analyses indicate amphiboles of Fe/(Fe + Mg + Ca) = 0.34-0.39, Ca/(Fe + Mg + Ca) = 0.03-0.04; and orthopyroxene of Fe/(Fe + Mg) = 0.44-0.55. Conditions of formation of the phenocrysts were inferred to be: 735°-780°C (final equilibration temperatures from oxygen isotopic studies); ∿1.5-2.3 kbar P_{H_2O}; and oxygen fugacities approximately equivalent to that of the NNO buffer. The breakdown of amphibole to opx + qtz was not investigated at the NNO buffer in this study. At P_{H_2O} = 2 kbar and the slightly lower f_{O_2} defined by the FMQ buffer, synthetic amphiboles chemically equivalent to the natural phenocrysts coexist with opx + qtz at 725°-735°C (Fig. II-6), which is in good agreement with the above temperature estimates. Under conditions of $P_{H_2O} = P_{total}$, this temperature range lies approximately 50°C above the granite minimum melting curve at 2 kbar (Tuttle and Bowen, 1958).

Part III: Stability of Fe-Mg Amphiboles with Respect to Sulfur Fugacity

Introduction

Subsolidus sulfide-silicate equilibria have important geological applications in regional metamorphism and emplacement of ore bodies. Studies such as those of Naldrett (1966), Fullagar *et al.* (1967), and Craig and Gilbert (1974) have shown the importance of sulfide-silicate interaction to the origin, emplacement, and metamorphism of natural sulfide ore bodies. Mallio and Gheith (1972) presented textural evidence that show such interactions to be operative during regional metamorphism of S-rich sediments. Field investigations of the type undertaken by Guidotti (1970) provide the basis for speculation on the composition of the S-containing volatile phase during metamorphism. Sulfur fugacity may also exert some control on isograd reactions. Mohr (1972) has suggested the shift of the kyanite isograd to lower metamorphic grade by the sulfurization of chlorite and consequent production of kyanite.

Early experimental studies of Kullerud and Yoder (1963, 1964) suggested the applicability of experimental techniques to the understanding of low pressure sulfide-silicate reactions. Although the majority of the experimental studies published to date have been concerned with the qualitative aspects of sulfurization reactions, several quantitative studies of coexisting sulfide-silicate assemblages have been reported. Clark and Naldrett (1972) reported equilibrium compositions of coexisting Fe-Ni olivines and Fe-Ni monosulfide solid solutions. Nadrett and Brown (1968), Hammerback and Lindquist (1972), and Popp and Gilbert (1974) have experimentally determined compositions of pyrrhotites coexisting with pyroxenes, biotites, or amphiboles, respectively. This section presents

the results of an experimental study of the effect of sulfur fugacity on amphiboles on the join $Mg_7...Fe_7Si_8O_{22}(OH)_2$. The qualitative effects of sulfurization and equilibrium amphibole-pyrrhotite compositions have been determined at P_{H_2O} = 2 kbar in the range 650° to 750°C.

Calculated Sulfide-Silicate Equilibria

The basic thermodynamic and phase equilibria principles of importance to sulfide-amphibole studies can be elucidated by considering the calculated phase relations of an Fe-Mg silicate solid solution for which sufficient thermodynamic data are available. A brief discussion of orthopyroxene-pyrrhotite equilibria follows. Figure III-1 shows the calculated stability field of the Mg-Fe orthopyroxene solid solution in terms of oxygen and sulfur fugacity at 980°C and 1 atm. These T-P conditions were chosen because the calculated coexisting pyrrhotite-pyroxene compositions can then be compared to the experimental data of Naldrett and Brown (1968). The reactions representing pyroxene oxidation

$$6FeSiO_3 + O_2 \rightarrow 2Fe_3O_4 + 6SiO_2 \qquad (1)$$

pyroxene vapor magnetite tridymite

and sulfurization

$$2FeSiO_3 + S_2 \rightarrow 2FeS + 2SiO_2 + O_2 \qquad (2)$$

pyroxene vapor pyrrhotite tridymite vapor

can be located in terms of f_{O_2} and f_{S_2} using the thermodynamic relation:

$$\underset{\rightarrow}{G}^\circ = -RT\ell nK \qquad (3)$$

where $\underset{\rightarrow}{G}^\circ$ is the standard state Gibbs free energy of reaction, K the equilibrium constant, R the gas constant, and T the absolute temperature. Standard state free energy values of tridymite and magnetite (assumed to be pure phases) were obtained from Robie and Waldbaum (1968); that of pyrrhotite from Barton and Skinner (1967); and that of $FeSiO_3$ was

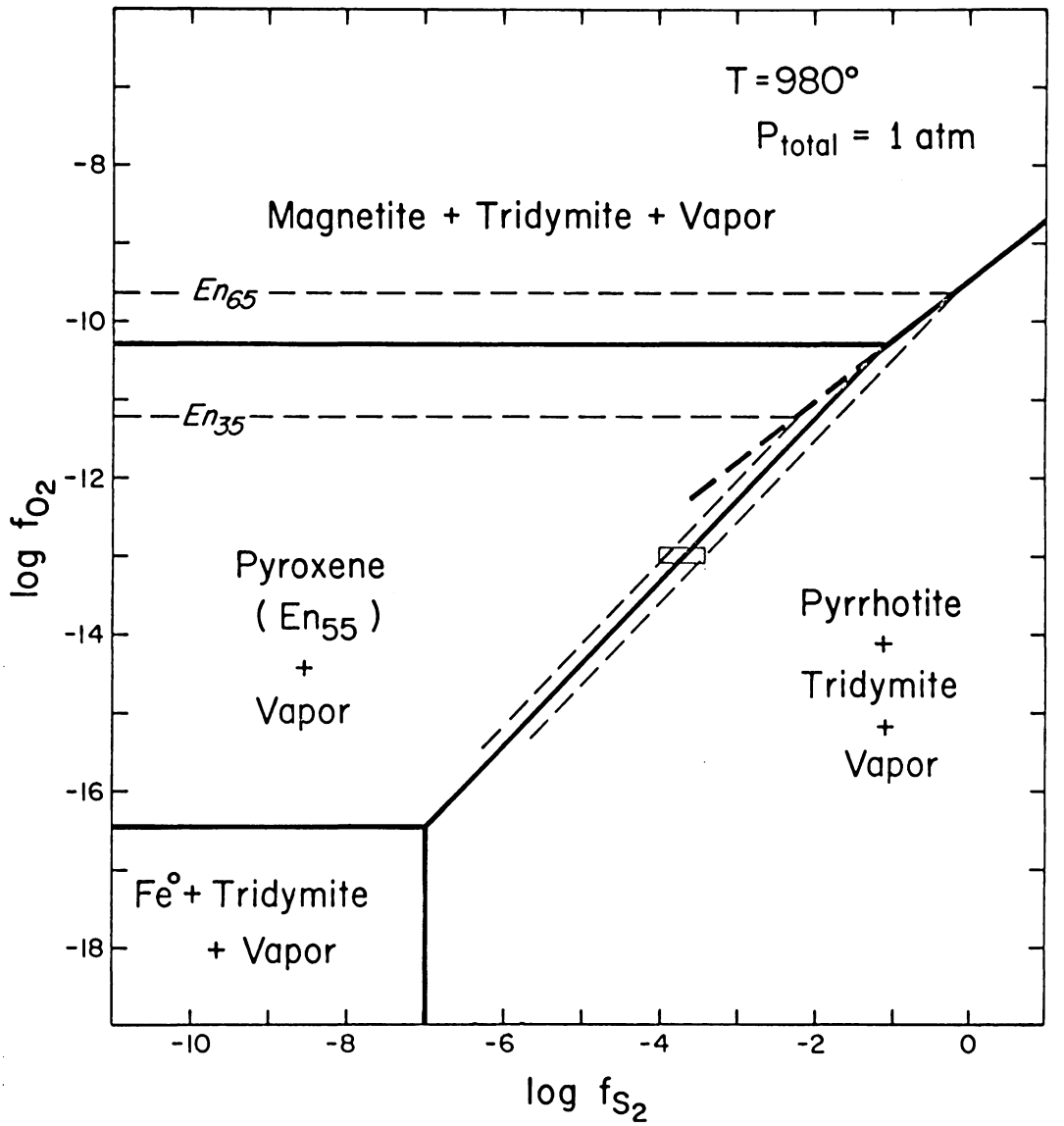

Figure III-1. Calculated phase relations for $MgSiO_3$-$FeSiO_3$ orthopyroxenes. Compositions expressed as mole % $MgSiO_3$. Shaded bar represents error in determination of log f_{S_2} using the method of Toulmin and Barton (1964).

calculated by the method described by Froese (1971) and utilizing Lindsley's data (1967). Assuming the pyroxene solid solution to be ideal at 980°C (e.g., Navrotsky, 1971) and using the relation between sulfur fugacity (f_{S_2}), activity of FeS in pyrrhotite (a^{po}_{FeS}), and pyrrhotite composition (N = 2 x atomic % Fe) as determined by Toulmin and Barton (1964), the stability field of any given pyroxene composition can be calculated. The calculated stability fields of several compositions expressed as mole % $MgSiO_3$ are shown in Figure III-1 (solid line = 55 mole %). The point of intersection of reactions 1 and 2 represents the equilibrium assemblage pyroxene + pyrrhotite + magnetite + tridymite (quartz actually reported) + vapor, which is that determined experimentally by Naldrett and Brown (1968). The calculated pyrrhotite composition (N = 0.954) coexisting with pyroxene En_{55} is in fair agreement with the experimental value of N = 0.944. Table III-1 summarizes the errors involved in the experimentally determined and calculated equilibria.

Two factors concerning experimental techniques for sulfide-silicate investigations are evident from Figure III-1. First, because f_{O_2} is as critical a variable as f_{S_2} in determining coexisting silicate-pyrrhotite compositions, knowledge of f_{O_2} during experimental runs is essential. Second, a typical error in measurement of pyrrhotite composition using the method of Toulmin and Barton (1964) is shown by the solid bar in Figure III-1 and represents approximately $\pm$30 mole % in pyroxene composition at the f_{S_2} and f_{O_2} values shown. Thus, a series of runs at varying f_{S_2} but constant f_{O_2} such as that imposed by standard solid buffer techniques (Eugster and Wones, 1962) may not yield pyrrhotite

TABLE III-1. Sources of Error in Calculated Orthopyroxene-Pyrrhotite Equilibrium

Source	Error in po Composition (N)
opx composition ($\pm$ 2 mole % $FeSiO_3$)	$\pm$0.002
po composition	$\pm$0.003
temperature $\pm$20°C	$\pm$0.002
tabulated G° values $\pm$1% error	$\pm$0.007

compositions precise enough to be of practical value. For this reason, and additional reasons to be discussed below, standard solid buffer techniques were not found applicable.

Experimental Procedures

Solid starting materials for all runs were crystalline natural or synthetic phases prepared as follows:

a. Amphiboles: synthesized to yield of >95% as discussed in Part I.

b. Pyrrhotite and pyrite: synthesized from iron sponge (reduced with H_2 at 700°C) and sulfur in standard evacuated silica glass tubes.

c. Magnetite: crystallized from amorphous reagent grade Fe_3O_4 + H_2O at 700°C, 2 kbar in sealed Au capsules.

d. Quartz: Lake Toxaway quartz; crushed, sieved, acid treated.

e. Sulfur: ASARCO, 99.999 pure.

Appropriate proportions of the above were weighed, mixed together in an agate mortar for several minutes, and then loaded into capsules along with a measured amount of distilled water.

All runs were carried out in the hydrothermal systems previously described in Parts I and II. Maximum variations of $\pm$3°C and $\pm$25 bars were noted during runs. At the termination of runs bombs were quenched at pressure, first in a stream of compressed air for 2-3 minutes, and then by immersion in water. In this manner, room temperature was reached within a maximum of five minutes.

The composition of capsule materials is an important consideration for runs in which the charge contains sulfur. Figure III-2 is a log f_{S_2} vs T plot at 1 atm of several relevant sulfurization curves calculated from the data of Barton and Skinner (1967). Shown as solid lines are curves for the equilibria Pt-PtS, Ag-Ag_2S, Fe-FeS, $Fe_{1-x}S$-FeS_2, and

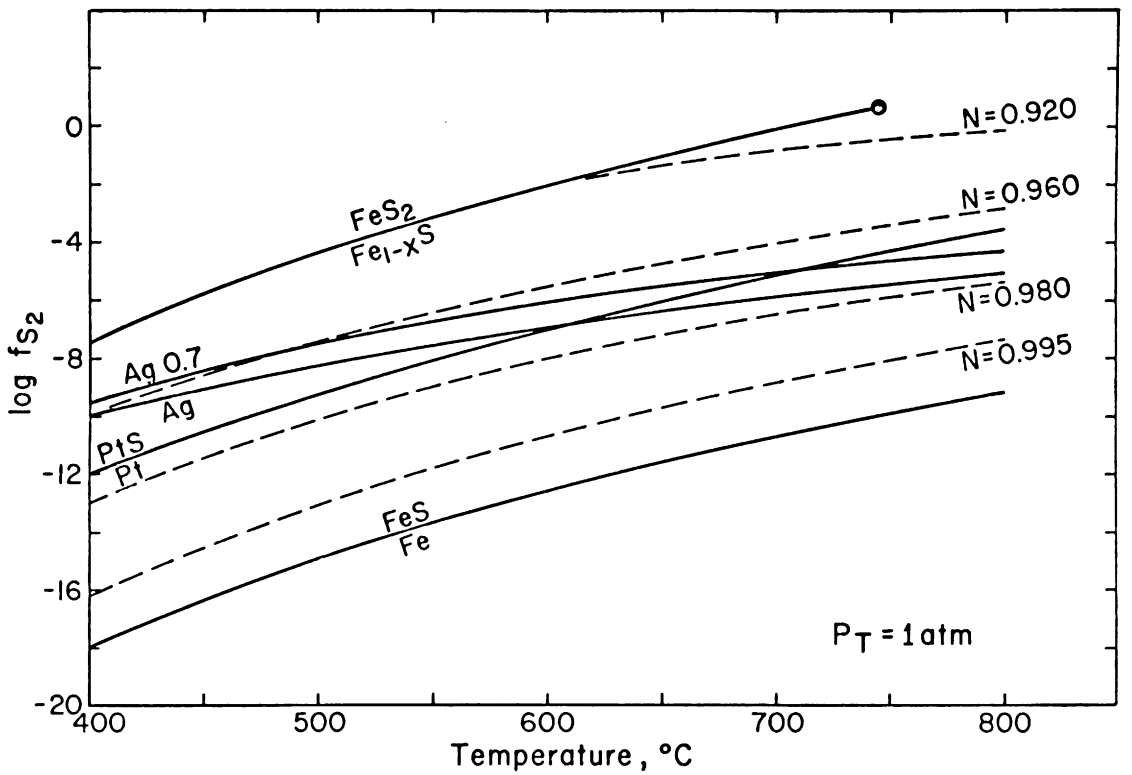

Figure III-2. Pertinent sulfurization curves calculated from the data of Barton and Skinner (1967). Dashed lines indicate pyrrhotite composition as a function of f_{S_2} and T (Toulmin and Barton, 1964).

$Ag_{70}Pd_{30}$-Ag_2S assuming $a_{Ag}^{AgPd} = 0.7$. The dashed lines indicate pyrrhotite composition (N) as a function of f_{S_2} and T as determined by Toulmin and Barton (1964). It is obvious that the standard noble metals will not be suitable capsule materials for assemblages containing pyrrhotite more sulfur-rich than N of approximately 0.970. Several preliminary runs containing the assemblage amphibole + troilite (N = 1.0) + iron + H_2O were carried out in Ag capsules surrounded by the standard solid buffer assemblages. The capsules were observed to be badly corroded after runs and Ag_2S was identified in the charge. Formation of Ag_2S was attributed to the oxidation of troilite and subsequent sulfurization of Ag due to an initial relatively high f_{O_2} generated by the dissociation of H_2O at the T and P of the runs.

Whereas the effect of increased pressure is to shift all of the curves in Figure III-2 to higher f_{S_2} by small but different amounts, the magnitude of this shift is not large enough to effect the above discussion. As a result, Au capsules, which are essentially inert to sulfur over the fugacity range investigated, were used for all runs reported here. Arnold (1962) reported exchange of Au and Fe between capsules and charges consisting of pyrrhotite-pyrite assemblages to be negligible at 2 kbar between 380° and 650°C. A run of Fe-rich amphibole at 2 kbar and 700°C carried out here indicated no loss of Fe to the capsule from the silicate.

Phase Identification and Characterization

All runs were opened immediately after quenching, checked for the presence of water, and X-rayed immediately thereafter. Charges were examined with the petrographic microscope, with the reflecting microscope

using standard polished sections, and by X-ray powder diffraction as described in Part I.

Amphiboles occur as needle-like crystals averaging approximately 1-2μ by 10-15μ, often intergrown in large fibrous clumps. In some cases a slight decrease in average grain size between reactant and product was noted. Compositions were obtained using the X-ray determinative curves discussed in Parts I and II. Peaks were located at the center of gravity at 2/3 peak height on two oscillations (4 scans) at 1/2° 2θ/minute using synthetic $MgAl_2O_4$ (a_o = 8.0831 Å) spinel as an internal standard. In most runs amphibole constituted a small enough proportion of the charge so that only the 440 peak could be measured precisely. Compositions determined in this manner are assumed to accurate to ±4 mole % Fe end-member. As in Part II, in a few runs a small percentage (∿ <5%) of the amphiboles were observed to have inclined extinction up to 10°. These amphiboles were confined to runs with an initially high f_{S_2}, or in double charge runs, to the initially S-rich end of the capsule. This was interpreted as indicating inversion of a portion of the orthoamphibole to a monoclinic form as a result of breakdown at high f_{S_2}. Since the total percentage of monoclinic amphibole in the charge was small and the molar volumes (i.e., unit cell parameters) of the synthetic orthoamphiboles are roughly equivalent to the natural *C2/m* monoclinic amphiboles, it is assumed that the determinative curves will still reflect the appropriate composition of these mixtures of the two types.

Pyrrhotite was identified by X-ray and reflected light methods and occurred as roughly equant anhedral to subhedral grains ranging in size from 40μ down to less than 1μ. Compositions were determined by the

location of the 102 peak (Toulmin and Barton, 1964) based on 3 oscillations (6 scans) at 1/2° 2θ/minute using synthetic spinel as an internal standard. As a check for systematic interlaboratory errors the curve of Toulmin and Barton was tested against and found to be consistent for four synthetic pyrrhotites of known composition. Since oxidation of fine grained pyrrhotite in air can significantly affect d-values, pyrrhotites were X-rayed immediately upon opening. However, no systematic shifts in composition were noted during X-ray scanning of a single sample for periods of up to two hours. Pyrrhotite compositions reported are assumed accurate in N to 0.003. Temperatures of all runs were within the stability field of hexagonal pyrrhotite and quenching rates were apparently rapid enough so that the complication of low temperature transitions was avoided (Scott, 1974). Splitting of the 102 peak, which would indicate presence of monoclinic pyrrhotite, was not observed.

Equilibrium sulfur fugacity was not high enough to yield pyrite as a stable phase in any runs reported. However, in several runs in which pyrite was a starting material, small ($\sim$3μ), equant grains of pyrite were identified optically in minor amounts (<1% total charge). The final pyrrhotite compositions in these runs was close to the pyrrhotite-pyrite solvus and pyrite was interpreted as being metastable. Arnold (1962) reported that sulfur-rich pyrrhotites quenched from temperatures higher than 650°C were found to exsolve pyrite regardless of the quenching rate. Contrary to that report, no exsolved pyrite was observed in polished sections of any runs of this study.

Magnetite was observed only in runs to which it was added as a starting material. It occurred as semi-equant anhedral to subhedral

grains ranging in size from 20μ to <1μ. In a number of runs it occurred as small blebs within large pyrrhotite grains and represents residual magnetite surviving after the replacement of a larger magnetite grain by pyrrhotite. Except for such grains, no reaction rims of pyrrhotite or magnetite were observed. For a number of magnetites coexisting with pyrrhotite, amphibole, and quartz, measured d_{400} values obtained were consistent with those given in the A.S.T.M. file (card 11-614), and thus solution of Mg into magnetite is assumed to be minor.

Several distinct forms of quartz were observed optically in run products. Lake Toxaway quartz, added to runs to serve as a source of SiO_2, was observed as large (20μ-30μ) equant anhedral grains. SiO_2 is also a product of the sulfurization reaction and as such occurred both as small anhedral grains down to <1μ, and as prisms up to 20μ x 5μ doubly terminated by pyramids.

Talc was identified primarily from X-ray scans. Optically it occurred as clumps of small shred-like grains roughly 1μ or smaller in size. When dispersed, it was very difficult to distinguish optically from very fine grained quartz.

Experimental Results

Preliminary Sulfurization Runs

Prior to attempting reversed equilibrium runs, preliminary runs were carried out in order to determine the qualitative effects of sulfur fugacity on the synthetic amphiboles as well as rates of the sulfurization reactions.

Elemental sulfur, 10-15 wt. % distilled H_2O, and synthetic amphiboles, ranging in composition from 14.3-71.3 mole % Fe end-member, were loaded into .120" O.D. Au capsules, placed within the standard FMQ buffer assemblage in large Au tubes, and run at 2 kbar in the range 650°-750°C for up to 3 weeks. Certain of the inner, charge-containing capsules were welded shut, some were merely crimped shut, and others left uncrimped. Upon opening, the capsules were carefully examined. Capsules of all three types were often considerably puffed after runs and the smell of H_2S was detected when capsules were pierced, indicating that all three types were effectively sealed during runs. A hard plug of sulfurized buffer material (magnetite, pyrrhotite, and quartz) was found in the open end of the unsealed and crimped capsules and apparently had effectively sealed the capsules from diffusion of the vapor.

In all runs at 700°C, regardless of starting amphibole composition, amphibole + pyrrhotite + quartz were the only products identified. Talc was present in all runs at 650°C and pyroxene in the 750°C runs. To avoid the complicating effect of the extra silicate phases, most additional preliminary runs were carried out at 700°C.

The results of a number of 700°C runs carried out in Au capsules surrounded by FMQ buffer are shown in Figure III-3. Initial and final amphibole compositions and final pyrrhotite compositions are plotted. The experimentally determined pyrrhotite composition coexisting with the assemblage FMQ is also shown by the heavy bar (determination of this value will be discussed below). Consideration of the range of amphibole and sulfide compositions of Figure III-1 suggests that f_{O_2} must vary considerably from run to run and that diffusion of H_2 through the Au capsule cannot have achieved equilibrium conditions. These runs, however, are of value in characterizing the sulfurization reaction at 700°C and 2 kbar which proceeds by the reaction:

$$[Fe_7Si_8O_{22}(OH)_2] \text{ in Fe-Mg amphibole} + 7/2\ S_2 \rightarrow$$
$$7[FeS] \text{ in pyrrhotite} + 8\ SiO_2 + 7/2\ O_2 + H_2O \qquad (4)$$

with equilibrium constant:

$$K = \frac{(a_{FeS}^{po})^7 (f_{O_2})^{7/2} (f_{H_2O})}{(a_{Fe}^{amph})^7 (f_{S_2})^{7/2}} \qquad (5)$$

where a denotes activity and SiO_2 is assumed a pure phase.

Since equilibration of H_2 between charge and buffer could not be achieved through Au capsules, even when capsules were initially unsealed, an alternate method was devised to equilibrate f_{O_2} between charge and buffer. Charges of amphibole + sulfur in the ratio of approximately 1:2 were sealed in Au capsules with 10-15 wt. % H_2O and then sealed in FMQ buffer assemblages. At the temperature of the runs, pressure exerted by the sulfur vapor is great enough to rupture the inner capsule during

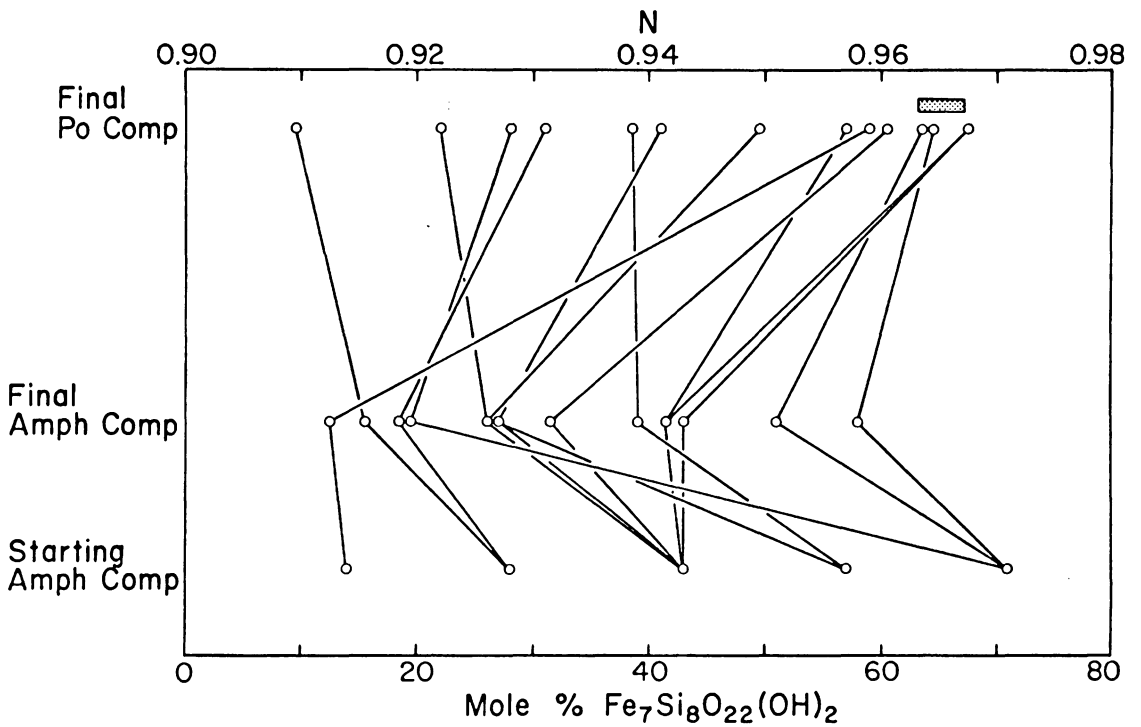

Figure III-3. Results of 700°C, 2 kbar runs starting with amphibole + sulfur + H_2O in sealed Au capsules surrounded by FMQ buffer. Shaded area indicates experimentally determined pyrrhotite in equilibrium with FMQ at 700°C; 2 kbar, along with experimental uncertainty.

the first several hours of the run, thus allowing interchange between the volatile phases of the charge and buffer. Exchange of solids between the charge and buffer is very small, but pyrrhotite is formed through sulfurization of the buffer. Oxygen fugacity in both the charge and buffer should thus be that defined by the FMQ buffer. In runs of sufficient length the composition of pyrrhotite in both charge and buffer is identical with the experimentally determined FMQ-po equilibrium composition.

Using the ruptured capsule method, identically prepared runs containing amphibole (57 mole % Fe end-member) + sulfur + H_2O were run at 700°C, 2 kbar in FMQ buffer for periods of 1-17 days to determine the effect of run time on the reaction. The results of these runs are given in Table III-2. The variation of amphibole and pyrrhotite compositions with time is plotted in Figure III-4. Open circles in Figure III-4 represent amphibole coexisting with talc, and open squares represent pyrrhotite coexisting with pyrite. The dashed line in the pyrrhotite diagram is the equilibrium composition of pyrrhotite for the assemblage FMQ-po at 700°C, 2 kbar. It is evident that equilibrium is not achieved in the shorter runs. Under the initially high f_{S_2}, amphibole is sulfurized to produce Fe-sulfides and talc. In runs of 11 days and longer, the metastable sulfides and silicates disappear leaving the assemblage amphibole + pyrrhotite + quartz.

Reversed Equilibrium Runs

Reversed tie lines between coexisting amphiboles and pyrrhotites were determined by single runs using a method similar to that of Naldrett and Brown (1968) and Clark and Naldrett (1972). The configuration of

TABLE III-2. Results of runs with f_{O_2} defined by FMQ buffer using the ruptured capsule method described in text. Starting materials for all runs were amphibole (57 mole % Fe_7) + sulfur + H_2O.

Duration (days)	Products*	Amph. comp. (mole % Fe, ± 4)	Po comp. (N, ± 0.003)
1	Py+K+Tc+A+Po+Q	53	0.932
3	Py+Tc+A+K+Q+Po	32	0.930
5	Q+A+Tc+Po+K+Py	31	0.928
7	Q+A+Po+Tc	25	0.951
11	A+Po+Q	40	0.960
17	A+Po+Q	54	0.964

**Products listed in decreasing order of abundance.*

Abbreviations: A - amphibole, Po - pyrrhotite, Q - quartz, Py - pyrite, Tc - talc, K - keatite.

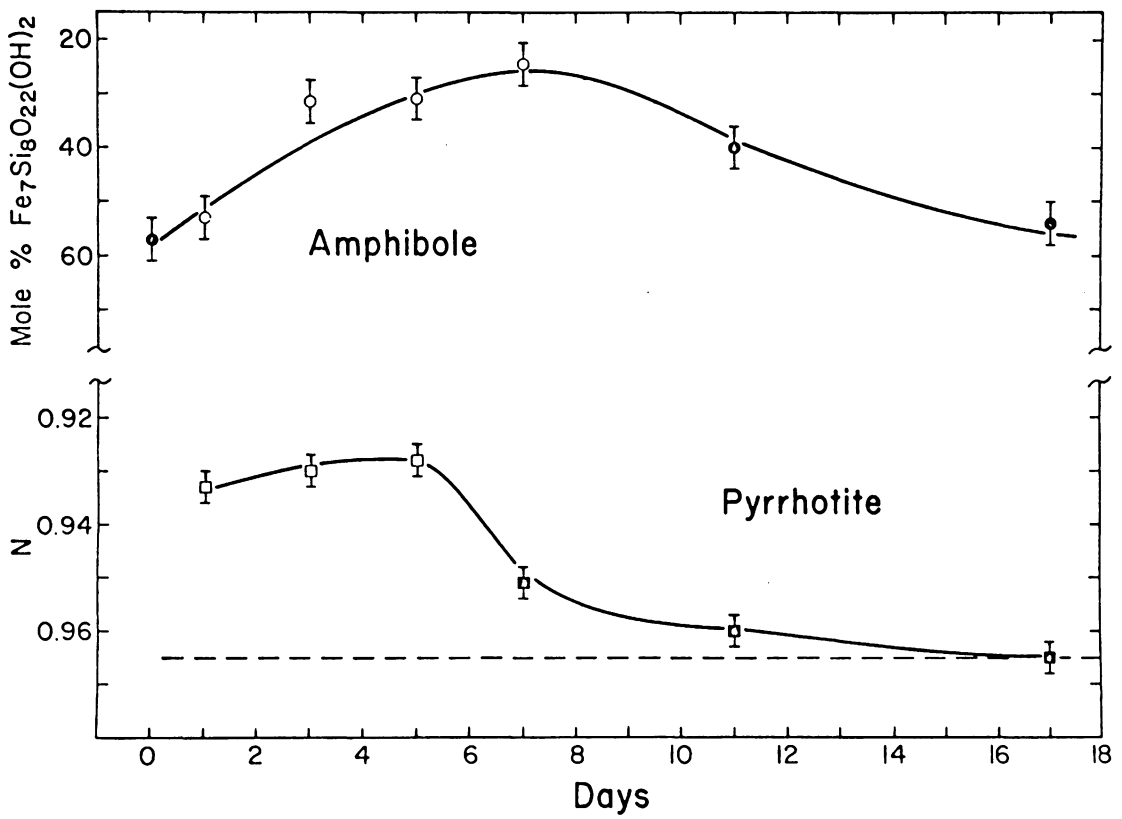

Figure III-4. Variation of amphibole and pyrrhotite compositions with time (700°C, 2 kbar, FMQ buffer). Starting materials for all runs: amphibole (57 mole % Fe_7) + sulfur + H_2O. Dashed line indicates equilibrium composition of pyrrhotite at FMQ buffer. See text for symbols.

sealed capsules for such runs is shown in Figure III-5b. The upper portion of the capsule initially contained the assemblage Mg-rich amphibole + troilite (N = 1.0) + quartz + magnetite, the lower portion Fe-rich amphibole + pyrite + quartz + magnetite, and the center portion magnetite + quartz. Ideally, the volatile phase should equilibrate throughout the entire capsule to produce a single pyrrhotite composition in all three layers and a single amphibole composition in the upper and lower layers. The presence of magnetite + quartz serves several purposes. First, the assemblage serves as a source of SiO_2 and Fe, which allows amphiboles to shift to more iron-rich compositions if the equilibrium relations so dictate. Second, the assemblage amphibole + magnetite + quartz should act as a buffer for f_{O_2}, and third, the assemblage magnetite + po allows calculation of the f_{O_2} defined by this buffer and thus f_{O_2} during runs is known. In several runs, diffusion of H_2 into the capsule resulted in the reaction of all the magnetite + quartz to amphibole. To minimize this effect, capsules were enclosed within larger Au capsules containing the assemblage magnetite + quartz + H_2O. In such a configuration f_{O_2} should not be drastically different on opposite sides of the inner capsule and thus diffusion should be minimized.

Table III-3 summarizes results of this series of runs. Within the error of measurement pyrrhotite compositions in the upper, lower, and middle (where measured) layers were identical in any single run. The amphiboles, however, react more sluggishly and equilibrium compositions can only be bracketed between wider limits.

In an attempt to achieve higher f_{O_2} and f_{S_2} certain of the runs in Table III-3 initially contained hematite plus quartz in the middle layer

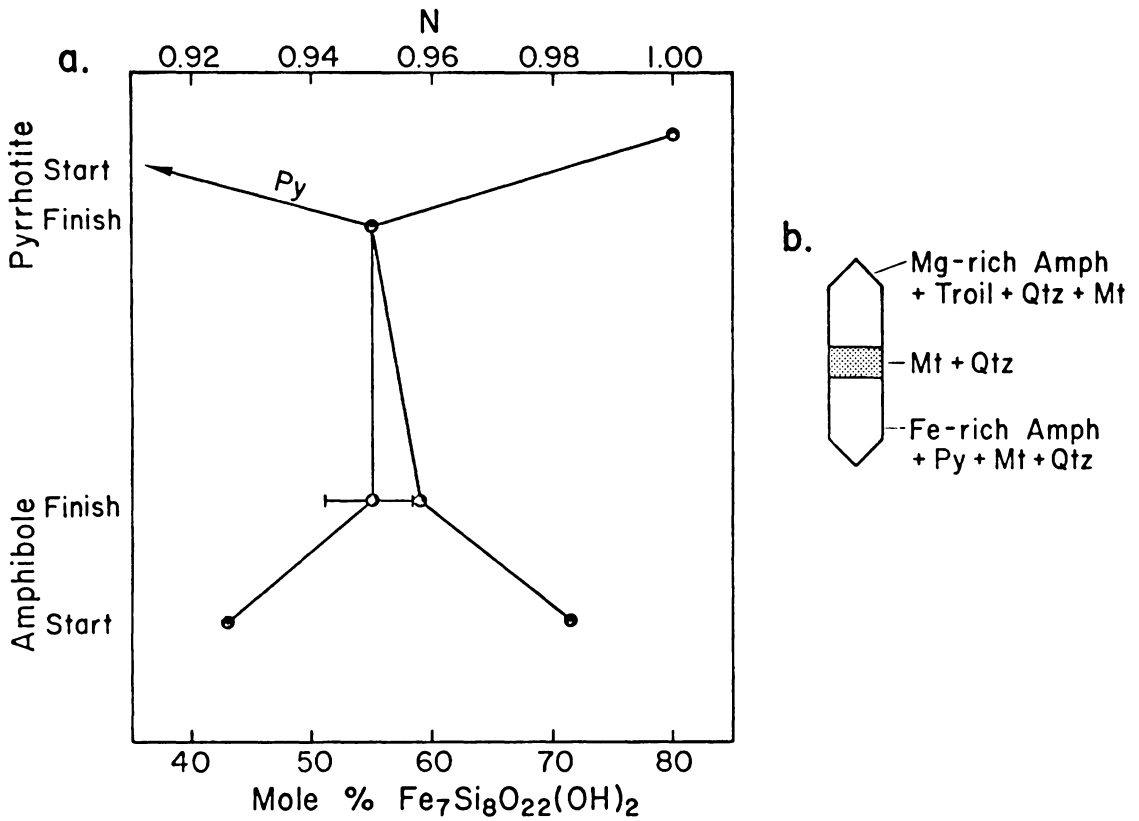

Figure III-5a. Results of a well-reversed experiment (700°C, 2 kbar). Error bar represents uncertainty in determination of amphibole composition. b. Starting configuration of reversal runs.

TABLE III-3. Results of Amphibole-Sulfide Runs at 2 kbar. Amphiboles and Pyrrhotites Coexisting with Magnetite and Quartz.

	Amphiboles[h]				Pyrrhotite[i]	
Run #	Starting Upper	Final Upper	Starting Lower	Final Lower	Final Upper	Final Lower
			725°C			
109	28.6	39	57.1	48	0.949	0.953
119	14.3	31	42.9	40	0.933	0.932
130	42.9	35	71.4	41	0.930	0.927
			700°C			
94	14.3	51	42.9	48	0.960	0.961
97	42.9	34	71.4	49	0.927	0.924
98	28.6	42	71.4	56	0.944	0.942
99	14.3	32	42.9	39	0.938	0.935
100	28.6	46	57.1	53	0.952	0.950
101	14.3	31	42.9	41	0.941	0.940
103	42.9	43	71.4	54	0.948	0.949
106	28.6	37	57.1	46	0.932	0.936
107	28.6	30	57.1	42	0.925	0.928
108	42.9	59	71.4	55	0.950	0.950
113[j]	14.3	26	42.9	33	0.927	0.929
131	14.3	33	28.6	36	0.952	0.953
			675°C			
111	28.6	36	57.1	41	0.937	0.937
118	14.3	31	42.9	42	0.942	0.942
126[j]	14.3	26	42.9	30	0.930	0.931
			650°C			
112	28.6	33	57.1	47	0.939	0.940
117	14.3	19	42.9	41	0.925	0.925
127[j]	14.3	23	42.9	33	0.928	0.930
			750°C			
120	14.3	30	42.9	38	0.929	0.928
			725°C			
125[j,f]	14.3	26	42.9	30	0.930	0.931

TABLE III-3 (continued).

Run #	Amphiboles[h] Starting Upper	Final Upper	Starting Lower	Final Lower	Pyrrhotite[i] Final Upper	Final Lower
			675°C			
128[k,e,g]	42.9	49	71.4	69	0.997	
			650°C			
129[k,e,g]	42.9	55	71.4	70	0.990	
			625°C			
132[k,e]	42.9	67	71.4	77	0.959	0.959

h - *amphibole composition reported as mole % $Fe_7Si_8O_{22}(OH)_2$; ± 4 for final compositions.*
i - *pyrrhotite composition reported as N; ± 0.003.*
j - *runs starting with hematite plus quartz in middle layer; pyrite in upper and lower.*
k - *runs starting with iron plus quartz in middle layer.*
e - *olivine observed in run products.*
f - *pyroxene observed in run products.*
g - *overlap of 102 pyrrhotite with magnetite 400 peak; may be seriously in error. Measurement based only on pyrrhotite in middle layer.*

of the capsule and pyrite in both the upper and lower layers. In all such runs magnetite + quartz was the final assemblage in the middle layer and a single pyrrhotite composition was observed in the upper and lower layers. Even though the pyrrhotite composition has not been reversed, i.e., both pyrrhotites formed from pyrite, the data of Table III-3 indicate that the final composition in either half of a true reversal is the same as the reversed composition within the error of measurement.

The results presented in Table III-3 can be grouped into four categories. (a) Runs in which both the upper and lower amphiboles show significant shift towards an intermediate composition and in which the final composition of both are within a bracket of 10 mole % or less. These runs are considered to be good reversals and the results of one such run are shown in Figure III-5a. (b) Runs in which both amphiboles show significant shifts towards an intermediate composition with a bracket of >10 mole % separating the final compositions. (c) Certain runs represent only one-sided reversals in that one amphibole showed significant reaction towards an intermediate composition but the other did not show significant reaction. (d) The final category is that in which both amphiboles shifted in the same direction, that is, to either more Fe- or more Mg-rich compositions.

Figure III-6 is a plot of amphiboles coexisting with pyrrhotite, magnetite, and quartz at 700°C and 2 kbar. Tie lines are drawn from the centers of pyrrhotite reversal brackets to the centers of amphibole brackets for type (a) runs. For type (b) and (c) runs, tie lines are drawn from pyrrhotites to amphibole compositions within the reversal

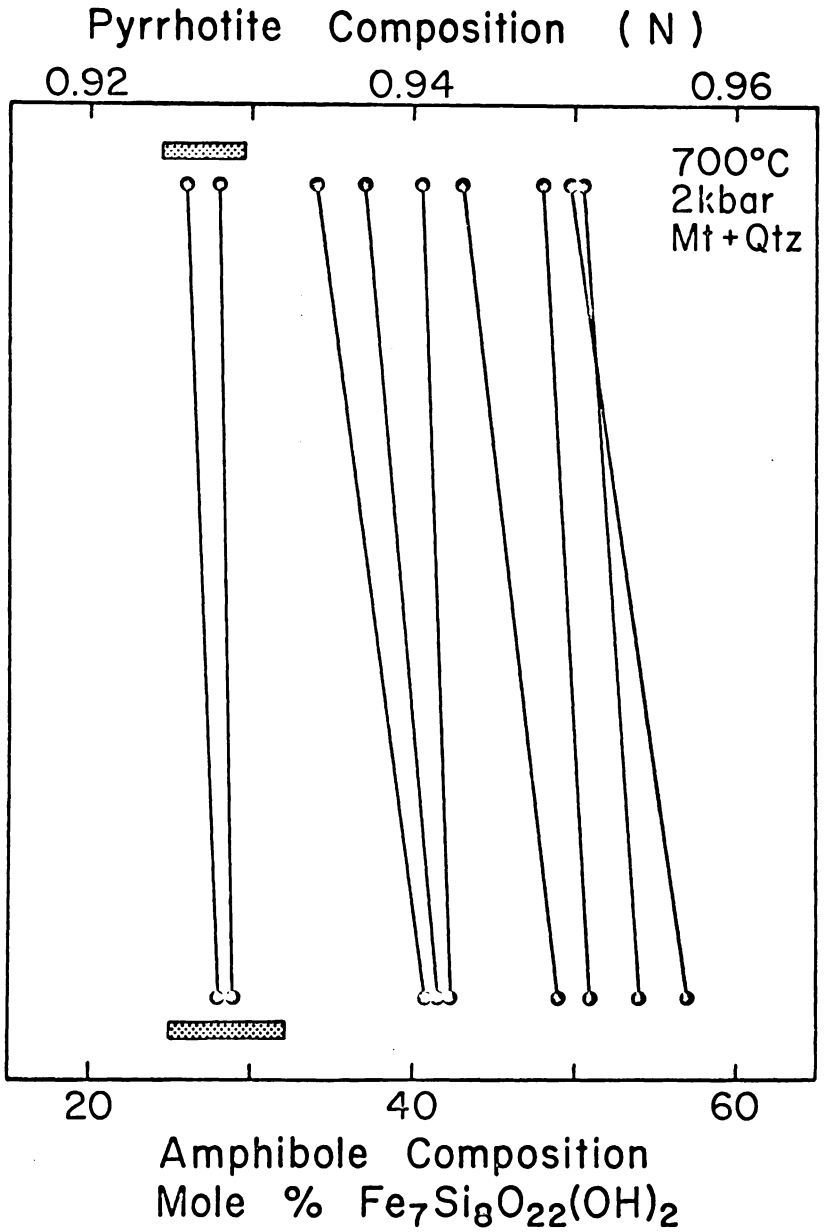

Figure III-6. Compositions of amphibole and pyrrhotite coexisting with magnetite and quartz. Error bars represent uncertainty in measurement of compositions of phases.

brackets such that the slopes are consistent with type (a) runs. Results of type (d) runs are not plotted.

A number of runs were made in which the middle layer initially contained iron plus quartz. In such runs lower f_{O_2} and f_{S_2} prevailed. Minor, but significant, amounts of olivine were observed to coexist with amphibole in the run products. At the lower f_{S_2}, overlap of the 102 pyrrhotite peak with the 400 magnetite peak introduces serious errors into the determination of pyrrhotite compositions, shifting observed compositions to more iron-rich values. Results of these runs are reported in Table III-3. All are of types (c) and (d) described above.

Determination of Oxygen Fugacity During Runs

As discussed above, the presence of magnetite + quartz in equilibrium with amphibole and pyrrhotite allows determination of f_{O_2} during runs. In Figure III-1, the intersections of the equilibria represented by equations 1 and 2 must lie on the curve representing the reaction:

$$\underset{\text{magnetite}}{Fe_3O_4} + 3/2\ \underset{\text{vapor}}{S_2} \rightleftarrows 3\ \underset{\text{pyrrhotite}}{FeS} + 2\ \underset{\text{vapor}}{O_2} \qquad (6)$$

Thus, for any given f_{S_2} (i.e., pyrrhotite composition), f_{O_2} is defined provided magnetite is present. Equilibrium f_{O_2} during the amphibole-sulfide runs can therefore be determined from an f_{O_2}-f_{S_2} plot of the magnetite-pyrrhotite equilibrium at the temperature and pressure in question. Magnetite-pyrrhotite curves were determined in two ways.

Equation 6 allows the direct calculation of the equilibrium. G° values at 1 atmosphere for magnetite and pyrrhotite were obtained from

the JANAF Tables (1971) and from Barton and Skinner (1967), respectively. G° of each gas is zero by definition. Thus $G^{\circ}_{\rightarrow}$ at one atmosphere is known for Equation 6, and K at one atm is determined by equation 3. The equilibrium constant is corrected from one atmosphere to the pressure in question (2000 bar) by the relation:

$$\ell n \frac{K_2}{K_1} = \frac{-V^{S}_{\rightarrow}}{RT} (P_2 - P_1) \tag{7}$$

where $V^{S}_{\rightarrow}$ is the volume of reaction of the solids, and P_2 and P_1 the pressures in question. Equation 7 follows directly from equation 3, the definition of standard states of solids and gases, and the relation

$$\left(\frac{\partial G}{\partial P}\right)_T = V \tag{8}$$

Assuming magnetite to be a pure phase and using the relation between f_{S_2}, a^{po}_{FeS}, and N (Toulmin and Barton, 1964) also corrected to 2000 bars by equation 7, the dashed mt-po equilibrium curves at 725° and 650°C, 2 kbar in Figure III-7 were calculated. The vertical error bar on the 650° curve represents the uncertainty based on the errors in the tabulated G° values.

The mt-po equilibrium was also located experimentally in the following manner. When plotted in terms of f_{O_2} and f_{S_2}, the equilibria

$$3\ Fe_2SiO_4 + O_2 \rightarrow 2\ Fe_3O_4 + 3\ SiO_2 \tag{9}$$

fayalite vapor magnetite quartz

$$Fe_2SiO_4 + S_2 \rightarrow 2\ FeS + SiO_2 + O_2 \tag{10}$$

fayalite vapor pyrrhotite quartz

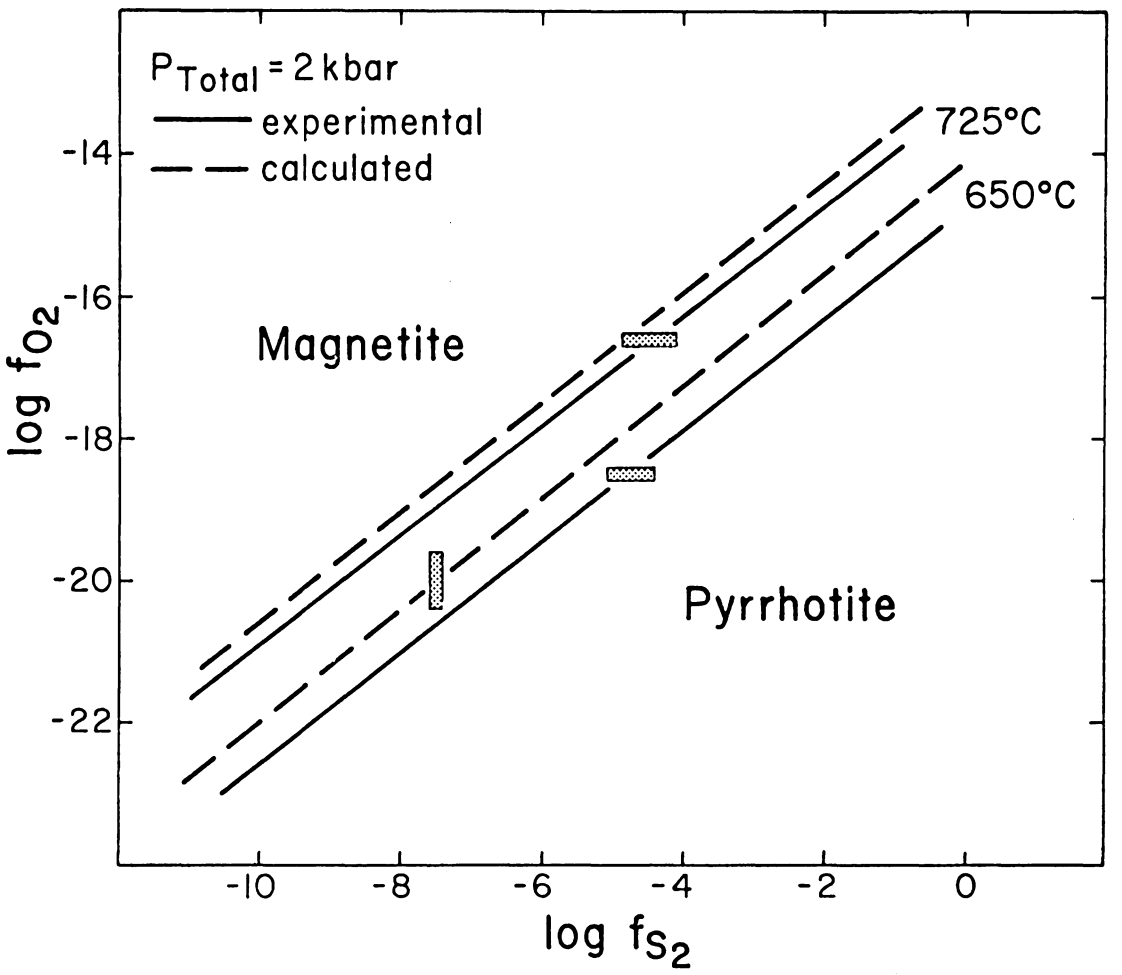

Figure III-7. Comparison of calculated and experimental magnetite-pyrrhotite equilibrium. Shaded bars represent error in location.

also intersect to define a point on the mt-po curve at a given T and P. Oxygen fugacity of the assemblage FMQ at temperature and one atmosphere can be evaluated from the equation of Wones and Gilbert (1969) and corrected to 2000 bar by equation 7. Since f_{S_2} is defined by the pyrrhotite composition, one point on the mt-po curve is located with respect to f_{O_2} and f_{S_2}. The slope of the curve is fixed by the equilibrium constant for reaction 6, i.e.,

$$\log K_{(6)} = 2 \log f_{O_2} + 3 \log a^{po}_{FeS} - 3/2 \log f_{S_2} \qquad (11)$$

Reversed pyrrhotite compositions coexisting with FMQ at 2 kbar and various temperatures were obtained by the double-charge capsule method used in amphibole runs. The assemblage FMQ-py was contained in one end of the capsule, and the assemblage FMQ-troil-qtz in the other. At the termination of runs the same composition pyrrhotite plus FMQ was observed in both ends of the capsule. The results of these runs are given in Table III-4. The experimental curves determined at 650°C and 725°C at 2 kbar are compared to the calculated curves in Figure III-7. The horizontal error bars associated with the experimental curves represent the uncertainty in f_{S_2} based on the accuracy in measurement of N_{po}, and represent an error of roughly 0.35 log units in f_{O_2}. The experimentally determined curves were used to determine f_{O_2} in amphibole-pyrrhotite runs.

Composition of the Vapor Phase

Assuming negligible solubility of the solids, the vapor phase is completely defined by the H-O-S system. Possible species in the system are taken to be H_2O, H_2, O_2, S_2, SO_2, SO, H_2S, HS, and H_2SO_4. If ideal

TABLE III-4. Reversed Fayalite-Magnetite-Quartz-Pyrrhotite Equilibria at 2 kbar

Temp. (°C)	Pyrrhotite Compositions (N, ± 0.0030) Upper	Lower	Average	log f_{S_2} (±0.3)	log f_{O_2} (±0.10)
725	0.9665	0.9635	0.9650	-4.48	-16.60
700	0.9650	0.9640	0.9645	-4.42	-17.27
675	0.9610	0.9610	0.9610	-4.43	-17.95
650	0.9612	0.9595	0.9604	-4.60	-18.68

mixing is assumed, the fugacity of each species can be calculated in the manner described by Eugster and Skippen (1967). Since temperature and total pressure are known, the following equations representing equilibria between the species can be solved simultaneously for log f_i:

$$P_{total} = \frac{f_{H_2O}}{\gamma_{H_2O}} + \frac{f_{H_2}}{\gamma_{H_2}} + \frac{f_{O_2}}{\gamma_{O_2}} + \frac{f_{S_2}}{\gamma_{S_2}} + \frac{f_{SO_2}}{\gamma_{SO_2}} + \frac{f_{SO}}{\gamma_{SO}} + \frac{f_{H_2S}}{\gamma_{H_2S}} + \frac{f_{HS}}{\gamma_{HS}} + \frac{f_{H_2SO_4}}{\gamma_{H_2SO_4}} \quad (12)$$

$$\log K_{H_2O} = \log f_{H_2O} - \log f_{H_2} - 1/2 \log f_{O_2} \quad (13)$$

$$\log K_{SO_2} = \log f_{SO_2} - 1/2 \log f_{S_2} - \log f_{O_2} \quad (14)$$

$$\log K_{SO} = \log f_{SO} - 1/2 \log f_{S_2} - 1/2 \log f_{O_2} \quad (15)$$

$$\log K_{H_2S} = \log f_{H_2S} - 1/2 \log f_{S_2} - \log f_{H_2} \quad (16)$$

$$\log K_{HS} = \log f_{HS} - 1/2 \log f_{S_2} - 1/2 \log f_{H_2} \quad (17)$$

$$\log K_{H_2SO_4} = \log f_{H_2SO_4} - 1/2 \log f_{S_2} - \log f_{H_2} - 2 \log f_{O_2} \quad (18)$$

$$\log f_{S_2} = x \quad (19)$$

$$\log f_{O_2} = y \quad (20)$$

where f_i's are the fugacities of the individual species, γ_i's the fugacity coefficients, K_i's the equilibrium constants for the formation of the given species, and x and y are the experimentally determined log fugacities of S_2 and O_2, respectively. Values of K_i were obtained from

the JANAF Tables (1971). The fugacity coefficient of H_2O was obtained from Burnham *et al.* (1969), that of H_2 from Shaw and Wones (1964), H_2S from Ryzhenko and Volkov (1971), and that of SO_2 was estimated from the reduced variable tables of Hougen *et al.* (1964). In the range of the experimental conditions the fugacities of the remaining species are so small that even large differences in an individual γ_i do not significantly effect the results, and therefore γ_i was set equal to unity for these species. The fugacities of O_2 and S_2 for each experimental run were determined as discussed above. Thus the fugacities of the individual species in the vapor phase coexisting with each amphibole + pyrrhotite + quartz + magnetite assemblage are known. The results for two runs at 700°C are compared below.

	$X_{Fe}^{amph} = 0.57$ $N_{po} = 0.950$	$X_{Fe}^{amph} = 0.29$ $N_{po} = 0.928$
$\log f_{S_2}$	-3.00	-1.24
$\log f_{O_2}$	-16.10	-14.75
$\log f_{H_2O}$	3.12	3.12
$\log f_{H_2}$	0.72	0.05
$\log H_2S$	1.51	1.72
$\log f_{SO_2}$	-1.93	0.29
$\log f_{SO}$	-6.18	-4.63
$\log f_{HS}$	-4.61	-4.07
$\log f_{H_2SO_4}$	-8.92	-6.02

Because amphiboles are hydrous phases, the fugacity of H_2O is an important variable in determining their field of stability. Even though it is assumed that sulfur does not enter into the amphibole structure, f_{S_2} can effect amphibole stability relations by influencing f_{H_2O} of the system as well as by direct reaction with the Fe component. Variation of f_{H_2O} at 700°C and 2 kbar total pressure is shown as a function of f_{O_2} and f_{S_2} in Figure III-8. The dashed line is the magnetite-pyrrhotite equilibrium curve which was experimentally determined. Over most of the range of f_{O_2} and f_{S_2} plotted, variation of f_{H_2O} is small. However, at relatively high f_{O_2} and f_{S_2}, SO_2 becomes the dominant species in the vapor phase and f_{H_2O} is substantially decreased. At relatively low f_{O_2} and high f_{S_2}, H_2S dominates the vapor phase and f_{H_2O} is again decreased.

log f_{O_2}-log f_{S_2} Plot of Amphibole Stability

The coexisting amphibole-pyrrhotite-magnetite-quartz assemblages listed in Table III-3 represent points that lie on the magnetite-pyrrhotite equilibrium curve in f_{O_2}-f_{S_2} space and are defined by the intersection of the following equilibria:

$$3\ Fe_7Si_8O_{22}(OH)_2 + 7/2\ O_2 \rightleftarrows 7\ Fe_3O_4 + 24\ SiO_2 + 3\ H_2O \qquad (21)$$

$$Fe_7Si_8O_{22}(OH)_2 + 7/2\ S_2 \rightleftarrows 7\ FeS + 8\ SiO_2 + H_2O + 7/2\ O_2 \qquad (22)$$

which represent amphibole oxidation and sulfurization, respectively. Assuming magnetite and quartz pure phases, the log form of the equilibrium constants for (21) and (22) are given by the expressions:

$$\log K_{(21)} = 3 \log f_{H_2O} - 21 \log a_{Fe}^{amph} - 7/2 \log f_{O_2} \qquad (23)$$

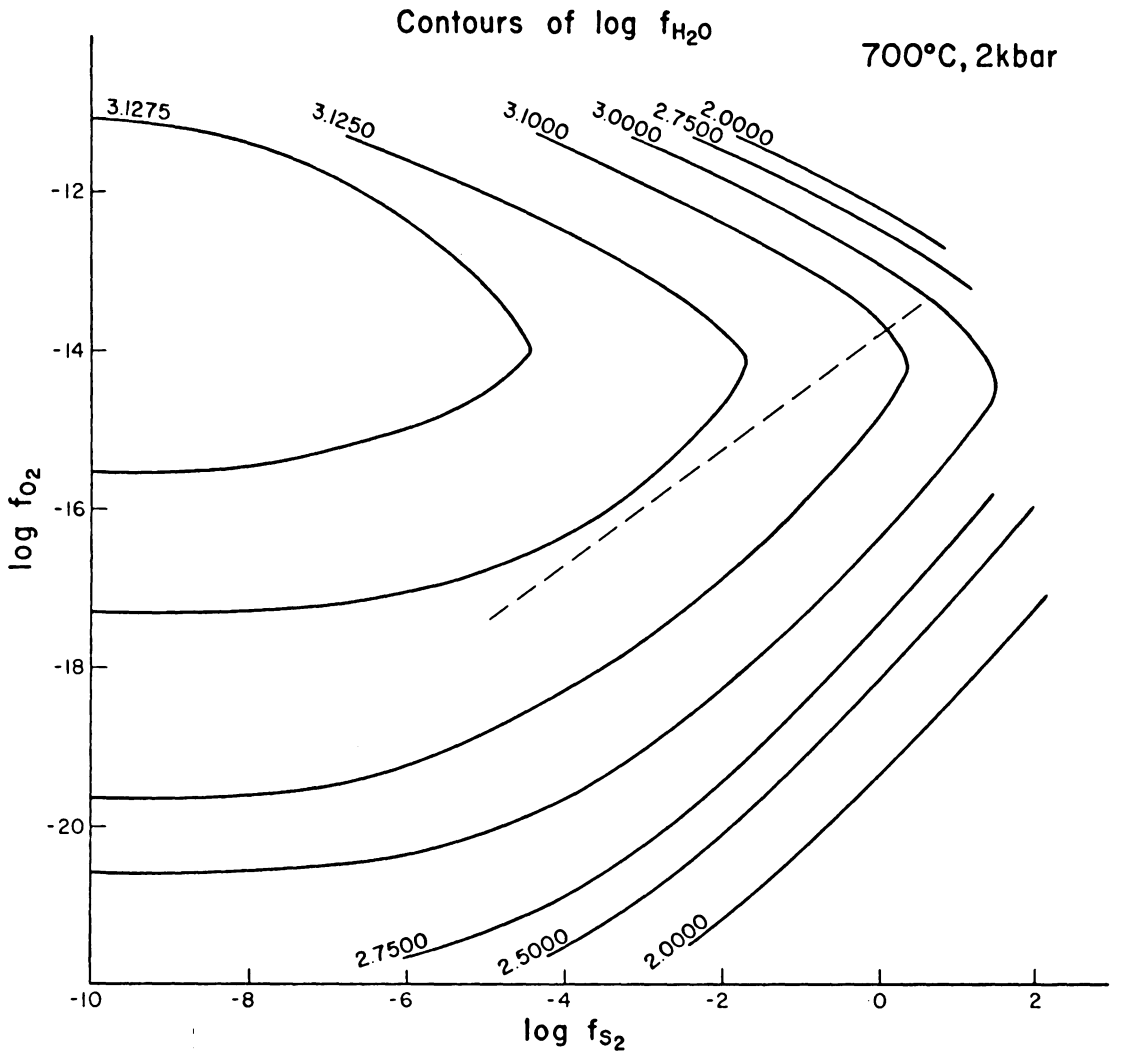

Figure III-8. Contours of calculated log f_{H_2O} in the H-O-S system at 700°C, 2 kbar. Dashed line: experimentally determined magnetite-pyrrhotite equilibrium at 700°C, 2 kbar.

$$\log K_{(22)} = 7 \log a_{FeS}^{po} + \log f_{H_2O} + 7/2 \log f_{O_2} - 7 \log a_{Fe}^{amph} - 7/2 \log f_{S_2} \quad (24)$$

Since the variation of f_{H_2O} with f_{O_2} and f_{S_2} is known, a_{FeS}^{po} is a function of f_{S_2} (Toulmin and Barton, 1964), and K_i's are constant at a given temperature, the only unknowns in (23) and (24) are the a_{Fe}^{amph} terms. It is therefore possible to extrapolate reaction (21) from the experimentally determined f_{O_2}-f_{S_2} conditions to other f_{O_2}-f_{S_2} conditions for constant amphibole composition even though the solution properties of the amphibole are not known. The extrapolation of the oxidation reaction for any amphibole composition is governed by the relation:

$$7/6 \Delta \log f_{O_2} = \Delta \log f_{H_2O} \quad (25)$$

where $\Delta \log f_{H_2O}$ is the difference in $\log f_{H_2O}$ between the experimental f_{O_2}-f_{S_2} conditions and any other conditions. Similarly, for constant amphibole compositions, equilibrium (22) can be extrapolated from the experimental f_{O_2}-f_{S_2} values by the relation:

$$7 \Delta \log a_{FeS}^{po} + \Delta \log f_{H_2O} + 7/2 \Delta \log f_{O_2} = 7/2 \Delta \log f_{S_2} \quad (26)$$

Figure III-9 is a $\log f_{O_2}$-$\log f_{S_2}$ plot of amphibole stability at 700°C and P_{total} = 2 kbar obtained in this manner. The stability fields of four well-reversed amphibole compositions are shown as solid lines. The shaded area represents the experimental uncertainty in location of the equilibria. The location of the pyrrhotite-pyrite equilibrium for the T-P conditions was obtained from Toulmin and Barton (1964), and the

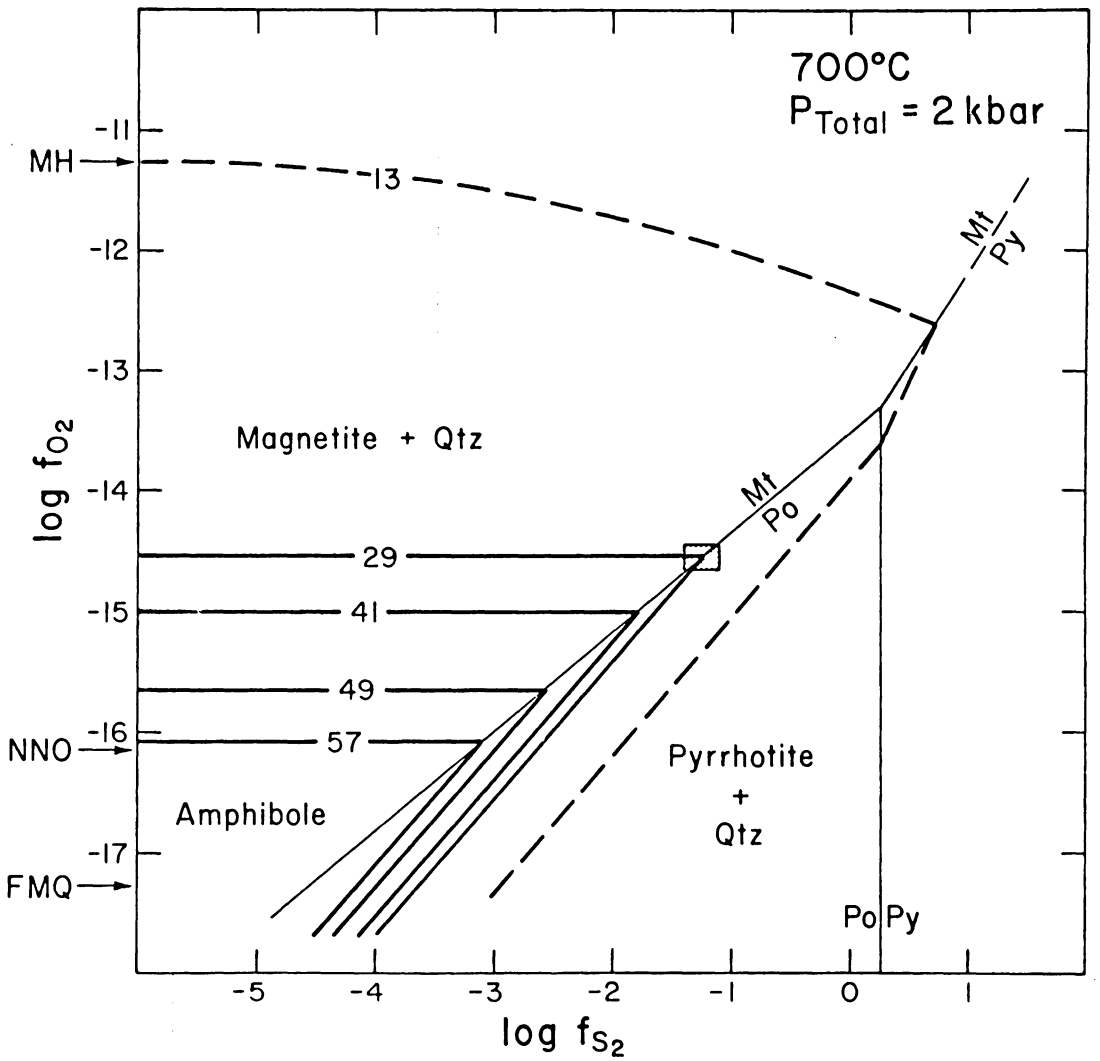

Figure III-9. Stability of amphiboles on a condensed f_{O_2}-f_{S_2} diagram. Compositions in mole % Fe_7. Dashed line was calculated starting from the amphibole composition determined in experiments in the S-free system. Shaded area indicates uncertainty in location of intersection. Symbols at left indicate f_{O_2} of solid buffer assemblages.

slope of the magnetite-pyrite curve was determined from the equilibrium constant for the reaction assuming pure solid phases.

The f_{O_2}-f_{S_2} conditions of the experiments lie in the range such that equilibria represented by equilibrium (21) (i.e., oxidation) are only very slightly affected by f_{S_2} variations. Extrapolation of these equilibria to the lowest f_{S_2}'s in Figure III-9 essentially represents amphibole stability in the S-free system. The log f_{O_2} value of -16.05 for oxidation of amphibole $X_{Fe}^{amph} = 0.57$ at low f_{S_2} is nearly identical with that of the Ni-NiO buffer (-16.16) at 700°C and 2 kbar (Heubner, 1971). The experimentally determined amphibole composition in the S-free system of 0.55 taken from Figure II-4 in Part II is in good agreement. For the S-free system, equilibrium (21) holds for an amphibole of $X_{Fe}^{amph} = 0.13$ at f_{O_2} defined by the M-H buffer (see Part II, Fig. II-1). The dashed line in Figure III-9 represents oxidation of this composition in f_{O_2}-f_{S_2} space determined by equation 25. The effect of f_{S_2} on amphibole oxidation reactions is much more pronounced at higher f_{O_2} and f_{S_2} values.

Equilibria represented by equations 22 and 26 (i.e., sulfurization) will also be effected by variation in f_{H_2O}. However, in the range of experimental conditions, the effect is too small to be detectable on the scale of Figure III-9, and the curves representing sulfurization of amphibole are identical to those for which f_{H_2O} is constant.

Amphibole Solution Models

The experimental results were tested against several solution models for the Fe-Mg amphiboles. The value of $K_{(21)}$ (eqn. 23) at 700°C and 2 kbar was calculated assuming the following three different amphibole models and

compared to an equilibrium constant obtained independent of a solution model. Because of the larger error in calculation of $K_{(22)}$, only $K_{(21)}$ was used in the comparison.

(1) Ideal solution, that is, Fe^{2+} and Mg^{2+}, are randomly distributed over all the M-sites within the amphibole structure and

$$a_{Fe}^{amph} = X_{Fe}^{amph} , \tag{27a}$$

$$\mu_{Fe}^{amph} = \mu^{\circ}{}_{Fe}^{amph} + 7\ RT\ \ell n\ X_{Fe}^{amph} \tag{27b}$$

where X_{Fe}^{amph} is the mole fraction of the Fe end-member in solution, and mixing is assumed to take place on seven cation sites within the amphibole structure.

(2) Ideal solution on the amphibole substructure (e.g., Mueller, 1962; Navrotsky, 1971), which assumes Fe^{2+} and Mg^{2+} to be preferentially segregated into specific structural sites but that mixing on an individual site is ideal. It was assumed that Fe^{2+} is preferentially segregated into the two M(4) sites and that Fe^{2+} and Mg^{2+} are equally distributed over the two M(1) sites, the two M(2) sites, and the M(3) site. The first assumption is consistent with previous crystal structure refinements and Mossbauer spectral studies of Fe-Mg amphiboles and the second assumption, while not strictly correct, is probably valid considering the precision of the experimental measurements of this study. For the ideal-substructure mixing model,

$$a_{Fe}^{amph} = (X_{Fe}^{M(4)})^{2/7}\ (X_{Fe}^{M(1)(2)(3)})^{5/7} \tag{28}$$

where $X_{Fe}^{M(4)}$ is the fraction of Fe^{2+} in the M(4) sites and $X_{Fe}^{M(1)(2)(3)}$ is

the fraction of Fe^{2+} in the M(1), M(2), and M(3) sites. Mueller (1962) found that such an expression gave a better approximation than an ideal solution model for empirically determined activity values of natural cummingtonites-grunerites. The variation in Fe^{2+}-Mg^{2+} distribution within the different structural sites as a function of total Fe/(Fe+Mg) ratio of the amphiboles was estimated from the data of Bancroft *et al.* (1967), Finger (1969, 1970), Ghose (1961), and Ghose and Weidner (1972). It should be noted, however, that this distribution is also a function of temperature, but that the variation of a_{Fe}^{amph} with temperature is negligible at the level of precision of the calculations.

(3) Symmetric regular solution (e.g., Thompson, 1967) in which

$$7\ RT\ell n\ a_{Fe}^{amph} = 7\ RT\ell n\ X_{Fe}^{amph} + (1-X_{Fe}^{amph})^2\ Wg \qquad (29)$$

where Wg is an excess mixing function.

Mean values of $\log K_{(21)}$ and estimated standard deviations ($\hat{\sigma}$) calculated from the 700°C data plotted in Figure III-6 using the above three models to define a_{Fe}^{amph} are reported in Table III-5. Using the regular solution model the equation defining $\log K_{(21)}$ contains two unknowns, log K and Wg. Thus equations from two different data points were solved simultaneously for the two unknowns. Mean Wg and the estimated standard deviation are also reported in Table III-5.

A value of $K_{(21)}$ that is independent of a solution model was obtained from equation 23. The function:

$$\log K_{(21)}/21 + \log a = 1/21(3 \log f_{H_2O} - 7/2 \log f_{O_2}) \qquad (30)$$

(for which the right hand side is known) was plotted against $\log X_{Fe}^{amph}$

TABLE III-5. Comparison of log $K_{(21)}$ Values at 700°, 2 kbar

	Ideal Solution	Ideal Sublattice Solution	Symmetrical Regular Solution	Extrapolation to log $X_{Fe}^{amph} = 0$
Mean log $K_{(21)}$	71.31	72.41	71.61	70.10
$\hat{\sigma}$	0.74	1.45	3.90	0.80
Mean Wg			-560	
$\hat{\sigma}$			2099	

for the same 700°C data used to calculate the equilibrium constant as just described. Linear regression analysis gave a best fit curve to the data defined by the equation:

$$(\log a + \log K_{(21)}/21) = 0.838(0.105)\ \log X + 3.336(0.04). \qquad (30a)$$

The slope ≈1 indicates log X ≈ log a, that is, ideal solution. At log $X_{Fe}^{amph} = 0$, by definition, log $a_{Fe}^{amph} = 0$, and thus log $K_{(21)}/21$ is defined by the intercept in equation 30a. The value of log $K_{(21)}$ obtained in this manner, along with the estimated standard deviation, is also given in Table III-5. Figure III-10 is a plot of X_{Fe}^{amph} vs a_{Fe}^{amph} calculated from the extrapolated value of the equilibrium constant. From Table III-5 and Figure III-10, it is concluded that for the precision of the experimental data, the amphibole solid solution behaves ideally.

Log K versus 1/T Plots; Enthalpy of Formation of Iron Amphibole

Assuming the amphibole solution to be ideal, mean values of log K for the oxidation reaction ($K_{(21)}$, eqn. 23) and sulfurization reaction ($K_{(22)}$, eqn. 24) were calculated at 725°, 700°, 675°, and 650°C from type (a), (b) and (c) runs (Table III-3). The values are plotted against 1/T (°K) in Figure III-11. Typical errors in log K reflect the precision of measurement of f_i's and X_{Fe}^{amph}. The standard state enthalpy of reaction ($H_{\rightarrow}^{\circ}$) is defined by the expression:

$$\frac{d \log K}{d\ (1/T)} = -\frac{H_{\rightarrow}^{\circ}}{2.303\ R} \qquad (31)$$

where R is the gas constant and the standard state is that in which the

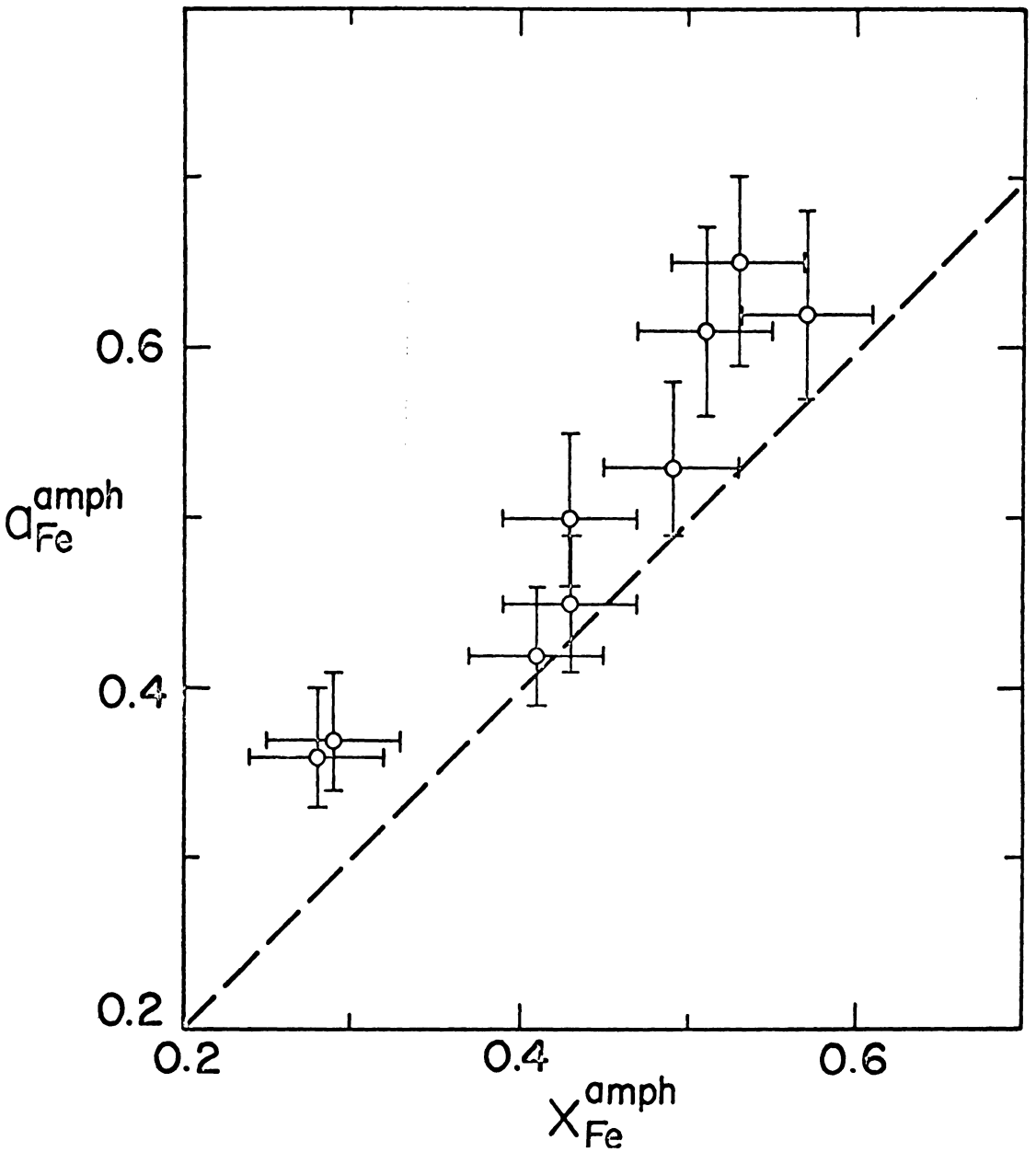

Figure III-10. Plot of a_{Fe}^{amph} vs X_{Fe}^{amph} (700°, 2 kbar) based on the value of log $K_{(21)}$ obtained by extrapolation to $X_{Fe}^{amph} = 1$. Uncertainty of a_{Fe}^{amph} represents 1 $\hat{\sigma}$ in log $K_{(21)}$. Uncertainty in X_{Fe}^{amph} represents minimum uncertainty in measurement of amphibole composition.

solids are at temperature, pressure, and pure composition; the vapor at temperature and one atmosphere; and mixing of the species in the vapor phase is ideal ($H^\circ_{mix} = 0$). Solid lines in Figure III-11 are least squares, straight line fits to the midpoints of the data, and the dashed lines represent maximum and minimum slopes that can be fit through the error bars. The values of $H^\circ_{\rightarrow}$ for each set of curves are given in Table III-6A. The rather large errors in determination of log K in turn result in quite large errors in $H^\circ_{\rightarrow}$ of reaction.

The value of $H^\circ_{\rightarrow}$ for each reaction was used to calculate H° of formation of $Fe_7Si_8O_{22}(OH)_2$ amphibole from the elements at 298° K and 1 atm. Assuming the curves in Figure III-11 to be linear down to 298° K, $H^\circ_{\rightarrow}$ at 298° K and 2 kbar is known. Values of H° of formation from the elements at 298° K and 1 atm for all phases except amphibole in equations 21 and 22 were obtained from Robie and Waldbaum (1968). Values of the solids were corrected to 2 kbar by the relation:

$$\left(\frac{\partial H}{\partial P}\right)_T = V(1 - T\alpha) \qquad (32)$$

where α, the coefficient of thermal expansion, was assumed to be negligible. The resulting H° of formation of Fe-amphibole at 298° K and 2 kbar was then corrected to 298° K and 1 atm by equation 32. The values obtained from the midpoints of the error bars, as well as the maximum and minimum values obtained from each reaction are summarized in Table III-6B. For comparison, $H^\circ_{298,1}$ of formation from the elements for anthophyllite (Zen, 1971), forsterite, fayalite (Robie and Waldbaum, 1968), annite (Eugster and Wones, 1962), and phlogopite (Bird and Anderson, 1973) are also listed in Table III-6B. Although the errors in the calculated $H^\circ_{298,1}$

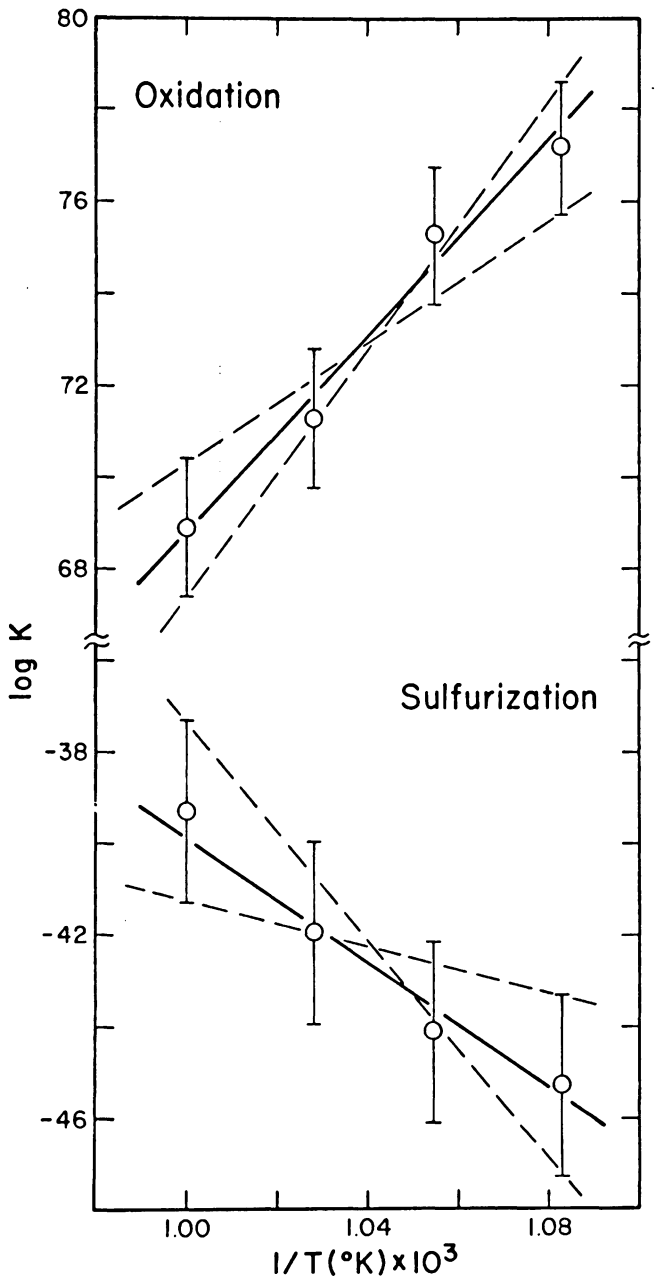

Figure III-11. Log K vs 1/T plots for sulfurization and oxidation reactions. Solid lines: linear regression through midpoints. Dashed lines: maximum and minimum slopes which can be drawn through error bars.

Table III-6

6A. Enthalpy of Reaction ($H^{\circ}_{\rightarrow}$, kcal)

	Oxidation (equation 21)	Sulfurization (equation 22)
Midpoints	-482	311
Maximum	-599	529
Minimum	-295	88

6B. Standard State Enthalpy of Formation from the Elements for Selected Silicates ($H^{\circ}_{298^{\circ}, 1\ atm}$ kcal/mole)

Fe End-members	Mg End-members
Fe_7 Amphibole (this study) oxidation: midpoints -2262; max. -2223; min. -2324 sulfurization: midpoints -2278; max. -2055; min. -2511	Mg_7 Anthophyllite -2888.1 (Zen, 1971)
Annite -1235 (Eugster and Wones, 1962) -1233.4 (Hammarback and Lindqvist, 1972)	Phlogopite -1482 (calculated from data in Bird & Anderson, 1972)
Fayalite -353.5 (Robie and Waldbaum, 1968)	Forsterite -520.4 (Robie & Waldbaum, 1967)

for Fe-amphibole are large, the difference between its value (-2270 kcal/mole average) and that of anthophyllite (-2888.1 kcal/mole; Zen, 1971) in the "right direction" when Fe and Mg end-members of other silicate solid solution series are considered (Table III-6B).

Geological Applications

The experimental results obtained in Part III may be applied towards an understanding of the volatile phase where Fe-Mg amphiboles and Fe-sulfides have crystallized together. Because Fe-sulfides continually re-equilibrate even at temperatures below 300°C, the more refractory amphiboles should better reflect the conditions of initial formation. As before, structural differences between synthetic and natural amphiboles are not considered, and the additional chemical components usually contained in natural amphiboles provide further complications. It is evident from Figures III-1 and III-9 that f_{O_2}, as well as f_{S_2}, is also a critical variable in determining equilibrium relations between silicates and Fe-sulfides. Estimation of f_{O_2} may be complicated unless additional specific phases, such as magnetite + quartz, are present. Although coexisting amphibole-sulfide assmeblages have been reported from sulfur-rich metamorphic terranes, perhaps a more common association is found in sulfide ore bodies. Amphiboles are common gangue minerals in the massive Ducktown-type ore bodies (Ross, 1935; Kinkel, 1967). The occurrence of cordierite-anthophyllite (gedrite) in association with volcanogenic sulfide deposits has also been discussed by numerous authors (e.g., Upadhyay and Smitheringale, 1972; Byers, 1969). Unfortunately, complete chemical analyses of amphiboles from such ore bodies are only rarely reported in the literature and no systematic studies of amphibole compositions within and around an ore body have been reported. In light of this scarcity of data only some very broad conclusions can be drawn.

Metamorphosed Iron Formation

Butler (1969) reported assemblages containing cummingtonite, orthopyroxene, Fe-sulfides, quartz, and magnetite from a regionally metamorphosed Fe-formation in the Gagnon, Quebec area. Three groups of assemblages were distinguished based on the Fe-sulfides: type I, pyrite only; type J, pyrrhotite only; type K, pyrite and pyrrhotite. Compositions (Fe/(Fe + Mg + Ca + Mn)) of orthopyroxene-cummingtonite pairs for each group are given below.

Type I (py): opx(0.56)-cum(0.51); opx(0.72)-cum(0.70)

Type J (po): opx(0.57)-cum(0.47)

Type K (po+py): opx(0.55)-cum(0.54)

Temperature-pressure estimates for metamorphism in the Gagnon area of 600°-700°C and 5.5-7.5 kbar were discussed in Part II. Since the pressure effect on the amphibole-sulfide compositions is small, Figure III-9 should give a good approximation to natural conditions. At 700°C, an amphibole of Fe/(Fe + Mg) = 0.18 coexists with py + po + mt + qtz, and more Mg-rich amphibole coexists with py + mt + qtz. As suggested by Butler, the natural assemblages clearly do not represent equilibrium assemblages. In support of this conclusion, calculated orthopyroxene-sulfide equilibria at 600°C (Froese, 1971) indicated orthopyroxene of Fe/(Fe + Mg) $\simeq$ 0.15 in equilibrium with py + po + mt + qtz. Since sulfides are only minor constituents of these rocks, interaction between sulfides and silicates may have been limited to areas immediately adjacent to sulfide grains, in which case silicate compositions may be unaffected by sulfurization.

Sulfide Ore Bodies

Froese (1969) reported cummingtonite, hornblende, and anthophyllite associated with sulfide minerals at the Coronation Mine, Saskatchewan. Anthophyllite and hornblende are reported to be incompatible but cummingtonite coexists with either. Pyrite, and pyrrhote + chalcopyrite, constitute the two major ore assemblages, with sphalerite and magnetite also reported from both. Although no specific textural relations are discussed, all three amphiboles apparently coexist with sulfides in places. Chemical compositions are reported only for anthophyllite. Approximate Fe/(Fe + Mg) in the range 0.54-0.72 were determined for anthophyllites by optical spectra. The structural formula:

$$Fe^{2+}_{3.19}Mg_{1.97}Al_{1.22}(Fe^{3+},Mn,Ti,Ca,Na)_{0.53}Al_{1.14}Si_{6.86}O_{22}(OH)_2$$

was calculated on the basis of 23 oxygens from the single complete chemical analysis given by Froese. Values of P_{H_2O} = 2-4 kbar, T = 550°-600°C have been estimated for the conditions of the final metamorphism under which the rocks from the Coronation Mine crystallized (Froese, 1969).

The significant amounts of aluminum in amphibole and the uncertain textural relations do not allow direct application of the experiment results. However, based on the observed assemblages, Froese (1971) has calculated the stability of amphiboles on the join $Mg_5...Fe_5Al_4Si_6O_{22}(OH)_2$ with respect to f_{O_2} and f_{S_2} at 600°C and P_{H_2O} = 3 kbar. Calculated amphibole compositions coexisting with quartz, magnetite, cordierite, and pyrrhotite range from ∿15% Fe end-member at pyrrhotite N = 0.930 to ∿25% at N = 0.940. Even though the 600°C temperature is below the experimental

range, comparison of these calculated values with experimental amphibole compositions (∿28-45 mole %) for the same pyrrhotite range (N = 0.93-0.94) at 650°C indicates that the iron end-member component is apparently destabilized by the addition of Al. It is important to note, however, that the calculations were based on a number of assumptions, including ideality of the amphibole and cordierite solid solutions.

Craig and Gilbert (1974) reported compositions of hornblendes from both ore and unmineralized wall rock from metamorphosed massive sulfide deposits at the Gossan Lead of Virginia, and Ducktown, Tennessee. Hornblendes in the ores have Fe/Mg ratios of ∿0.3, whereas those from adjacent nonmineralized wall rock are in the range Fe/Mg $\geq$ 1.0. Pyrrhotite constitutes the major sulfide mineral in both ore bodies. The estimated temperature of metamorphism at the Gossan Lead mine studied (∿400°C, Craig *et al.*, 1971) and chemical complexity of the amphiboles again do not allow direct application of the experimental results. It is obvious, however, that significant interaction between sulfides and amphiboles has taken place.

It is clear that sulfur fugacity exerts a strong control on the iron content of amphiboles. The assemblages: pyrrhotite + pyrite + magnetite; and fayalite + magnetite + quartz + pyrrhotite may be taken to limit the geologically reasonable range of f_{O_2}-f_{S_2} conditions. For the Fe-Mg amphiboles, the corresponding range of composition at 700°C 2 kbar is ∿18-84 mole % Fe end-member based on an equilibrium constant determined assuming ideality of the amphibole solution. The latter value, however, does not represent a stable composition at 700°C and f_{O_2} defined by the FMQ buffer.

In terms of present knowledge of amphibole compositions from S-rich environments, the results of this study have somewhat limited application. Although interest in silicates from these environments has increased considerably in recent years, more field and laboratory data are needed. Because of the economic importance of sulfides in massive ore bodies, additional research is needed in order to define, quantitatively and accurately, the conditions of ore formation. As is obvious from the above discussion, knowledge of the specific textural relations between opaques and silicates is necessary for meaningful interpretation. Finally, the results of this study should serve as a starting point for additional experimental studies of more chemically complex amphiboles which have a more widespread occurrence.

REFERENCES

Arnold, R. G. (1962), Equilibrium relations between pyrrhotite and pyrite from 325° to 743°C. Econ. Geol. v. 57, p. 72-90.

Bancroft, G. M., Burns, R. G., and Maddock, A. G. (1967), Determination of cation distribution in the cummingtonite-grunerite series by Mossbauer spectra. Am. Mineral. v. 52, p. 1009-1026.

Barr, A. J. and Goodnight, J. H. (1972), Statistical Analysis System. Student Supply Store, North Carolina State University, Raleigh, North Carolina.

Barton, P. B. and Skinner, B. J. (1967), Sulfide mineral stabilities. In: *Geochemistry of Hydrothermal Ore Deposits*, H. L. Barnes, ed., Holt, Rinehart, and Winston, New York, 670p.

Beyers, A. R. (1969), *Symposium on the Geology of the Coronation Mine, Saskatchewan.* Geol. Surv. Canada, Paper 68-5, 329p.

Bird, G. W. and Anderson, G. M. (1973), The free energy of formation of cordierite and phlogopite. Am. Jour. Sci. v. 273, p. 84-91.

Bonnichsen, B. (1969), Metamorphic pyroxenes and amphiboles in the Biwabik iron formation, Dunka River area, Minnesota. Min. Soc. Am. Spec. Paper 2, p. 217-239.

Boyd, F. R. (1955), The anthophyllite-cummingtonite group. *Ann. Report Director Geoph. Lab. 1945-55*, Yearbook 54, p. 117-118.

Burnham, C. W., Holloway, J. R., and Davis, N. F. (1969), Thermodynamic properties of water to 1000°C and 10,000 bars. G.S.A. Special Paper 132, 96p.

Butler, P. (1969), Mineral compositions and equilibria in the metamorphosed iron formation of the Gagnon region, Quebec, Canada. Jour. Pet. v. 10, p. 56-101.

Cameron, K. L. (1975), An experimental study of actinolite-cummingtonite phase relations with notes on the synthesis of Fe-rich anthophyllite. Am. Mineral. v. 60, p. 375-390.

Charkraborty, K. L. (1963), Relationship of anthophyllite, cummingtenite, and mangano-cummingtenite in the metamorphosed Wabush iron-formation, Labrador. Can. Mineral. v. 7, p. 738-750.

Clark, T. and Naldrett, A. J. (1972), The distribution of Fe and Ni between synthetic olivine and sulfide at 900°C. Econ. Geol. v. 67, p. 939-952.

Craig, J. R., Sears, C. E., Gilbert, M. C., and Hewitt, D. A. (1971), The Gossan Lead district, in *Guidebook to Appalachian Tectonics and Sulfide Mineralization of Southwestern Virginia*, Guidebook #5, VPI & SU, p. 25-34.

_____ and Gilbert, M. C. (1974), Amphiboles in Appalachian ores (abstr.) G.S.A. Abstr. with Prog. v. 6, no. 4, p. 346.

Ernst, W. G. (1966), Synthesis and stability relations of ferrotremolite. Am. Jour. Sci. v. 264, p. 37-65.

_____ (1968), *Amphiboles: Crystal Chemistry, Phase Relations and Occurrence*, Springer-Verlag, New York, 125p.

Eugster, H. P. and Wones, D. R. (1962), Stability of the Ferruginous biotite, annite. Jour. Pet. v. 3, p. 82-125.

_____ and Skippen, G. (1967), Igneous and metamorphic reactions involving gas equilibria. In: *Researches in Geochemistry, Vol. 2*, D. H. Ableson, ed., John Wiley & Sons, New York, 663p.

Evans, B. W., Ghose, S., Rice, J. M., and Trommsdorf, V. (1974), Cummingtonite-anthophyllite phase transition in metamorphosed ultramafic rocks, Ticino, Switzerland (abstr.). EOS, Trans. Am. Geoph. Union v. 55, no. 4, p. 469.

Evans, H. T., Appleman, D. E., and Handwerker, D. S. (1963), The least squares refinement of crystal unit cells with powder diffraction data by an automated computer indexing method (abstr.). Prog. Abstr. Amer. Cryst. Ass. Meet., Cambridge, Mass., p. 42.

Ewart, A., Green, D. C., Carmichael, I. S. E., and Brown, F. H. (1971), Voluminous low temperature rhyolitic magnas in New Zealand. Cont. Min. Pet. v. 33, p. 128-144.

Finger, L. W. (1969), The crystal structure and cation distribution of a grunerite. Min. Soc. Am. Special Paper no. 2, p. 95-100.

_____ (1970), Refinement of the crystal structure of anthophyllite. *Ann. Report Dir. Geoph. Lab. 1968-69*, Yearbook 68, p. 283-288.

Fisher, G. W. (1967), Fe-Mg olivine solid solutions, *Ann. Report Dir. Geoph. Lab. 1965-66*, Yearbook 65, p. 209-217.

Forbes, W. C. (1969), Unit-cell parameters and optical properties of talc on the join $Mg_3Si_4O_{10}(OH)_2$-$Fe_3Si_4O_{10}(OH)_2$. Am. Mineral. v. 54, p. 1399-1408.

_____ (1971), Synthesis of grunerite, $Fe_7Si_8O_{22}(OH)_2$. Nature Phys. Sci. v. 232. Aug. 2, p. 109.

French, B. M. (1968), *Progressive Metamorphism of the Biwabik Iron-Formation, Mesabi Range, Minnesota.* Minn. Geol. Soc. Bull. 45, 103p.

Froese, E. (1969), Metamorphic rocks from the Coronation Mine and surrounding area. In: *Symp. on the Geology of the Coronation Mine, Saskatchewan*, A. R. Beyers, ed., p. 55-78.

_____ (1971), The graphical representation of sulfide-silicate equilibria. Econ. Geol. v. 66, p. 335-341.

Fullagar, P. D., Brown, H. S., and Hagner, A. F. (1967), Geochemistry of wall rock alteraction and the role of sulfurization in the formation of the Ore Knob sulfide deposit. Econ. Geol. v. 62, p. 798-825.

Ghose, S. (1961), The crystal structure of a cummingtonite. Acta. Cryst. v. 14, p. 622-627.

_____ and Weidner, J. R. (1972), Mg^{2+}-Fe^{2+} order-disorder in cummingtonite, $(Mg,Fe_7)Si_8O_{22}(OH)_2$ a new geothermometer. Earth Planet. Sci. Let. v. 16, p. 346-354.

Gibbs, G. V. (1969), Crystal structure of protoamphibole. Mineral. Soc. Am. Spec. Pap. 2, p. 101-109.

_____ and Louisnathan, S. J. (1971), *Powder Diffractometry in Geology*, Short Course Lecture Notes, 5th Ann. Mtg. S.E. Sec. G.S.A., 190p.

Greenwood, H. J. (1963), The synthesis and stability of anthophyllite. Jour. Pet. v. 4, pt. 3, p. 317-351.

Guidotti, G. V. (1970), The mineralogy and petrology of the transition from lower to upper sillimanite zone in the Oquossoc area, Maine. Jour. Pet. v. 11, p. 277-336.

Gundersen, J. N. and Schwartz, G. M. (1962), *The Geology of the Metamorphosed Biwabik Iron Formation, Eastern Mesabi District, Minnesota.* Minn. Geol. Soc. Bull. 43, 139p.

Hammarback, S. and Lindquist, B. (1972), The hydrothermal stability of annite in the presence of sulfur. Geologiska Forren. i Stockholm Forrhandl. v. 94, p. 549-564.

Huebner, J. S. (1971), Buffering techniques for hydrostatic systems at elevated pressures. In: *Research Techniques for Highland High Temperature*, G. C. Ulmer, ed., Springer-Verlag, New York, 367p.

Himmelberg, G. R. and Phinney, W. C. (1967), Granulite-facies metamorphism Granite Falls-Montevideo area, Minnesota. Jour. Pet. v. 8, p. 325-348.

Hinrichsen, T. (1967), Uber den stabilitatsberich der Mg-Fe^{2+}-Al-mischkristallreihe rambisher hornblenden, Teil I: Hydrothermale untersuchungen der anthophyllit-ferroanthophyllit-mischkristall-reiche. N. Jahrbuch. f. Mineral. Monatschafte, p. 257-270.

Hougen, O. A., Watson, K. M., and Ragatz, R. A. (1964), *Chemical Process Principle Charts*, Third Edition, John Wiley & Sons, New York.

JANAF Thermochemical Tables (1971), Nat. Stand. Ref. Data Ser., Nat. Bur. Stand., 37, 1141p.

Johannson, K. (1930), Vergleichende untersuchungen an Anthophyllits, Grammatit, and Cummingtonit. Zeits. Krist. b. 73, p. 31-51.

Kinkel, A. R., Jr. (1967), *The Ore Knob Copper Deposit, N. C., and Other Massive Sulfide Deposits in the Appalachians.* U.S.G.S. Prof. Paper 558, 58p.

Klein, K., Jr. (1964), Cummingtonite-grunerite series: a chemical, optical, and x-ray study. Am. Mineral. v. 49, p. 963-982.

_____ (1966), Mineralogy and petrology of the metamorphosed Wabush iron formation, southwestern Labrador. Jour. Pet. v. 7, p. 281-330.

_____ and Waldbaum, D. R. (1967), X-ray crystallographic properties of the cummingtonite-grunerite series. Jour. Geol. v. 75, p. 379-392.

_____ (1968), Coexisting amphiboles. Jour. Pet. v. 9, p. 281-330.

Kranck, S. H. (1961), A study of phase equilibria in a metamorphic iron formation. Jour. Pet. v. 2, p. 137-184.

Kullerud, G. and Yoder, H. S. (1963), Sulfide-silicate relations. *Ann. Report Dir. Geoph. Lab. 1962-63*, p. 215-218.

_____ and _____ (1964), Sulfide-silicate relations. *Ann. Report Dir. Geoph. Lab. 1963-64*, p. 218-222.

Layton, W. and Phillips, R. (1960), The cummingtonite problem. Min. Mag. v. 32, p. 659-663.

Lindemann, W. (1964), Beitrag zur struktur des anthophyllits (abstr.). Nortschr. Mineral. b. 42, p. 205.

Mallio, W. J. and Gheith, M. A. (1972), Textural and chemical evidence bearing on sulfide-silicate reactions in metasediments. Mineral. Deposita. v. 7, p. 13-17.

Mohr, D. W. (1972), Stratigraphy, structure, and metamorphism of the eastern part of the Fontant Lake Reservoir, Great Smokey Mtns., N. C. Ph.D. Dissert., Dept. Geol. Sci., Univ. Chicago, Chicago, Ill.

Mueller, R. F. (1960), Compositional characteristic and equilibrium relations in mineral assemblage of a metamorphosed iron formation. Am. Jour. Sci. v. 258, p. 449-497.

_____ (1962), Energetics of certain silicate solutions. Geochim. Coschim. Acta. v. 26, p. 581-598.

Naldrett, A. J. (1966), The role of sulfurization in the genesis of iron-nickel sulfide deposits of the Porcupine District, Ontario. Can. Mining and Metallur. Bull. v. LXIX, p. 147-155.

_____ and Brown, G. M. (1968), Reaction between pyrrhotite and enstatite-ferrosilite solid solutions. *Ann. Report. Dir. Geoph. Lab. 1966-67*, p. 427-429.

Navrotsky, A. (1971), The intracrystalline cation distribution and the thermodynamics of solid solution formation in the system $FeSiO_3$-$MgSiO_3$. Am. Mineral. v. 56, p. 201-211.

Papike, J. J., Ross, M., and Clark, J. R. (1969), Crystal-chemical characterization of clinoamphiboles based on five new structure refinements. Mineral. Soc. Am. Spec. Pap. 2, p. 117-136.

Perry, E. C., Jr. and Bonnichsen, B. (1966), Quartz and magnetite: oxygen-18-oxygen-16 fractionation in metamorphosed Biwabik iron formation. Science v. 153, p. 528-529.

Popp, R. K. and Gilbert, M. C. (1974), Sulfurization of intermediate Fe-Mg amphiboles (abstr.). G.S.A. Abstr. with Prog. v. 6, no. 7, p. 1058.

_____, Gilbert, M. C., and Craig, J. R. (1974), Effect of oxygen fugacity on the stability of Fe-Mg amphiboles (abstr.). EOS, Trans. Am. Geoph. Union v. 56, no. 12, p. 1200.

Ramberg, H. (1952), Chemical bonds and distribution of cations in silicates. Jour. Geol. v. 60, p. 331-355.

Rice, J. M., Evans, B. W., and Trommsdorff, V. (1974), Widespread occurrence of magnesocummingtonite in ultramafic schists, Cime di Gagnore, Ticino, Switzerland. Contr. Min. and Pet. v. 43, p. 245-251.

Richardson, S. W., Gilbert, M. C., and Bell, P. M. (1969), Experimental determination of kyanite-andalusite and andalusite-sillimanite equilibrium: the aluminum silicate triple point. Am. Jour. Sci. v. 267, p. 259-272.

Robie, R. A. and Waldbaum, D. R. (1968), Thermodynamic properties of minerals and related substances at 298.15°K (25.0°C) and one atmosphere (1.013 bars) pressure and at higher temperatures. U.S.G.S. Bull. 1259, 256p.

Ross, C. S. (1935), *Origin of the Copper Deposits of the Ducktown Type in the Southern Appalachian Region.* U.S.G.S. Prof. Paper 179, 165p.

Ryzhenko, B. N. amd Volkov, V. P. (1971), Fugacity coefficients of some gases in a broad range of temperatures and pressures. Geochemistry International v. 8, no. 4, p. 468-481.

Schurmann, K. (1974), Stability relations of amphiboles in the tremolite-ferrotremolite-anthophyllite-grunerite quadralateral (abstr.). Inter. Min. Assoc. Collected Abstracts, p. 85.

Scott, S. D. (1974), The Fe-S system. In: *Sulfide Mineralogy,* P. H. Ribbe, ed., M.S.A. Short Course Notes, v. 1.

Seifert, F. and Virgo, D. (1974), Temperature dependence of intracrystalline Fe^{2+}-Mg distribution in a natural anthophyllite. *Ann. Report Dir. Geoph. Lab. 1973-74*, Yearbook 73, p. 405-411.

Shaw, H. R. (1967), Hydrogen osmosis in hydrothermal experiments. In: *Researches in Geochemistry, Vol. 2*, P. H. Ableson, ed., John Wiley & Sons, New York, 663p.

_____ and Wones, D. R. (1964), Fugacity coefficients for hydrogen gas between 0° and 1000°C for pressures to 3000 atm. Am. Jour. Sci. v. 262, p. 918-929.

Simmons, E. C., Lindsley, D. H., and Papike, J. J. (1974), Phase relations and crystallization sequence in a contact metamorphosed rock from the Gunflint iron formation, Minnesota. Jour. Pet. v. 15, p. 539-565.

Sueno, S., Papike, J. J., Prewitt, C. T., and Brown, G. E. (1972), Crystal structure of high cummingtonite. Jour. Geoph. Res. v. 77, no. 29, p. 5767-5777.

Thompson, J. B., Jr. (1967), Thermodynamic properties of simple solutions. In: *Researches in Geochemistry, Vol. 2*, D. H. Ableson, ed., John Wiley & Sons, New York, 663p.

Toulmin, P. and Barton, P. B. (1964), A thermodynamic study of pyrite and pyrrhotite. Geochim. Cosmochim. Acta. v. 28, p. 641-671.

Tuttle, O. F. and Bowen, N. L. (1958), *Origin of Granite in the Light of Experimental Studies in the System* $NaAlSi_3O_8$-$KAlSi_3O_8$-SiO_2-H_2O. G.S.A. Memoir 74, 153p.

Upadhyay, H. D. and Smitheringale, W. G. (1972), Geology of the Gullbridge copper deposit, Newfoundland: volcanogenic sulfides in cordierite-anthophyllite rocks. Can. Jour. Earth Sci. v. 9, p. 1060-1073.

Winkler, H. G. F. (1967), *Petrogenesis of Metamorphic Rocks, 2nd ed.* Springer-Verlag, New York, 237p.

Wones, D. R. and Eugster, H. P. (1965), Stability of biotite: experiment, theory, and application. Am. Mineral. v. 50, p. 1228-1272.

_____ and Gilbert, M. C. (1969), The fayalite-magnetite-quartz assemblage between 600° and 800°C. Am. Jour. Sci., Schairer Vol. 267-A, p. 480-488.

Zen, F. (1971) Comments on the thermodynamic constants and hydrothermal stability relations of anthophyllite. Am. Jour. Sci. v. 270, p. 136-150.

The vita has been removed from the scanned document

IRON MAGNESIUM AMPHIBOLES: SYNTHESIS AND STABILITY WITH RESPECT TO TEMPERATURE, PRESSURE, OXYGEN FUGACITY AND SULFUR FUGACITY

by

Robert K. Popp

(ABSTRACT)

Standard hydrothermal and gas-buffering techniques have been used to synthesize and investigate phase relations of amphiboles on the join $Mg_7Si_8O_{22}(OH)_2$-$Fe_7Si_8O_{22}(OH)_2$. Synthesized amphiboles from $Mg_6Fe_1Si_8O_{22}(OH)_2$ to $Mg_1Fe_6Si_8O_{22}(OH)_2$ are optically orthorhombic. Variation of unit cell parameters with composition suggests that they are members of a single, continuous solid solution.

$$a(\text{Å}) = 18.577(12) + 0.001284(190)X_{Fe},$$
$$b(\text{Å}) = 17.942(11) + 0.004862(170)X_{Fe},$$
$$c(\text{Å}) = 5.285(3) + 0.000617(50)X_{Fe},$$
$$V(\text{Å}^3) = 1760.8(1.7) + 0.8226(280)X_{Fe};$$

(X_{Fe} = mole % Fe end-member)

Electron diffraction patterns of composition Mg_5Fe_2 are consistent with that of an orthorhombic amphibole with an a unit cell repeat of $\sim$18.6 Å, but are unlike any known amphibole structure type. Even though the structure type is unknown, measured shifts in peak locations on the powder X-ray diffraction patterns allow compositions to be measured to within $\pm$3 mole % Fe end-member. Combining these results with those of Forbes (1971) and Greenwood (1963), it is now clear that the entire range of amphiboles across the join can be synthesized.

No change in unit cell parameters as a function of f_{O_2} was observed, and thus there is no evidence for solution of oxy-amphibole component.

At 2 kbar and f_{O_2} defined by the MH buffer the maximum extent of solution of Fe end-member in amphibole is 12 and 22 mole % at 725° and 630°C respectively; amphibole is unstable below 630°C, being replaced by the assemblage + talc + quartz + magnetite + hematite. At f_{O_2} defined by the NNO buffer the extent of solid solution expands to 54, 62, and 65 mole % Fe end-member at 725°, 625°, and 600°C, respectively.

Results obtained in this study have been combined with previously published data to produce a T-X section of the upper thermal stability of amphibole at 2 kbar and f_{O_2} defined by the FMQ buffer. Temperatures for the reaction: amphibole → pyroxene + quartz + vapor decrease from ∿765°C for the pure Mg end-member to ∿710°C for 62 mole % Fe end-member. The breakdown reaction: amphibole → olivine + quartz + vapor, was observed for the more iron-rich amphiboles, and takes place at ∿675°C for amphibole of 73 mole % Fe end-member.

Reversed tie lines have been determined between Fe-Mg amphiboles and pyrrhotites in the presence of excess magnetite and quartz at 2 kbar, and 650°, 675°, 700°, and 725°C. This assemblage represents the simultaneous equilibria:

$$\text{amphibole} + O_2 \rightarrow \text{magnetite} + \text{quartz} + H_2O \qquad (1)$$

$$\text{amphibole} + S_2 \rightarrow \text{pyrrhotite} + \text{quartz} + H_2O + O_2. \qquad (2)$$

At 700°C, amphiboles of 29, 41, 49, and 57 mole % Fe end-member coexist with pyrrhotites of N = 0.928, 0.934, 0.943, and 0.950, respectively. Compositions of coexisting amphibole-pyrrhotite pairs apparently are not

seriously affected by temperature over the range investigated although scatter of the amphibole data does not allow a rigorous analysis. Sulfur fugacity for runs was determined from pyrrhotite compositions while f_{O_2} was known from an experimentally determined magnetite-pyrrhotite curve. Knowledge of these two fugacities allowed calculation of fugacities of all species, including H_2O, assuming an H-O-S vapor, and thus reactions (1) and (2) were located in terms of f_{O_2} and f_{S_2}.

Several models for the amphibole solid solution were used to explain the variation in composition of coexisting amphibole-pyrrhotite pairs at 700°C. The precision of measurement of both the amphibole compositions and the fugacities of volatile species does not justify other than an ideal solution model. A standard state enthalpy of formation ($H^{\circ}_{298°;1\ atm}$) of $Fe_7Si_8O_{22}(OH)_2$ amphibole from the elements of -2262 kcal/mole was calculated from a log K_{eq} vs 1/T plot for reaction (1).

The results in the S-free system have been used to estimate temperatures of formation of amphibole-bearing metamorphic and extrusive igneous rocks. Application of the results in the S-containing system is limited by the scarcity of data on natural amphibole-sulfide assemblages.